Studies on Brain MR Image Segmentation and Visualization

Thesis submitted by

Madhumita Ray

Doctor of Philosophy (Engineering)

Department of Computer Science and Engineering
Faculty Council of Engineering and Technology
Jadavpur University
Kolkata, India
2024

Jadavpur University
Kolkata 700032, West Bengal, India

Index No: 009/18/E

- **1. Title of the Ph.D thesis:**

  Studies on Brain MR Image Segmentation and Visualization.

- **2. Name, Designation and Institution of the Supervisor:**

  Dr. Jamuna Kanta Sing

  Professor

  Department of Computer Science and Engineering

  Jadavpur University

  Kolkata - 700032

- **List of publications:**
  - **List of Journal Papers:**
    - M. Ray, N. Mahata, and J. K. Sing, "Uncertainty parameter weighted entropy-based fuzzy c- means algorithm using complemented membership functions for noisy volumetric brain MR image segmentation," *Biomedical Signal Processing and Control, Elsevier*, vol. 85, p. 104925, April 2023. [Impact Factor: 5.1, SCIE Indexed]

  - **List of Conference Papers:**
    - M. Ray, N. Mahata and J. K. Sing, "A novel entropy-based FCM algorithm using inverse fuzzy membership framework and uncertainty measure for segmentation of brain MR images," in *Proc. 2nd International Conference on Artificial Intelligence: Advances and Applications (ICAIAA)*, Poornima College of Engineering, Jaipur and Rajasthan Technical University, Kota, Rajasthan, India, March 27-28, 2021, pp. 57-67.
    - M. Ray and J. K. Sing, “A novel relative entropy based FCM algorithm using interval type-2 fuzzy set at local membership functions for brain MR image segmentation,” in *Proc. 2024 3rd International Conference on Control, Instrumentation, Energy & Communication (CIEC)*, Calcutta University, Kolkata, India, January 25-27, 2024, pp. 91-96.

    * M. Ray and J. K. Sing, “3D brain MR image segmentation using a fuzzy entropy-based fuzzy clustering algorithm,” in *Proc. 2nd International Conference on Advancement in Computation & Computer Technologies (InCACCT)*, Chandigarh University, Chandigarh, Punjub, India, May 2-3, 2024.

- **4. List of Patents:** NIL

- **5. List of presentations in International Conferences:**

- M. Ray, N. Mahata and J. K. Sing, "A novel entropy-based FCM algorithm using inverse fuzzy membership framework and uncertainty measure for segmentation of brain MR images," in *Proc. 2nd International Conference on Artificial Intelligence: Advances and Applications (ICAIAA)*, Poornima College of Engineering, Jaipur and Rajasthan Technical University, Kota, Rajasthan, India, March 27-28, 2021, pp. 57-67.

- M. Ray and J. K. Sing, “A novel relative entropy based FCM algorithm using interval type-2 fuzzy set at local membership functions for brain MR image segmentation,” in *Proc. 2024 3rd International Conference on Control, Instrumentation, Energy & Communication (CIEC)*, Calcutta University, Kolkata, India, January 25-27, 2024, pp. 91-96.

- M. Ray and J. K. Sing, “3D brain MR image segmentation using a fuzzy entropy-based fuzzy clustering algorithm,” in *Proc. 2nd International Conference on Advancement in Computation & Computer Technologies (InCACCT)*, Chandigarh University, Chandigarh, Punjub, India, May 2-3, 2024.

Statement of Originality

I, **Madhumita Ray, Registration No. 1021804005 of 18-19** registered on **5th June, 2018** do hereby declare that this thesis entitled "**Studies on Brain MR Image Segmentation and Visualization**" contains literature survey and original research work done by the undersigned candidate as part of Doctoral studies.

All information in this thesis have been obtained and presented in accordance with existing academin rule and ethical conduct. I declare that, as required by these rules and conduct, I have fully cited and referred all materials and results that are not original to this work. I also declare that I have checked this thesis as per the "Policy on Anti Plagiarism, Jadavpur University, 2019", and the level of similarity as checked by iThenticate software is **2** %.

Madhumita Ray.
Signature of Candidate:
Date: 03/06/24

Certified by Supervisor:

03/06/24
(Signature with date, seal)

Jamuna Kanta Sing, Ph.D.
Professor
Dept. of Computer Science & Engineering
Jadavpur University, Kolkata-700032

Certificate from the supervisor

This is to certify that the thesis entitled "**Studies on Brain MR Image Segmentation and Visualization**" submitted by **Smt. Madhumita Ray**, who got her name registered on 5th June, 2018 for award of Ph. D. (Engg.) degree of Jadavpur University is absolutely based upon her own work under supervision of **Dr. Jamuna Kanta Sing**, Professor, Department of Computer Science and Engineering, Jadavpur University and that neither her thesis nor any part of the thesis has been submitted for any degree/ diploma or any other academic award anywhere before.

Signature of the Supervisor and date with Official Seal

03/06/24

Dr. Jamuna Kanta Sing, Professor
Department of Computer Science and Engineering
Jadavpur University
Kolkata, India

Jamuna Kanta Sing, Ph.D.
Professor
Dept. of Computer Science & Engineering
Jadavpur University, Kolkata-700032

Acknowledgements

I am very much thankful and expressing my sincere gratitude to my Ph.D research guide and supervisor **Prof (Dr.) Jamuna Kanta Sing** for his continuous encouragement and valuable advice for my research work. At the time of crisis he continuously support me. His trust on my potential make the whole journey smooth and successful. His outstanding knowledge and excellence ideas in this domain inspired me much and make me affectionate in the field of medical imaging. In the whole journey of my Ph.D research work I have faced many ups and downs , I have passed through my maternity period. It was a very tough time for me to balance my research work and my little one's responsibility. Without help of 'Sir' (my supervisor) I couldn't be able to carry on my work. Thank you so much sir.

I am very much obliged to my parents for their continuous encouragement, support and enthusiastic words. Their blesses always give me strength to fight against my adverse states of mind at this whole journey. My mother is my strength and for her today I am here. Her blesses and strong wishes make me achieve success to complete my Ph.D research work. I am very much thankful to my brother for his continuous inspiring words and mental support. He always boost up and encourage me to continue and complete my research work.

I am thankful to my husband for his support and inspiration. He always support me in each and every steps of my whole journey. Without him I could not be able to continue my research work. His support and inspiration make me complete my research work successfully.

I am expressing my sincere gratitude to my mother-in-law and father-in-law for their tremendous support and love which

make me succeed to complete this research work and thesis. I am blessed and grateful to my two little sweet heart my daughter and little son for their love and affection. Their love is my strength and make me succeed to overcome the ups and downs of my whole journey.

I am grateful to Manas Da for his continuous support and encouragement as a dada in the whole period of my research work. I am thankful to Nabanita for her support and suggestions in my research work.

I am thankful to HoD, CSE, Dr. Subhrapratim Nath of my present institution Meghnad Saha Institute of Technology for giving me the opportunity to successfully complete my thesis at the time of submission.

I am thankful to Sayan, Sudip Da, Aniruddha, Arannya, Arkadeep, Sulagna for their support to do my research work.

I am thankful to my friends Ritu, Mousumi for their support.

I am thankful to all other persons who indirectly support in my research work.

I express my sincere thanks to EKO X-ray and Imaging Institute and AMRI Hospital Dhakuria, Kolkata, India, for providing clinical brain MR image data.

Last but not the least I sincerely express my thanks to all of my critics, without their opinions the research work may not complete.

Abstract

The thesis on "Studies on Brain MR Image Segmentation and Visualization" consists of three different improved, modified fuzzy c-means based frameworks for brain magnetic resonance (MR) image segmentation. These frameworks segment the dominating regions of human brain namely, cerebro spinal fluid (CSF), gray matter (GM) and white matter (WM). The necessity of this task is very crucial in medical image analysis field as it is the fundamental requirement to diagnosis of any deformities in human brain by using MR images. In MR imaging, the scanned images are drastically affected by noise and intensity inhomogeneity (IIH), because of the uneven distribution of radio frequency, generation of Eddy current and unconscious movement of patient. Further, noise and IIH make the MR images blur, mostly at the boundaries of different tissue regions and increase the difficulties to get correct segmentation results.

The fuzzy c-means (FCM) clustering algorithm is most studied algorithm to segment the images, but has limitation for high noisy images. The conventional FCM algorithm does not consider the spatial information of the images and therefore its performance decreases for the images that are highly affected by noise.

The developed three improved enhanced FCM-based frameworks address this issue and successfully segment high noisy volumetric brain MR images. The first method is based on the

complemented fuzzy membership functions. It utilizes a class-level uncertainty parameter for each voxel and incorporates complemented global and spatially constraint local fuzzy membership functions in the fuzzy objective function. It also incorporates total uncertainties in the 3D image domain by means of Shannon entropy. The complemented local fuzzy membership function estimates the degree of non-association for a voxel at the particular region, constraint by the local region-level intensity distribution. This framework allows the algorithm to utilize the spatial intensity distribution both in locally and globally within the image domain and produce more accurate cluster prototypes.

The second method is based on interval type-2 based FCM framework. In this work, a multi-objective framework is developed for segmentation of 3D brain MR image volumes using relative entropy-based type-1 and interval type-2 fuzzy c-means (FCM) algorithms. The first objective function uses a relative entropy-based type-1 FCM algorithm utilizing spatial information and locally biased class-level possibility parameter to yield local as well as global membership functions (MFs). In doing so, it utilizes the intensity dispersion within a cubic neighborhood of the center voxel under consideration. The total uncertainty is measured by using relative entropy and it is defined by local and global MFs. Whereas, the second objective function uses this global MFs and introduces an interval type-2 fuzzy MFs, weighted by the above possibility parameters. Specifically, it utilizes the local MFs as the secondary MFs in the interval type-2 fuzzy sets for better realization of correlation between the neighboring voxels. The framework calculates the final cluster centers as the arithmetic mean of those yielded by the two objective functions. Finally, it generates the final MFs by combining the

global and interval type-2 based fuzzy MFs using two weighting parameters to resolve the trade-off between them.

The third method is based on fuzzy entropy-based FCM framework. The fuzzy entropy has been utilized by incorporating the local membership functions to mitigate the underlying uncertainty for voxel classification. In the objective function, the global membership functions and the local membership functions, weighted by class-specific possibility parameters are incorporated. It also incorporates the fuzzy entropy to define total uncertainty.

The performances of the contributed algorithms have been investigated both in qualitatively as well as quantitatively using several volumes of brain MR images. The outcomes of the experiments indicate the supremacy of the developed frameworks over recently developed standard state-of-the-art algorithms.

Contents

List of Figures

List of Tables

Chapter 1

Introduction

The thesis consists of overview of image segmentation, followed by different algorithmic approaches, which are developed based on the fuzzy c-means (FCM) algorithm for segmentation of brain magnetic resonance (MR) image volumes and their visualization.

In medical image analysis, image segmentation is the primary requirement to examine different types of soft tissues of human body. The thorough investigation of the correctly segmented regions makes the whole treatment procedure easy and safe for the patients. It also helps doctors to choose correct diagnosis procedures by providing detailed insight visualization of each segmented regions. In particular, the segmentation of brain MR images is a prime concern in medical image analysis domain for diagnosis and treatment of various kinds of diseases and deformities of human brain.

However, the brain MR images are contaminated by noise and intensity inhomogeneity (IIH) mainly due to nonuniform radio frequency distribution of the scanner and movements of the patient at the time of scanning. As a result, MR images appear to be low in resolution and blurry. The conventional FCM algorithm is unable to segment these images properly, as it does not consider the spatial information as well as the correlation between the neighbouring pixels/voxels.

Three different enhanced frameworks based on the FCM algorithm have been developed for high noisy and IIH contaminated 3D brain MR image segmentation. These contributions are tested and validated by using several 3D image volumes of brain MR images, which contain simulated as well as real patient image volumes. Experiments also carried out using a synthetic image volume by adding Rician noise. The results are found to be superior to some of the state-of-the-art methods.

1.1 Introduction

The magnetic resonance images of human brain is abruptly affected by noise and intensity inhomogeneity (IIH) at the time of scanning. Different factors are responsible for this phenomena. The factors are non-uniform distribution of radio frequency throughout the entire object, generation of Eddy current as the faster variation of gradient of magnetic field happened and patient's unconscious movement during scanning. As a result, the distribution of a voxel intensity varies over the image domain and makes the images foggy or blurry, particularly at the different tissue boundary regions. This incident makes the brain magnetic resonance image segmentation procedure very challenging and complex. This gives a motivation to address these issues with the objectives to achieve better segmentation results. The motivation and objectives are discussed in the subsequent sections.

To handle these issues and segment the blurry, low resolution and high noisy and IIH affected 3D brain MR images accurately, three main contributions are made. In the first contribution, an entropy-based modified FCM algorithm has been developed by utilizing the complemented global membership functions and

the local membership functions by associating the uncertainty parameters and Shannon entropy. In the second contribution, a multi-objective based framework is developed using relative entropy-based fuzzy c-means algorithm by incorporating type-1 and interval type-2 fuzzy membership functions in association with possibility parameters. Finally, in the third contribution, a fuzzy entropy-based framework has been developed by incorporating fuzzy entropy, which is defined with the help of the local membership functions for better realization of the above issues. These contributions are also briefly discussed in the subsequent section. Further, to make the thesis self contained, different medical imaging modalities and different methods for medical image segmentation are briefly discussed along with scope of the thesis in the remaining sections.

1.2 Medical imaging modalities

With the advancement of medical imaging, detailed views of the internal organs' of human body can be generated without open surgery, by using different kind of advanced imaging techniques, called medical imaging modalities. The visual representations of internal regions are used for accurate diagnosis, monitoring the medical conditions of the patients and to plan for the correct treatment as well. By utilizing medical imaging modalities doctors can examine and visualize the internal tissue regions, including muscles, bones, blood vessels, organs and other internal structures for accurate treatment. Different medical imaging modalities [1] are discussed briefly at the following subsections.

1.2.1 X-ray

The imaging technique, X-ray [1][2] generates high-resolution images of the internal anatomical structure like, bones. In the X-ray technique, an electromagnetic radiation passes through the object of interest like, a human body. The digital detector or the X-ray film detect the rays. The high dense object like, bones absorb more x-rays and make the object whiter and the reverse effect happens for low dense or softer objects like, muscles. So, image quality is dependent on the amount of radiation from the x-ray beam as well as proper positioning of the body parts. X-ray imaging generates two-dimensional images for the three dimensional objects. So, it creates difficulties for visualization of three-dimensional images in details.

Within an evacuated glass tube, electromagnetic radiation, or X-rays, are generated. The different voltage between anode and cathode of the glass tube generates high-speed electrons which hit on the anode and emits x-rays and heat. As the X-rays can absorbed by hard tissues properly and not by the soft tissues, its not suitable for soft tissue's visual representation. It provides the 2D image of any 3D objects, so its difficult to get significant view of the internal structures of human body.

1.2.2 Computed Tomography (CT)

Computed Tomography (CT) imaging [1][3] uses X-ray to generate detail images of the internal structures of the body. It capture the images from different angles and measure the passing X-ray's intensity by using detectors. In this purpose, multi-slice detector is used. The multi-slice detector is able to capture multiple images from different directions at a single instance of time and develop cross-sectional images of the internal parts of the

human body. By utilizing spatial filtering for noise reduction, various levels of X-ray beam for capturing various information, CT imaging make a significant improvement of image qualities. The CT imaging process has side effect of ionizing radiation. To avoid this side effect it utilizes dose modulation and adjust the radiation based on the shape, size and other composition of organs. Though CT imaging generates high resolution images and has a dose control mechanism, yet it has major risk of causing cancer for ionizing radiation.

1.2.3 Ultrasound Imaging (US)

The ultrasound (US) imaging technique [2] uses sound waves of high-frequency to generate the detail structural images of internal organs. It uses transducer, which emits high frequency sound waves and detects the bouncing wave from the different tissue boundary of the body. The captured bouncing waves are converted into electrical signals and processed to generate the detailed structural images. The ultrasound images provide depth information which is used to create the detail volumetric view of the images.

1.2.4 Magnetic Resonance Imaging (MRI)

The magnetic resonance imaging technique [1] is a powerful imaging technique having the capacity of capturing the detail images of spinal cord, brain, etc. It is used to diagnose the critical diseases like, disorders in spinal cord, brain tumor, cardiovascular diseases, joint and bone problems, etc. It uses powerful magnetic field and radio waves to capture detail information of organs.

The powerful magnatic field align the hydrogen atom's nuclei of water molecules on the body and create a magnetic moment on the body. The organization of the nucli atoms are changed by radio frequency (RF) pulses and make the emission of the radio signals weaker. The detector capture the radio signal, processed and generate the detail images of the internal organs of the body. The energy level of hydrogen nuclei increased under the magnetic field and drop when it is in the normal microscopic stage. This is called relaxation. The level of hydrogen atoms or the relaxation rate are different for various tissue types and generate different radio signals. The magnetic resonance imaging modalities generates images in different plane that is axial, sagittal and coronal and provides 3D view of the internal structure of the body. In MRI, non-ionizing radiations happens at the time of scanning, so it is safe over CT scanning [3] [2].

Hence, among all the medical imaging methodologies, which are discussed so far, MRI modality is more efficient and safest modality technique to investigate any deformities and anomalies in the soft tissues of human body.

For more accurate investigation, these soft tissue regions need to be segmented to analyze the particular regions and get more insight view of the internal soft tissue regions. In the next section, different image segmentation methodologies has been discussed.

1.3 Overview of the image segmentation methodologies

Image segmentation [4][5] is a very important and crucial task to analyze any image thoroughly and extract the detail information from the image. These detail information are required to

generate any productive framework for the advancement of the different research fields like, medical imaging, machine vision, content-based image retrieval, object detection and recognition, video surveillance, etc. Image segmentation is the technique for partitioning an image into several parts having similar properties like, intensity, color and texture, etc. By virtue of segmentation, the analysis procedure becomes more easy and smooth.

The two fundamental image segmentation approaches are i) discontinuity detection and ii) similarity detection. At the first approach the segmented regions are partitioned according to the discontinuity. Edge detection is the example of the discontinuity based segmentation technique. The second segmentation approach is based on the similarity among the image elements. The intensity or threshold based segmentation, region based segmentation, clustering based segmentation techniques follow the similarity based segmentation approach. In the next sections these methods are described briefly.

1.3.1 Edge based segmentation

This segmentation technique [6] [4] [7] utilizes sudden changes in intensities of the images. Edge is generated by connecting the pixels on the boundary of regions. The regions are segmented by generating the edge boundary of the region. The edges are formed when the intensity value of the neighbouring pixels/voxels significantly changes in a certain direction, as a results discontinuity among the elements happens. To detect the edges, the first order derivative of the images are conducted. Zero crossing is detected by zero crossing method by utilizing second order derivative. The edge strength is measured by this second order derivative.

The first order derivative is conducted by using Prewitt operator, Sobel operator, Canny operator. These operators have different functionality. Prewwit operator estimates gradient of image intensity, sobel operator utilizes small valued filter to involution the images in vertical and horizontal direction. It is computationally expensive. The canny edge detector utilizes multistage algorithms for different range of edges.

The Second order derivative utilizes Laplacian operator and zero crossing. The zero crossing point has to be detected for edge detection. It detects by utilizing second order derivative.

1.3.2 Intensity or threshold based segmentation

In this approach, segmentation procedure [4] [5] is carried out by considering the intensity or threshold value. It segments the images into two different classes. If the particular pixel value belongs within the threshold range then it belongs to one class and other elements which are not within the threshold range belongs to another class. The thresholding procedure [8] is two types i) global thresholding and ii) local thresholding. In global thresholding approach, the whole image is segmented into two different classes: background and object. The values, which are greater than or equal to the threshold value, considered as the object and denoted by '1' and others are considered as background and denoted by '0'. It is defined in the following function (1.1).

$$O(x,y) = \begin{cases} 1 & , \ if \ I(x,y) \geq T \\ 0 & , \ if \ I(x,y) < T \end{cases} \tag{1.1}$$

where, $O(x,y)$ is the segmented image, $I(x,y)$ is the input image and T is the threshold value. The local thresholding method

is based on the characteristics of the subdivided sector locally and the threshold value is selected according to that. Though thresholding technique is fast but it does not consider the spatial information of the image and highly sensitive in the presence of noise. Moreover, threshold selection is a crucial task, which may be erroneous, that yields faulty segmentation results.

1.3.3 Region based segmentation

Region based segmentation procedure [4] [9] [5] is based on the homogeneous characteristics of the neighbouring pixels/voxels in the image domain. The region is formed by considering the pixels or voxels having similar characteristics by comparing with its neghbouring pixels/voxels. The region based segmentation process consists of two different methods i) region growing and ii) region split and merge.

i) Region growing methods: The region growing method [10] [5] [7] segments the image based on the homogeneous property between the pixels/voxels. Region growing procedure can be seeded or unseeded.

In seeded region growing method [11], a seed is specified and the seed pixel/voxel satisfies all the characteristics of the region of interest. So, very cautious attention is required for seed selection as the whole segmentation procedure is based on the seed pixel/voxel. The pixels/voxels are compared with the seed values and added to that region whose seed value matches most.

On the other way, unseeded region growing procedure is an automatic process of segmentation in which the process starts with a single region say, R_1 with single pixel/voxel and provide multiple regions like, $(R_1, R_2, R_3, ..., R_n)$ as a outcome. The test pixel/voxel is compared with the mean value of the predefined

region and if the difference is less than the predefined threshold, it belongs to the region, otherwise creates a new region.

ii) Region split and merge method: In this region split and merge method [12][5], the image is considered as a single region. Then, it divides into four quadrants according to predefined criteria and tests the homogeneity between them. If fails, it divides each quadrant again into four quadrants. This repetitive process continues until the homogeneity criteria is satisfied. The regions will be merged if they have similar homogeneous characteristics.

The region based segmentation procedure provides better segmentation results than the other segmentation procedure discussed so far, as the region grows from inner to outer direction to generate clear region boundary. It generates better segmentation results if seed selection is correct. However, its success is highly depends on manual selection of the seed point and thereby prone to error. It is also tedious to formulate the terminating condition of the region growing process. Moreover, its success is limited if the input image is noisy.

The aforesaid segmentation procedures have several limitations, specifically, they cannot segment images affected with high noise.

1.3.4 Clustering based segmentation

The clustering based segmentation technique [13] is mostly used in noisy image segmentation. In this method, the segmentation occur by grouping the pixels/voxels of similar characteristics. Among the various kind of clustering-based segmentation approaches, k-means and fuzzy c-means clustering techniques are mostly used.

The k-means algorithm

In the k-means algorithm [14][15][16] [17], first it selects the k number of clusters and initializes them with different values. A pixel or voxel becomes a member of a particular cluster or region, whose centre is closest to that particular pixel or voxel. A pixel or voxel can belong to a cluster entirely.

Objective function of the k-means algorithm is defined as follows:

$$J = \sum_{k=1}^{K} \sum_{t=1}^{T} \left(d_{k_t}^2 \right) \tag{1.2}$$

where, T indicates the dimension of input image, K represents the number of clusters and $d_{k_t}^2$ is the square of the Euclidean distance between the t^{th} pixel or voxel x_t and k^{th} cluster centre v_k. The distance is calculated as follows:

$$d_{k_t}^2 = ||x_t - v_k||^2 \tag{1.3}$$

The fuzzy c-means algorithm

The fuzzy c-means (FCM) algorithm [18] is widely used segmentation technique for image segmentation. It considers that a pixel/voxel may belong to multiple clusters or regions with possibly different membership values. By minimizing the quadratic cost function and by imposing certain predefined criteria on the parameters, the FCM algorithm segments the whole image domain into predefined number of clusters according to the centroid of each region. For each pixel/voxel the algorithm generates C number of membership values. The membership value

decreases as the distance is increases away from the cluster centroid. A pixel/voxel is assigned to a cluster for which it has maximum membership value. The objective function of the FCM algorithm is as follows:

$$J = \sum_{c=1}^{C} \sum_{i=1}^{I} \left(\mu_{c_i}^{m} d_{c_i}^{2} \right) \tag{1.4}$$

where, I indicates dimension of the input image or total number of pixels/voxels, C represents the number of clusters. μ_{c_i} indicates the fuzzy membership value of the i^{th} pixel or voxel x_i for the c^{th} cluster centre v_c, $d_{c_i}^2$ is the square of the Euclidean distance between the i^{th} pixel or voxel x_i and c^{th} cluster centre v_c and m denotes the fuzzyfier having value > 1. The distance is calculated as follows:

$$d_{c_i}^2 = ||x_i - v_c||^2 \tag{1.5}$$

However, (1.4) emphasizes the following constraints:

$$\sum_{c=1}^{C} \mu_{c_i} = 1, \forall c \tag{1.6}$$

By minimizing the equation (1.4) with Lagrange multipliers the algorithm finds the iterative equations for the membership functions and the cluster centres. The equations for the membership functions and the cluster centres are stated as follows.

$$\mu_{c_i} = \frac{1}{\sum_{n=1}^{C} \left(\frac{d_{c_i}^2}{d_{n_i}^2} \right)^{\frac{-1}{m-1}}} \forall c, i \tag{1.7}$$

$$v_c = \frac{\sum_{i=1}^{I}\left(\mu_{c_i}^{m}\, x_i\right)}{\sum_{i=1}^{I}\left(\mu_{c_i}^{m}\right)} \forall c \tag{1.8}$$

The algorithm is summarized below:

Algorithm 1: FCM

Input: Brain MR image I
Output: Segmented region of the CSF, GM and WM

Initialize the m, iteration number $b = 0$ and threshold ϵ;
Initialize the cluster centre $v_c^{(b)}, \forall c$;
repeat
    Evaluate the fuzzy MFs $\mu_{c_i}^{(b)}, \forall c, i$ by using (1.7);
    Evaluate the new cluster centres ${v_c}^{b+1}, \ \forall c$ by using (1.8);
    $b = b + 1$;
until $||v_c^{(b)} - v_c^{(b-1)}|| < \varepsilon, \forall c$

In the next section, the importance of segmentation is discussed in the context of medical image analysis.

1.4 Segmentation in the context of medical image analysis

In recent days, different segmentation techniques [19] [20] are utilized vastly in medical image analysis field. More specifically, fuzzy c-means algorithm has been used mostly for segmentation. Today, in the field of medical science, although there is a substantial development in all the related sectors, there is still a need for improvement as it deals with the human body. For accurate diagnosis, various kind of detailed investigation has been performed by examining different kind of pathological reports like, MRI, X-ray, blood test, etc., which are suitable for the particular disease identification. From these different kind

of pathological reports, the MRI reports are mostly used to investigate severe fatal diseases of internal organs. Among these organs, human brain is the most crucial part of human body and any kind of abnormalities or deformities of brain will be identified by thorough scanning of brain using MRI scanner. These scanned brain MR images become ambiguous and low resolution due to limitation of scanner, movements of human body, etc. The results may also vary from scanner to scanner. To examine the brain MR images correctly, segmentation is a most required and obvious step. Though segmentation by expert radiologist is convincing but it is time consuming and can vary person to person according to person's individual expertise. That's why some automation is required in this purpose. Fuzzy c-means algorithm is mostly used and studied algorithm for the brain MR image segmentation. The FCM algorithm does not consider the spatial dependencies between the pixels/voxels, so fails to segment very high noisy images. To overcome the limitation of traditional FCM algorithm, researchers develop different improved and modified FCM algorithms.

Among the different FCM-based improved and modified algorithms, some recently developed algorithms are discussed in this section.

Halder et al. [21] developed FCM-based algorithm by combining rough set, fuzzy set for segmentation of brain MR images. The algorithm also considers the spatial correlation of the pixels. Aqad et al. [22] incorporated FCM-based improved algorithm by utilizing ant-colony optimization technique to determine the initial centre of the most dominating regions namely, GM, WM and CSF for clustering. They have used Mahalanobis distance for segmentation. Zaniani et al. [23] suggested a modified FCM method for brain MR image segmentation by utilizing

the neighbouring spatial information and kernel distance matrix of pixels. Shankar et al. [24] developed an improved FCM algorithm based on bat optimization algorithm. The algorithm uses echolocation of bats for clustering. Alrosan et al. [25] suggested mean ABC algorithm which is based on an artificial bee colony optimization technique for brain MR image segmentation. Kamarujjaman et al. [26] developed a modified FCM framework by utilizing 3D dynamic mask for spatial correlation measurement among the neighbouring voxels. Alomoush et al. [27] incorporates a firefly mate algorithm, for image segmentation. To segment the image regions, the algorithm utilizes fire fly algorithm with mate list.

1.5 Motivation of the thesis work

Now a days, the deformities or anomalies of human brain have increased rapidly. To provide right treatment, accurate diagnosis is required. To analyze the deformities, MRI scanning is the first step. These MR images need to be examined region wise for detail visualization. To find out the regions correctly and thoroughly, segmentation is an obvious step. Moreover, since the 2D image does not provide any information regarding the internal structure and shape of the object, we need to investigate the 3D image volume as a whole for identifying the different tissue regions within the brain. Due to the nature of the brain MR image volume, fuzzy clustering algorithm may play important role to yield correct segmentation results. This provides a motivation to investigate the fuzzy clustering algorithm and develop different variants for the purpose of 3D brain MR image segmentation and visualization, especially in the presence of high noise and intensity inhomogeneity.

1.6 Objectives of the thesis work

The main objective of the thesis is to segment the 3D brain MR images into different soft tissue regions, especially in the presence of high noise and intensity inhomogeneity. As a 2D brain MR image does not provide any information of the internal tissue structures and shapes, we investigate the 3D brain MR image volumes as a whole to identify the different tissue regions. Usually, the brain MR image volumes are affected by noise and intensity inhomogeneity (IIH) at the time of MR scanning. Therefore, uncertainty arises during the segmentation process and it maximizes at the tissue boundary regions within the image domain. To address these issues, the thesis embodies the following objectives.

To study the effectiveness of the complemented fuzzy membership functions along with uncertainty parameters to address the inherent image uncertainty and segment noisy 3D brain MR images.

To study the effectiveness of the type-1 and interval type-2 fuzzy membership functions by means of a multi-objective framework for 3D brain MR image segmentation.

To study the fuzzy entropy-based FCM algorithm for better realization of the uncertainty and segmentation of noisy 3D brain MR images.

1.7 Organization of the thesis

- **Chapter 1: Introduction**

Chapter 1 describes the necessity of brain MR image segmentation along with its difficulties, especially in the presence of high noise and IIH. It also briefly describes the different segmentation procedures. The motivation and objectives of the thesis work are described in this chapter. Finally, it summarizes the contributions of the thesis work in the form of different Chapters.

- **Chapter 2: Entropy-based FCM algorithm for brain MR image segmentation**

  This chapter demonstrates an uncertainty parameter weighted entropy-based fuzzy c-means clustering algorithm for noisy volumetric (3D) brain MR image segmentation using complemented global and spatially constraint local membership functions. Due to inherent noise and intensity inhomogeneity (IIH), the acquired MR images have blurry tissue boundaries. This leads to a situation where uncertainty arises while lebeling a pixel/voxel into its proper tissue region. Further, it magnifies in the regions of different tissue boundaries. The proposed algorithm addresses this issue by introducing a class-level uncertainty parameter for each voxel and weightedly incorporating in the fuzzy objective function using complemented global and spatially constraint local fuzzy membership functions. It also incorporates total uncertainties in the 3D image domain by means of Shannon entropy. The complemented local fuzzy membership function estimates the degree of non-association, constraint by the local region-level intensity distribution. This framework allows the algorithm to utilize the spatial intensity distribution both in locally and globally within the

image domain and produce more accurate cluster prototypes. The experimental results demonstrate its superiority over some of the state-of-the-art methods.

- **Chapter 3: Multi-objective framework for brain MR image segmentation**

  This chapter consists of a multi-objective framework for segmentation of 3D brain MR image using relative entropy-based type-1 and interval type-2 fuzzy c-means (FCM) algorithms. The first objective function uses a relative entropy-based type-1 FCM algorithm utilizing spatial information and locally biased class-level possibility parameter to yield local as well as global membership functions (MFs). In doing so it utilizes the intensity dispersion within a cubic neighborhood of the center voxel under consideration. Whereas, the second objective function uses this global MF and introduces an interval type-2 fuzzy MF, weighted by the above possibility parameter. Specifically, it utilizes the local MFs as the secondary MFs in the interval type-2 fuzzy sets for better realization of correlation between the neighboring voxels. The framework calculates the final cluster centers as the arithmetic mean of those yielded by the two objective functions. Finally, it generates the MF by combining the global and interval type-2 based fuzzy MFs using two weighting parameters to resolve the trade-off between them. The segmentation results prove its efficiency over other state-of-the-art methods.

- **Chapter 4: Fuzzy Entropy-based FCM algorithm for brain MR image segmentation**

  This chapter presents a fuzzy clustering algorithm by incorporating fuzzy entropy for segmentation of 3D brain

magnetic resonance (MR) images. Intensity inhomogeneity (IIH) and noise strongly affect brain MR images because of improper scanning environment or patient's unconscious movements at the time of image acquisition. The occurrence of this phenomenon makes the soft tissue regions blurry, specifically at the boundary region and imposes uncertainty for clustering the soft tissue regions. The presented algorithm utilizes fuzzy entropy, which associates with the local membership functions to mitigate the underlying uncertainty for voxel classification. It integrates fuzzy entropy with the membership functions of local neighbouring regions of the voxel. The objective function conjugates global membership functions with the distance of the cluster center and the voxel along with a controlling factor as a first term. The multiplicative factor of the local membership function, the mean distance of neighboring voxels from the cluster center, possibility parameter and a complemented controlling factor is added as the second term. Finally, the third term is the fuzzy entropy defined with the local membership function. It provides superior results as compared with some of the state-of-the-art methods.

- **Chapter 5: Concluding remarks and future directions of work**

  This chapter summarizes the contributions of the thesis work and highlights the future directions of research work.

Chapter 2

Entropy-based FCM algorithm for brain MR image segmentation

2.1 Source of the Chapter

Chapter 2 is based on the research work [28].

2.2 Introduction

Brain magnetic resonance (MR) image analysis is one of the major and important tasks for diagnosis of any kind of abnormalities of human brain. It helps doctors to analyze different kind of diseases of human brain by observing the classified soft tissue regions and to diagnose and doing treatment correctly. The brain MR image become blurry when noise and intensity inhomogeneity affect the image. The reason behind this blurry image is due to non-uniformly passing of signals of radio frequency (RF) coil, gradient driven eddy currents and movement of patient during the image scanning. The segmentation procedure becomes challenging as noise and intensity inhomogeneity make the soft tissue regions fuzzy and imposes uncertainty at clustering and recognizing each voxel separately. Fuzzy c-means algorithm (FCM) [18] is mostly studied in this regard. As

the FCM algorithm has limitation when high noise and intensity inhomogeneity (IIH) associate with the image, many variants are proposed in the past by incorporating local information, entropy and other contextual information. To reduce the shortcomings of conventional FCM algorithm, Ji et al. [29] proposed an adaptive scale fuzzy local Gaussian mixture model (AS-FLGMM) algorithm for brain MR image segmentation. For small neighborhood, the algorithm ignores the difference between variance of the sub regions. Based on local scale calculation method, the algorithm evaluates the variance of the local Gaussian mixture model. Sing et al. [30] proposed a modified FCM (mFCM) algorithm by utilizing the scale control spatial information for high noisy brain MR image segmentation. The algorithm introduces a probability function for local membership function. The final membership function and the cluster centers were calculated by utilizing the global and local membership functions. Furthermore, Adhikari et al. [31] proposed a conditional spatial fuzzy c-means (csFCM) algorithm for segmentation of brain MR images. It introduces an auxiliary variable, which defines the belongingness of the pixel in the cluster for each pixel. In addition to the global fuzzy membership function, it also introduces a conditional spatial fuzzy membership function, which are then used to calculate a weighted membership function. Verma et al. [32] proposed an improved intuitionistic FCM (IIFCM) for brain image segmentation. The algorithm utilizes the property of intuitionistic fuzzy set theory in association with local gray level and local spatial information. Kahali et al. [33] proposed a fuzzy clustering (2sFMoF) algorithm that uses multi-objective functions in two stages. The algorithm incorporates 3D spatial fuzzy c-means (3DSpFCM) algorithm at stage one by considering spatial neighborhood information of

the 3D brain MR image volume for local membership function, which is associated with global membership function for each voxel. At the second stage, the cluster prototypes, which are generated at the earlier stage, are set as an input of 3D modified fuzzy c-means (3DMFCM) algorithm, which also utilizes local voxel information and generates the final result. Namburu et al. [34] modified the conventional FCM algorithm by soft fuzzy rough c-means hybrid segmentation algorithm for brain MR image segmentation. The algorithm considers bias field correction and extracts the rough regions of the image. In particular, it utilizes fuzzy rough approximation by excluding the negative regions. The soft set utilizes the similarity coefficients of the pixels for clustering the image. Further, Singh et al. [35] proposed a bias corrected FCM (LZM-UNLM-BCFCM) algorithm by utilizing local Zernike moment (LZM) and unbiased non local means to segment brain MR images. It utilizes the LZMs to filter the regions having similar values and uses pixel-wise bias field to reduce IIH. Ren et al. [36] incorporated the kernel-based FCM (KFCM) and weighted fuzzy kernel clustering (WK-FCM) algorithms to propose a new algorithm for brain image segmentation. Singh et al. [37] proposed local Zernike moments (LZM)–based unbiased nonlocal means FCM algorithm. The algorithm calculates the Zernike moments for all neighboring values for each pixel. It follows two steps. In the first step, it reduces the noise from the input data by considering local data values of LZMs and generates another image, which is considered as global data value. Whereas, in the second step, the noisy original image and the noise free image are used for proper segmentation by considering both the local and global data values. Pham et al. [38] proposed two stage algorithm for brain MR image segmentation. At the first stage, the algorithm incorporates

kernelized fuzzy clustering based on entropy by considering local spatial information and bias correction. At the second stage, it considers an adaptive energy weight global and local fitting energy active contour (AWGLAC) model, which is the combination of region-based active contour model and adaptive model with energy elements. Mahata et al. [39] proposed a fuzzy clustering algorithm using local contextual information and Gaussian function to segment brain MR image and IIH correction. It estimates the bias field by fitting a Gaussian function over the local image gradients.

Recently, in line with these variants, Alruwaili et al. [40] proposed a weighted spatial fuzzy c-means (wsFCM) clustering algorithm for brain MR image segmentation. It utilizes the value of neighboring pixels of each pixel and imposes more weights on them to make the objective function strong enough to handle the noise and IIH. Basnet et al. [41] proposed a deep dense residual neural network architecture for volumetric brain MR image segmentation. To enhance the gradient flow with few number of parameters, the network model considers the contracting and expanding path and establishes residual skip connection between them. Further, Singh et al. [42] proposed a multi-objective antlion optimization algorithm to improve the traditional FCM. It utilizes LMMSE filtered local spatial information for the classification purpose. Xu et al. [43] proposed an adaptive interval fuzzy c-means algorithm to classify satellite images of land cover by considering spatial information. The algorithm integrates adaptive interval-valued modelling and spatial information to reduce the uncertainty of land cover classification. Hua et al. [44] proposed an improved multi view fuzzy c-means (IMV-FCM) algorithm to segment brain MRI images. It uses multiple views and for each view, the algorithm

produces optimal weight for the correct cluster. Xu et al. [45] proposed a reliability-based spatial context fuzzy c-means (RS-FCM) algorithm for image segmentation. The algorithm utilizes the correlation between neighboring pixels. It establishes the reliability for the spatial relationship among the pixels of noisy input data and reduces the blur effect at the edge of the region. Feng et al. [46] proposed an interval-valued fuzzy c-means algorithm to classify ambiguity of objects. The algorithm uses mean-square-error to adjust the interval width and also considers the boundary factor for optimal feature calculation. Very recently, Devi et al. [47] proposed a clustering algorithm based on hybrid deep learning for brain tumor classification and segmentation. The algorithm utilizes stationary wavelet packet transformation technique for feature extraction and hybrid adaptive black widow optimization in association with Moth flame optimization (HABWMFO) for optimal feature selection. Classification and segmentation are performed in two steps; (i) an adaptive kernel fuzzy c-means clustering (AKFCM) algorithm and (ii) a hybrid convolution neural network long short-term memory (CNN-LSTM) model. Wei et al. [48] proposed a fuzzy subspace clustering with adaptive local variance, non-local information and mean-membership linking (FSC-LNML) algorithm for noisy image segmentation. The algorithm utilizes the local variance and non-local information in the objective function. It also incorporates the mean membership value as well as the inverse of local variance. It imposes weights to each intensity value of the input image adaptively and establishes the concept of subspace.

Apart from the above variants of the FCM algorithm, researchers also proposed some entropy-based FCM algorithms. Li et al.

[49] proposed the first integration of entropy into a fuzzy clustering algorithm by incorporating maximum-entropy inference (MEI) algorithm. A small artificial data set is used to evaluate the algorithm. Yasuda et al. [50] proposed modified entropy-based fuzzy-c means method (MEFCM) which incorporates two entropies by means of membership functions and also using their complements. It encounters with two problems; (i) deterministic annealing (DA), which takes long time to execute and (ii) use of the Fermi-Dirac-like membership function, which is difficult to interpolate the required parameters. The algorithm does not consider local information of the image and so is prone to noise. Zarinbal et al. [51] proposed the relative entropy fuzzy clustering method (REFCM) by integrating relative entropy with the fuzzy membership values. The relative entropy functions act as a regularizing function, which is a convex and non-negative function. Gharieb et al. [52] proposed a different formulation of entropy-based FCM algorithm (MRE-FCM) by means of two membership relative entropy functions. This mechanism makes the possibility for more fuzziness. The resulting iterative equation for the cluster centers shows that this formulation still does not consider local data while computing their membership and cluster center functions. So, this algorithm is also prone to noise. Kahali et al. [53] proposed a fuzzy c-means clustering algorithm using entropy and Gaussian function to segment brain MR images. It utilizes the local correlations between the pixels to reduce the effects of noise. Furthermore, Kumar et al. [54] proposed kernel intuitionistic fuzzy entropy c-means (KIFECM) algorithm for MRI image segmentation. The algorithm addresses the uncertainty of input data by using intuitionistic fuzzy set and the nonlinear structure of data by measuring kernel distance. The algorithm uses

Sugeno and Yager's negation function as an intuitionistic fuzzy set generators. Mahata et al. [55] proposed another entropy-based fuzzy clustering algorithm by utilizing global and local entropy for noisy 3D brain MR image segmentation. Recently, Wu et al. [56] proposed an entropy-based symmetric regularized picture FCM algorithm for image segmentation. It utilizes the neighboring pixels' information for fuzzy clustering. Salehi et al. [57] proposed a multiple kernel FCM algorithm by using entropy and relative entropy. The entropy and relative entropy control the fuzziness of the segmented regions. Ouchicha et al. [58] proposed a fuzzy c-means algorithm based on exponential entropy with modified kernel for brain MR image segmentation. The algorithm utilizes the exponential entropy and addresses the penalty for misclassification as a logarithmic term.

In this work, we presented a fuzzy c-means clustering algorithm, which uses class-level uncertainty parameter and utilizes it to estimate total information uncertainty by means of entropy using Shannon function. Unlike FCM algorithm, it uses complemented global and spatially constraint local fuzzy membership functions to define degrees of non-association to a class or cluster. The complemented fuzzy membership functions, uncertainty parameter and the entropy are judiciously incorporated into the fuzzy objective function. Finally, we integrate the global and local membership functions by two weighting parameters to generate the final membership function, based on which a voxel is classified and image volume is segmented. The main motivation of this work is how to incorporate the class-level uncertainty parameter into the a fuzzy clustering algorithm so that the fuzzy membership function and the cluster prototypes are influenced by this parameter. We summarize the main contributions below.

1) Unlike conventional fuzzy membership functions, we use complemented global and local fuzzy membership functions. The later one is constraint by the intensity distribution around the center voxel under consideration. In particular, it utilizes the association of the intensity distribution in the close proximity of the voxel and influences more to estimate the final membership function.

2) As the brain MR images are blurry, especially in the regions of different tissue boundaries, there is always an uncertainty to find actual class of a voxel lying in these regions. We address this issue by defining class-level uncertainty parameter for each voxel and using it weightedly with the two complemented fuzzy membership functions.

3) We estimate the total information uncertainty in a form of entropy by using the weighted class-level uncertainty parameter.

4) We generate the final fuzzy membership function to classify a voxel by integrating the complemented global and local fuzzy membership functions, weighted by two controlling parameters.

The qualitative and quantitative analysis of the algorithm, with six different volumes of T1-weighted simulated brain MR images with different percentage of noise and intensity inhomogeneity as well as four volumes of clinical real patient 3D brain MR images and a synthetic 3D image volume with high Rician noise, has shown its efficiency and superiority over some of the state-of-the-art algorithms developed in recent past.

The work is organized as follows. In Section 2, we present the developed fuzzy clustering algorithm. In Section 3, we present the comprehensive studies based on the experimental results.

Section 4 presents the complexity analysis of the developed algorithm. Finally, Section 5 draws the concluding remarks.

2.3 Uncertainty parameter weighted entropy-based fuzzy c-means clustering algorithm using complemented global and spatially constraint local membership functions

Due to the limitations of MR scanners, brain MR images are usually contaminated by noise and intensity inhomogeneity (IIH), resulting blurry and low resolution images. Because of this, intensity distribution of a brain soft tissue becomes irregular across the whole image domain. In other words, it produces an image, where it appears visually as brighter in some regions and as darker in other regions for the same brain tissue. As a result, it makes the segmentation of soft tissue regions uncertain and challenging. Moreover, this class-level uncertainty increases towards the unshrap tissue boundaries of different regions. In addition, in brain MR image volume, the voxels of soft tissue regions are tightly bounded with its neighboring voxels. To address the above limitations, we propose an class-level uncertainty parameter weighted entropy-based fuzzy clustering algorithm using complemented global and spatially constraint local fuzzy membership functions. In particular, we introduce a class-level uncertainty parameter for each voxel, which in turn weightedly used in conjunction with the above two fuzzy membership functions. This framework makes the complemented fuzzy membership functions and cluster prototypes to be influenced by the class-level uncertainty parameter. Unlike conventional FCM algorithm, we introduce two complemented fuzzy

membership functions in line with the uncertainty to define the degrees of non-association to a class. The complemented local fuzzy membership function uses the intensity distribution around the close proximity of the center voxel to incorporate the tightly coupled nature of the neighnouring voxels. Furthermore, to measure the total information uncertainty in the form of entropy, we use this uncertainty parameter, weighted by the degree of fuzzyness, in the Shannon entropy. The framework also uses this entropy to define its objective function. Its objective function is defined as follows.

$$J = \sum_{i=1}^{C}\sum_{d=1}^{D}\sum_{h=1}^{H}\sum_{w=1}^{W}\Bigg(\Big(\big(1-\mu_{i_{dhw}}^{m}\big)||x_{dhw}-v_i||^2+\big(1-u_{i_{dhw}}^{m}\big)||\bar{x}_{dhw}-v_i||^2\Big)p_{i_{dhw}}^{m}-p_{i_{dhw}}^{m}\ln p_{i_{dhw}}^{m}\Bigg) \tag{2.1}$$

subject to the following constraints-

$$\sum_{i=1}^{C}\mu_{i_{dhw}}=1,\forall d,h,w \tag{2.2}$$

$$\sum_{i=1}^{C}u_{i_{dhw}}=1,\forall d,h,w \tag{2.3}$$

$$\sum_{i=1}^{C}p_{i_{dhw}}=1,\forall d,h,w \tag{2.4}$$

where C is the number of segments or cluster or class and D is the depth or total number of images in the image volume, H and W are the height and width of an image, respectively. $\mu_{i_{dhw}}$ and $u_{i_{dhw}}$ are the complemented global and spatially constraint local fuzzy membership functions, respectively for the voxel x_{dhw} with respect to the class i. v_i is the i^{th} cluster center. The variable $\bar{x}_{dhw}$ is the mean of the voxels lying within the immediate

cubic neighborhood of the center voxel x_{dhw}. v_i is the i^{th} cluster center, $p_{i_{dhw}}$ is the class-level uncertainty parameter for the voxel $x_{i_{dhw}}$ with respect to class i and $m > 1.0$ is the degree of fuzziness.

The first term of (2.1) is responsible for grouping the homogeneous voxels as close to their actual cluster center by considering intensity distribution both locally and globally with respect to the 3D image domain. Whereas, the second term is responsible for estimating total information uncertainty within the 3D image domain. To achieve the goal, we need to minimize the objective function with respect to different parameters satisfying all the constraints. The objective function in (2.1) by considering its constraints in (2.2) - (2.4) is solved by using the Lagrange multipliers. The augmented objective function with the Lagrange multipliers is defined as follows:

$$J = \sum_{i=1}^{C}\sum_{d=1}^{D}\sum_{h=1}^{H}\sum_{w=1}^{W}\Bigg(\Big((1-\mu_{i_{dhw}}^{m})||x_{dhw}-v_i||^2 + (1-u_{i_{dhw}}^{m})||\bar{x}_{dhw}-v_i||^2\Big) p_{i_{dhw}}^{m} - p_{i_{dhw}}^{m}\ln p_{i_{dhw}}^{m}\Bigg) - \sum_{d=1}^{D}\sum_{h=1}^{H}\sum_{w=1}^{W}\Bigg(\lambda_{dhw}\sum_{i=1}^{C}(\mu_{i_{dhw}}-1) + \gamma_{dhw}\sum_{i=1}^{C}(u_{i_{dhw}}-1) + \delta_{dhw}\sum_{i=1}^{C}(p_{i_{dhw}}-1)\Bigg) \tag{2.5}$$

The final iterative equations with respect to $\mu_{i_{dhw}}$, $u_{i_{dhw}}$, $p_{i_{dhw}}$ and v_i are achieved by performing partial derivatives of (2.5) with respect to the corresponding parameters and equating them to zero, as stated below.

$$\frac{\delta J}{\delta \mu_{i_{dhw}}} = 0; \tag{2.6}$$

$$\frac{\delta J}{\delta u_{i_{dhw}}} = 0; \tag{2.7}$$

$$\frac{\delta J}{\delta p_{i_{dhw}}} = 0; \tag{2.8}$$

$$\frac{\delta J}{\delta v_i} = 0; \tag{2.9}$$

By using (2.6), the calculations of $\mu_{i_{dhw}}$ is given below.

$$-m\, \mu_{i_{dhw}}^{m-1}\, ||x_{dhw} - v_i||^2\, p_{i_{dhw}}^m - \lambda_{dhw} = 0 \tag{2.10}$$

$$or, \mu_{i_{dhw}} = \left(- \frac{\lambda_{dhw}}{m\, p_{i_{dhw}}^m\, ||x_{dhw} - v_i||^2} \right)^{\frac{1}{m-1}} \tag{2.11}$$

Since, $\sum_{l=1}^{C} \mu_{l_{dhw}} = 1$, by replacing the value of $\mu_{l_{dhw}}$ in (2.11), we get the following equation.

$$-\lambda_{dhw}^{\frac{1}{m-1}} = \frac{1}{\sum_{l=1}^{C} \left(\frac{1}{m\, p_{l_{dhw}}^m\, ||x_{dhw} - v_l||^2} \right)^{\frac{1}{m-1}}} \tag{2.12}$$

Finally, from (2.11) and (2.12) we get the iterative equation of $\mu_{i_{dhw}}$ as follows:

$$\mu_{i_{dhw}} = \frac{1}{\sum_{l=1}^{C} \left(\frac{p_{i_{dhw}}^m\, ||x_{dhw} - v_i||^2}{p_{l_{dhw}}^m\, ||x_{dhw} - v_l||^2} \right)^{\frac{1}{m-1}}} \tag{2.13}$$

Similarly, by using (2.7), the calculations of $u_{i_{dhw}}$ is shown below.

$$-m\, u_{i_{dhw}}^{m-1}\, ||\bar{x}_{dhw} - v_i||^2\, p_{i_{dhw}}^m - \gamma_{dhw} = 0 \tag{2.14}$$

$$or, u_{i_{dhw}} = \left(- \frac{\gamma_{dhw}}{m\, p_{i_{dhw}}^{m}\, ||\bar{x}_{dhw} - v_i||^2} \right)^{\frac{1}{m-1}} \tag{2.15}$$

Since, $\sum_{l=1}^{C} u_{l_{dhw}} = 1$, by replacing the value of $u_{l_{dhw}}$ in (2.15), we get the following equation.

$$-\gamma_{dhw}^{\frac{1}{m-1}} = \frac{1}{\sum_{l=1}^{C} \left(\frac{1}{m\, p_{l_{dhw}}^{m}\, ||\bar{x}_{dhw} - v_l||^2} \right)^{\frac{1}{m-1}}} \tag{2.16}$$

Finally, from (2.15) and (2.16), we get the iterative equation of $u_{i_{dhw}}$ as follows:

$$u_{i_{dhw}} = \frac{1}{\sum_{l=1}^{C} \left(\frac{p_{i_{dhw}}^{m}\, ||\bar{x}_{dhw} - v_i||^2}{p_{l_{dhw}}^{m}\, ||\bar{x}_{dhw} - v_l||^2} \right)^{\frac{1}{m-1}}} \tag{2.17}$$

Likewise, by using (2.8) the calculations of $p_{i_{dhw}}$ is given below.

$$\begin{aligned} &\left((1 - \mu_{i_{dhw}}^{m})\, ||x_{dhw} - v_i||^2 + (1 - u_{i_{dhw}}^{m})\, ||\bar{x}_{dhw} - v_i||^2 \right) m\, p_{i_{dhw}}^{m-1} \\ &\quad - p_{i_{dhw}}^{m} \frac{1}{p_{i_{dhw}}^{m}}\, m\, p_{i_{dhw}}^{m-1} - m\, p_{i_{dhw}}^{m-1} \ln \left(p_{i_{dhw}}^{m} \right) - \delta_{dhw} = 0 \end{aligned} \tag{2.18}$$

$$\begin{aligned} or, m\, p_{i_{dhw}}^{m-1} \Big(&(1 - \mu_{i_{dhw}}^{m})\, ||x_{dhw} - v_i||^2 + (1 - u_{i_{dhw}}^{m})\, ||\bar{x}_{dhw} - v_i||^2 \\ &-1 - \ln \left(p_{i_{dhw}}^{m} \right) \Big) = \delta_{dhw} \end{aligned} \tag{2.19}$$

or,

$$p_{i_{dhw}} = \left(\frac{\delta_{dhw}}{m\left(\left(1-\mu_{i_{dhw}}^{m}\right)||x_{dhw}-v_i||^2 + \left(1-u_{i_{dhw}}^{m}\right)||\bar{x}_{dhw}-v_i||^2 - 1 - \ln\left(p_{i_{dhw}}^{m}\right)\right)} \right)^{\frac{1}{m-1}} \tag{2.20}$$

Since, $\sum_{l=1}^{C} p_{l_{dhw}} = 1$, by replacing the value of $p_{l_{dhw}}$ in (2.20), we get the following equation.

$$\delta_{dhw}^{\frac{1}{m-1}} = \frac{1}{\sum_{l=1}^{C}\left(\frac{1}{m\left(\left(1-\mu_{l_{dhw}}^{m}\right)||x_{dhw}-v_l||^2+\left(1-u_{l_{dhw}}^{m}\right)||\bar{x}_{dhw}-v_l||^2-1-\ln\left(p_{l_{dhw}}^{m}\right)\right)} \right)^{\frac{1}{m-1}}} \tag{2.21}$$

From (2.20) and (2.21), we get the iterative equation for $p_{i_{dhw}}$ as follows:

$$p_{i_{dhw}} = \frac{1}{\sum_{l=1}^{C}\left(\frac{\left(\left(1-\mu_{i_{dhw}}^{m}\right)||x_{dhw}-v_i||^2+\left(1-u_{i_{dhw}}^{m}\right)||\bar{x}_{dhw}-v_i||^2-1-\ln\left(p_{i_{dhw}}^{m}\right)\right)}{\left(\left(1-\mu_{l_{dhw}}^{m}\right)||x_{dhw}-v_l||^2+\left(1-u_{l_{dhw}}^{m}\right)||\bar{x}_{dhw}-v_l||^2-1-\ln\left(p_{l_{dhw}}^{m}\right)\right)} \right)^{\frac{1}{m-1}}} \tag{2.22}$$

Finally, by using (2.9) we derive the iterative equation of cluster center, as given below.

$$\sum_{d=1}^{D}\sum_{h=1}^{H}\sum_{w=1}^{W}\Bigg(\left(1-\mu_{i_{dhw}}^{m}\right)2\left(x_{dhw}-v_i\right)\left(-1\right)p_{i_{dhw}}^{m}+\left(1-u_{i_{dhw}}^{m}\right)\left(\bar{x}_{dhw}-v_i\right)\left(-1\right)p_{i_{dhw}}^{m}\Bigg)=0 \tag{2.23}$$

or,

$$v_i\sum_{d=1}^{D}\sum_{h=1}^{H}\sum_{w=1}^{W}\left(\left(1-\mu_{i_{dhw}}^{m}\right)p_{i_{dhw}}^{m}+\left(1-u_{i_{dhw}}^{m}\right)p_{i_{dhw}}^{m}\right)= \sum_{d=1}^{D}\sum_{h=1}^{H}\sum_{w=1}^{W}\left(\left(1-\mu_{i_{dhw}}^{m}\right)p_{i_{dhw}}^{m}x_{dhw}+\left(1-u_{i_{dhw}}^{m}\right)p_{i_{dhw}}^{m}\bar{x}_{dhw}\right) \tag{2.24}$$

or,

$$v_i=\frac{\sum_{d=1}^{D}\sum_{h=1}^{H}\sum_{w=1}^{W}\left(\left(1-\mu_{i_{dhw}}^{m}\right)p_{i_{dhw}}^{m}x_{dhw}+\left(1-u_{i_{dhw}}^{m}\right)p_{i_{dhw}}^{m}\bar{x}_{dhw}\right)}{\sum_{d=1}^{D}\sum_{h=1}^{H}\sum_{w=1}^{W}\left(\left(1-\mu_{i_{dhw}}^{m}\right)p_{i_{dhw}}^{m}+\left(1-u_{i_{dhw}}^{m}\right)p_{i_{dhw}}^{m}\right)} \tag{2.25}$$

The final membership function $g_{i_{dhw}}$ with respect to class i by which the voxel x_{dhw} is classified is calculated by taking the complement of the weighted value, which integrates the complemented global and local fuzzy membership functions with two weighting parameters. It is defined as follow.

$$g_{i_{dhw}}=1-\frac{(\mu_{i_{dhw}})^{p}(u_{i_{dhw}})^{q}}{\sum_{l=1}^{C}(\mu_{l_{dhw}})^{p}(u_{l_{dhw}})^{q}} \tag{2.26}$$

For better understanding of the developed algorithm, it is summarized below.

Input: A volumetric (3D) brain MR image of size $H \times W \times D$.

Assign the values for m, p, q, error ϵ and $k = 0$.
1. Initialize the cluster center $v_i^{(k)}, \forall i$ from image histogram.
2. Set the initial value of the uncertainty parameter ${p_{i_{dhw}}^m}^{(k)}, \forall i, d, h, w$.
3. Repeat

(a) Calculate the complemented global fuzzy membership function $\mu_{i_{dhw}}^{(k+1)}, \forall i, d, h, w$ by using (2.13).

(b) Calculate the complemented local fuzzy membership function $u_{i_{dhw}}^{(k+1)}, \forall i, d, h, w$ by using (2.17).

(c) Calculate the new uncertainty parameter $p_{i_{dhw}}^{(k+1)}, \forall i, d, h, w$ by using (2.22).

(d) Calculate the new cluster center ${v_i}^{(k+1)}, \forall i$ using (2.25).

(e) $k = k + 1$

4. Until $||v_i^{(k)} - v_i^{(k-1)}|| < \varepsilon, \forall i$
5. Calculate the final fuzzy membership function $g_{i_{dhw}}, \forall i, d, h, w$ by using (2.26).
6. Get the final cluster centers $V = \{v_1, v_2, v_3, ..., v_C\}$ and the membership matrix $M = \{g_{i_{dhw}}\}, \forall i, d, h, w$.
7. Assign the voxel x_{dhw} to a class that yields maximum membership value.

Output: Segmented 3D brain MR image volumes.

The work flow of the presented algorithm is shown in FIGURE 2.1.

2.4 Experimental studies

To evaluate the classification effectiveness of the presented algorithm, we perform several experiments on 6 simulated, 4 real patient clinical 3D brain MR image volumes and a 3D synthetic

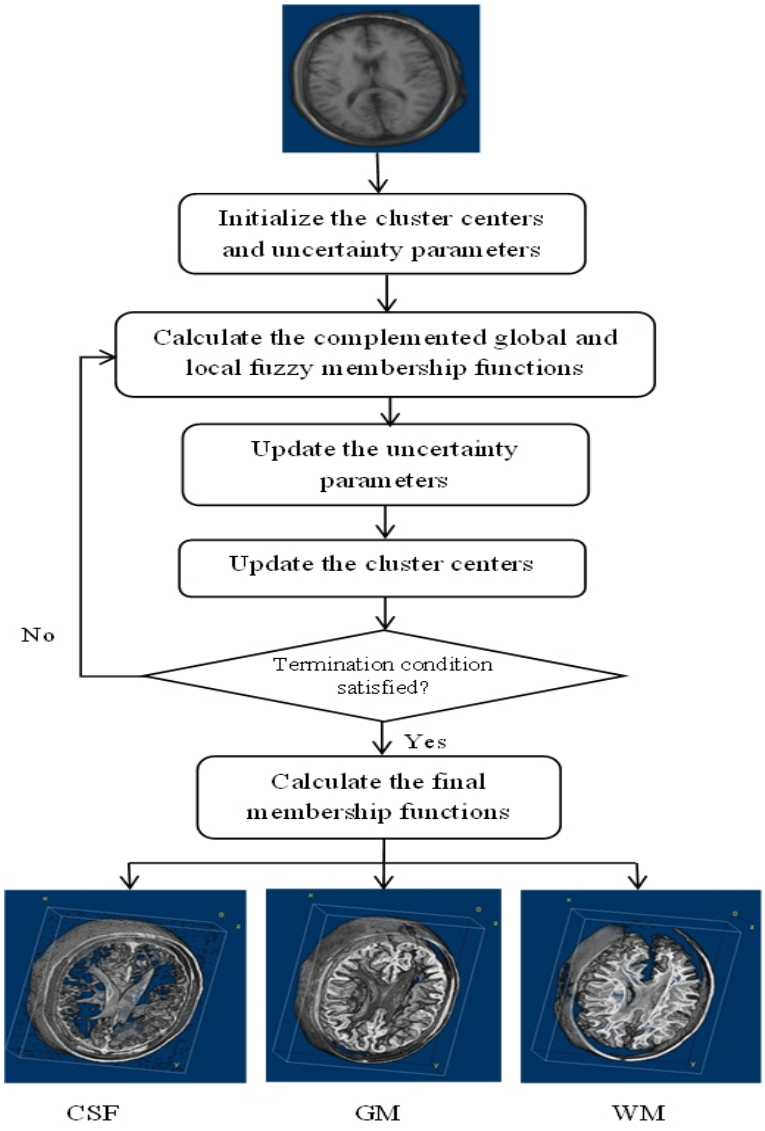

FIGURE 2.1: Work flow of the developed algorithm

image, where high Rician noise is added. We collect the simulated 3D brain MR image data from the BrainWeb [59]. The data contain different levels of noise (1%-9%) and intensity inhomogeneity (IIH) (20%-40%). In this study, we use 5%, 7% and 9% of noise and 20% and 40% of IIH. The size of each image volume is $181 \times 217 \times 181$ $(height \times width \times depth)$ and voxel thickness is $1 \times 1 \times 1$ mm^3. The real patient clinical image volumes of brain MR have the resolutions of $256 \times 150 \times 20$, $350 \times 206 \times 20$, $1105 \times 649 \times 20$ and $552 \times 325 \times 58$. Whereas, the size of the 3D synthetic image is $200 \times 200 \times 80$ that contains four different

non-overlapping regions.

2.4.1 Parameter estimation of the developed algorithm in the context of optimal result

We need to tune-up the developed algorithm to achieve optimal result. In line with this, we test the algorithm by setting different combinations of the controlling parameters, like (i) weighted parameters (p, q), (ii) degree of fuzzyness m and (iii) size of the neighborhood window. First, we optimize the pair (p, q) by conducting the experiments using different combinations. The combination that gives best result is taken as the optimized value of (p, q). We present the Dice similarity coefficient (DSC) values in FIGURE 2.2. We conduct this experiment by using $m = 2.0$ and neighborhood window size as $3 \times 3 \times 3$ on a T1-weighted simulated brain MR image volume that contains 9% noise and 40% IIH. From the results, we set $(p, q) = (3, 2)$. Next, we find the optimal value of m. We conduct the experiments on the same image volume using $(p, q) = (3, 2)$ and same neighborhood window. The results are shown in FIGURE 2.3, which gives optimal value of m as 2.0. Finally, to find the optimal neighborhood window size, again we conduct the experiments on same image volume using $(p, q) = (3, 2)$ and $m = 2.0$. We present the results in FIGURE 2.4. The window size of $3 \times 3 \times 3$ gives best result. Therefore, we analyze the effectiveness of the presented algorithm using $(p, q) = (3, 2)$, $m = 2.0$ and neighborhood window size of $3 \times 3 \times 3$ in all the remaining experiments.

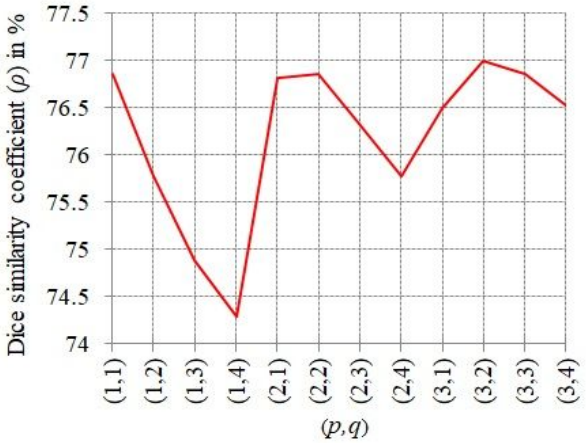

FIGURE 2.2: Dice similarity coefficients by using different combinations of (p, q).

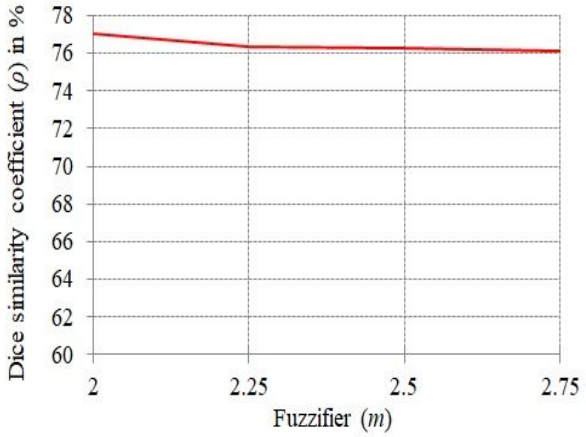

FIGURE 2.3: Dice similarity coefficients by using different values of m.

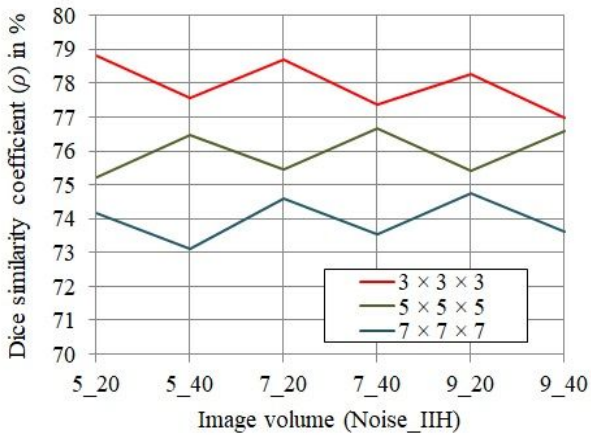

FIGURE 2.4: Dice similarity coefficients by using different window sizes.

2.4.2 Qualitative Evaluation

In this section, we present the visual outputs of the developed algorithm. First, we conduct experiments on the simulated brain MR image volumes, then on the clinical brain MR image volumes and finally on the synthetic image volume.

Qualitative results on simulated BrainWeb image volumes

In this section, we present the efficiency of the developed algorithm by displaying the segmented three soft tissue regions, namely white matter (WM), gray matter (GM) and cerebro spinal fluid (CSF). We conduct experiments on 6 image volumes. For better understanding of the segmented results, we compare with that of the ground truths and find that it satisfactorily perform the task in all the cases. One of the results is presented in FIGURE 2.5. In FIGURE 2.5(A), the 3D brain MR image volume with 9% noise and 40% IIH is shown. In FIGUREs 2.5(B)-2.5(D), the ground truths of the CSF, GM and WM, respectively are shown. Whereas, in FIGUREs 2.5(E)-2.5(G), we show the segmented CSF, GM and WM, respectively. Furthermore, for better visualization, we present the lower two-third portion of these regions in FIGURE 2.5(H)-2.5(J). Careful investigation reveals that the algorithm can efficiently segment the 3D brain MR image volumes. Further, for better understanding the 2D color mapped of the segmented image volumes and the ground truths are presented in FIGURE 2.6.

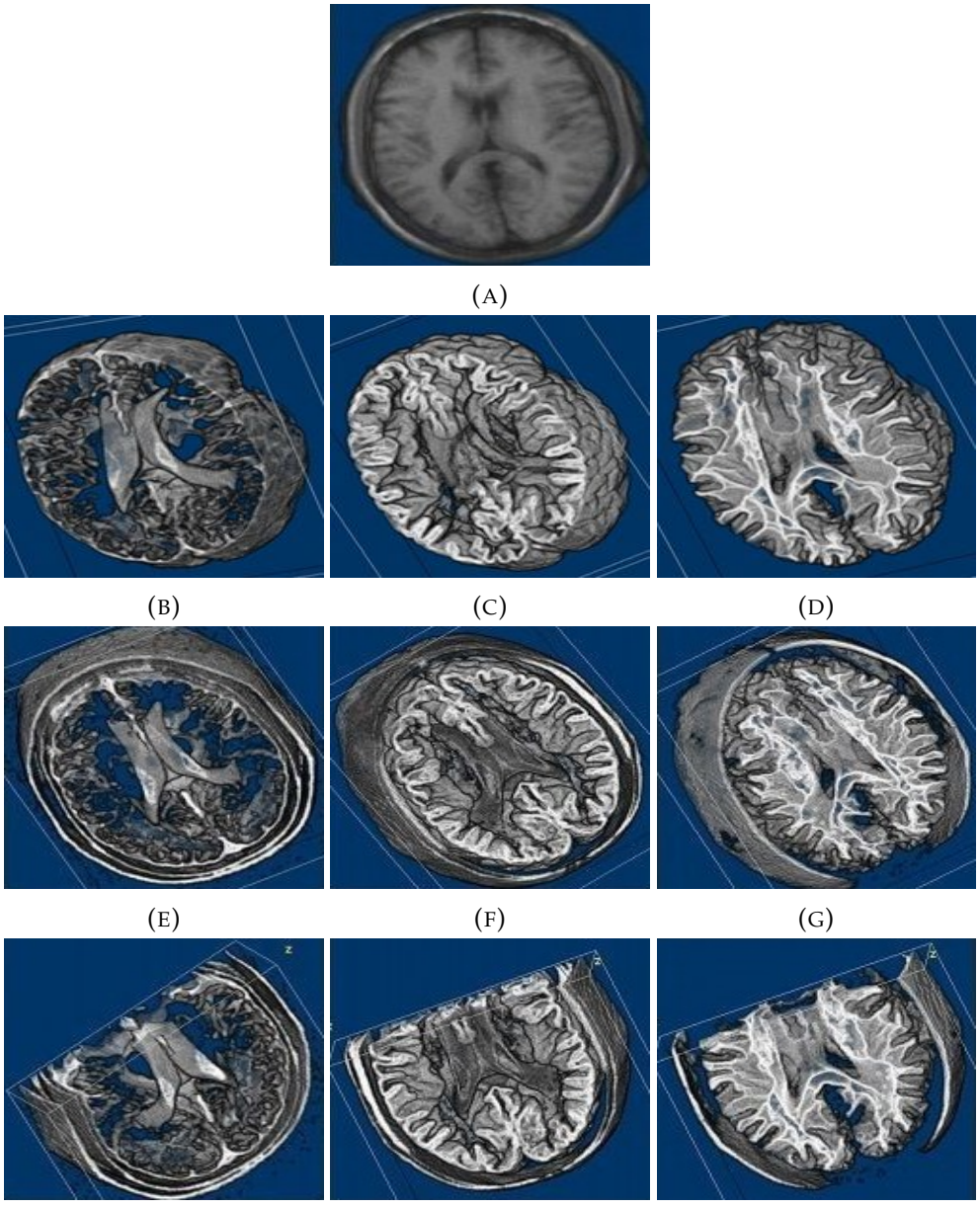

(A)

(B) (C) (D)

(E) (F) (G)

(H) (I) (J)

FIGURE 2.5: Segmented outputs of the developed algorithm. (A) Input image volume, (B)-(D) Ground truths of the CSF, GM and WM, respectively, (E)-(G) Segmented CSF, GM and WM, respectively and (H)-(J) Lower two-thirds of the CSF, GM and WM, respectively.

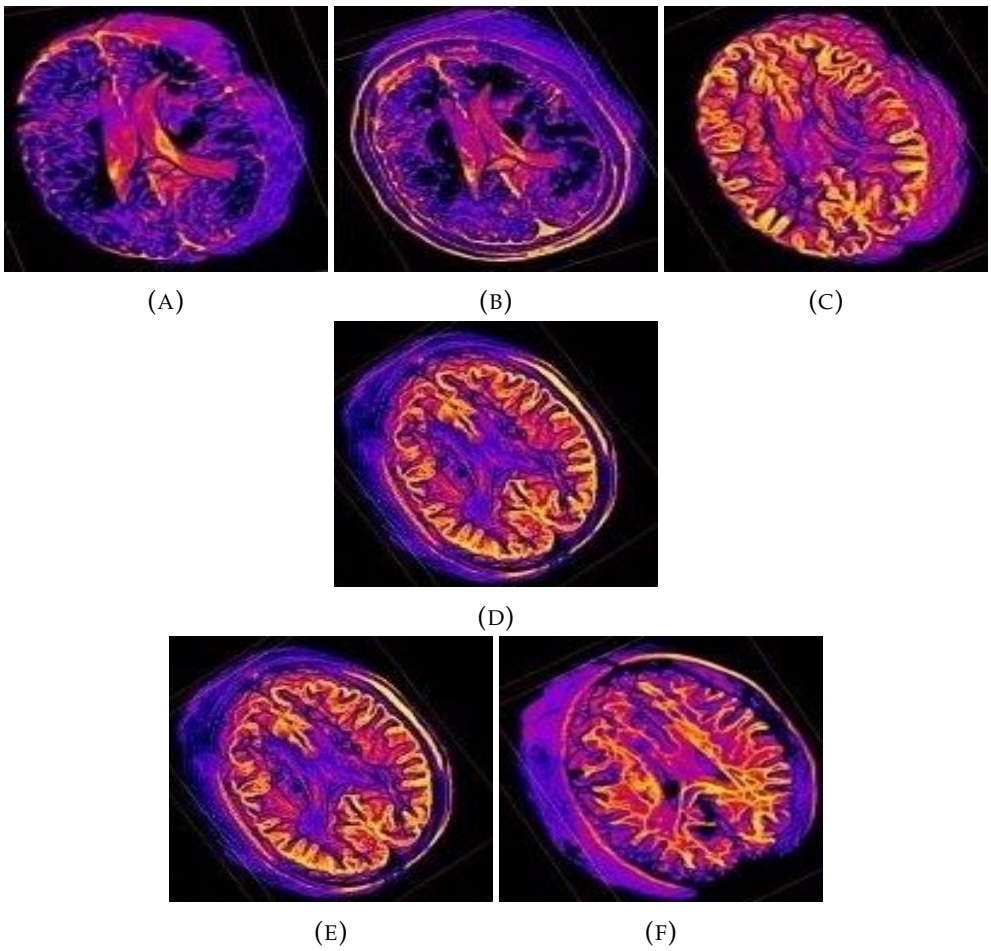

(A) (B) (C)

(D)

(E) (F)

FIGURE 2.6: 2D color mapped of the segmented results. (A)-(B) Ground truth and segmented CSF, respectively, (C)-(D) Ground truth and segmented GM, respectively and (E)-(F) Ground truth and segmented WM, respectively.

Qualitative results on clinical real patient image volume

In this section, we display the segmented results on four clinical real patient brain MR image volumes. There are collected from the AMRI Hospital and the EKO X-ray and Imaging Institute, Kolkata, India. All the image volumes are acquired by 1.5T MRI machines. Like the previous section, we present the segmented results of an image volume in FIGURE 2.7. Its 2D color mapped segmented results are also presented here. In this case also the presented algorithm shows its effectiveness.

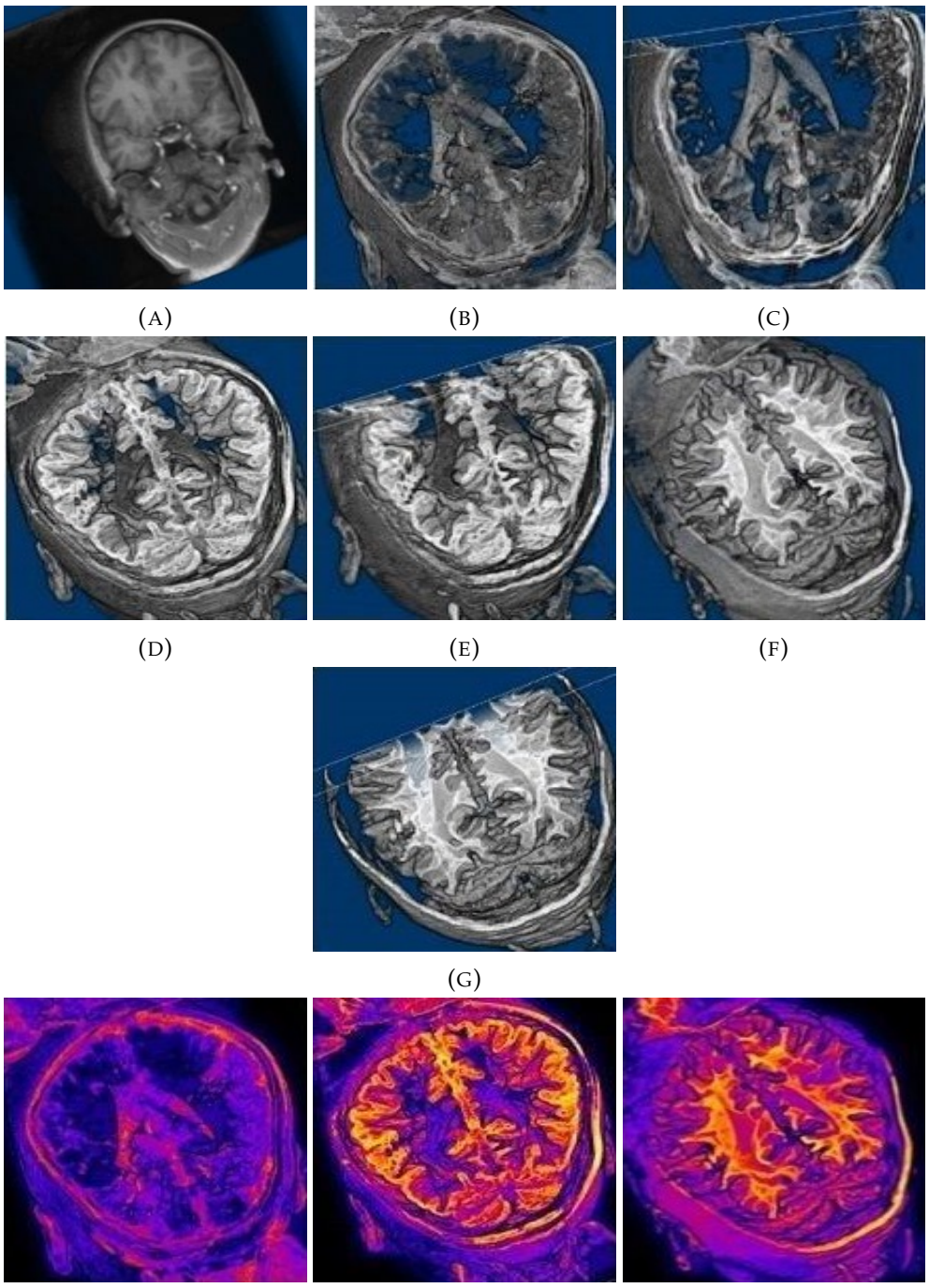

(A) (B) (C)

(D) (E) (F)

(G)

(H) (I) (J)

FIGURE 2.7: Segmented outputs on a clinical data. (A) 3D input image, (B)-(C) CSF and its lower two-thirds, respectively, (D)-(E) GM and its lower two-thirds, respectively, (F)-(G) WM and its lower two-thirds, respectively, and (H)-(J) 2D color mapped of the segmented CSF, GM and WM, respectively.

Qualitative results on a synthetic image volume

In this section, we test the algorithm on a synthetic image volume, which is manually corrupted by Rician noise. It is generally believe that the intensity distribution due to Rician noise is quite similar to that of a MR image [60]. The synthetic image volume and its noisy version are shown in FIGURE 2.8(A)-(B). Whereas, the segmented volume is shown in FIGURE 2.8(C). Again, the developed algorithm shows its effectiveness.

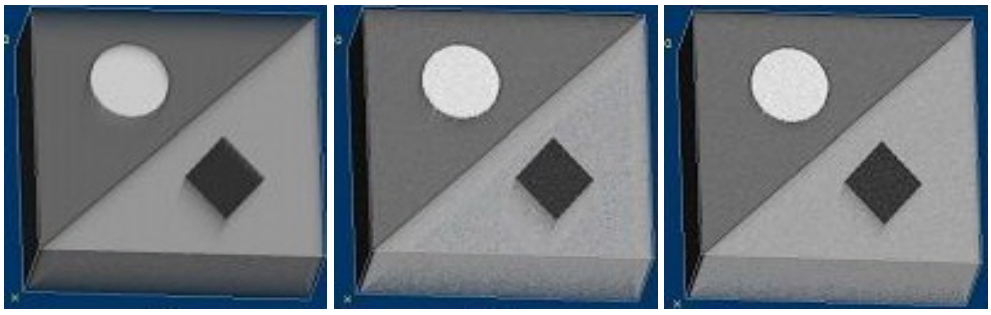

(A) (B) (C)

FIGURE 2.8: Segmented output over a synthetic image volume. (A)-(C) Input, corrupted and segmented image volumes, respectively.

2.4.3 Quantitative evaluation

In this section, we present comparative performance evaluation by means of several indices, namely (i) partition coefficient (v_{pc}), (ii) partition entropy (v_{pe}), (iii) Dice similarity coefficient (ρ), (iv) segmentation accuracy (SA) and (v) tissue segmentation accuracy (TSA) ([31]).

Quantitative Analysis of simulated MR image volume

We present the efficacy of the developed algorithm in different figures along with the similar and state-of-the-arts methods. In particular, these methods are MEI [49], REFCM [51], MEFCM

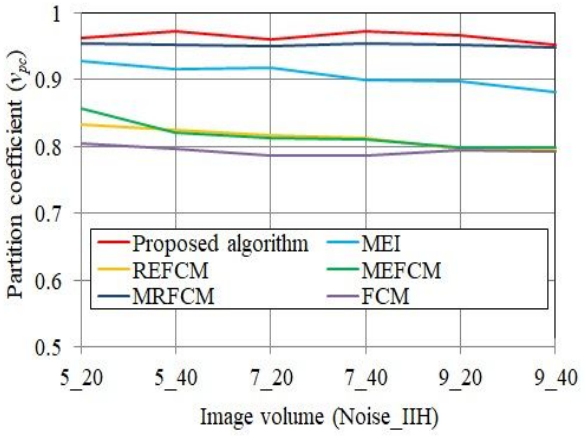

FIGURE 2.9: Results of different algorithms using V_{pc} on 3D simulated images.

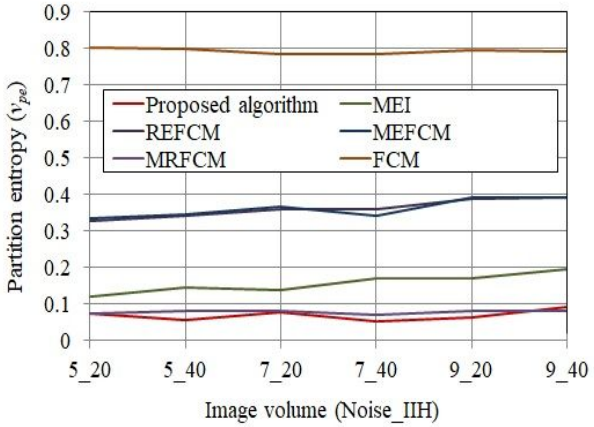

FIGURE 2.10: Results of different algorithms using V_{pe} on 3D simulated images.

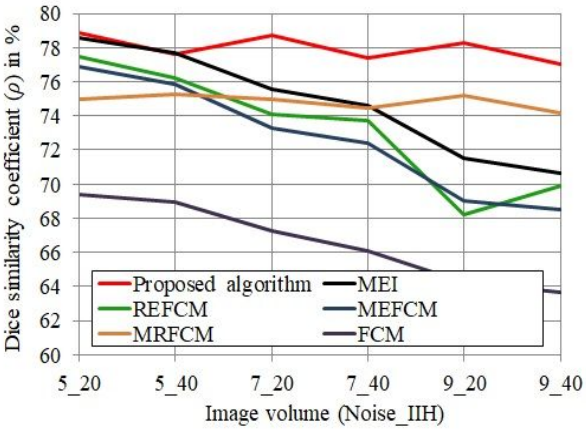

FIGURE 2.11: Results of different algorithms using ρ on 3D simulated images.

[50], MREFCM [52] and FCM [18]. It may be noted that all the comparative methods are implemented and their results are presented in this section. FIGURE 2.9 and FIGURE 2.10 show the comparative performance in terms of v_{pc} and v_{pe}, respectively. From the figures one can find that the developed algorithm is superior to the other methods. We present the Dice similarity coefficient of different methods in FIGURE 2.11. In this case also, the presented algorithm outperforms the other methods.

We also present the performance indices of the developed algorithm in different tabular form in terms of SA, TSA along with other comparative methods. For SA index, we present the results in TABLE 2.1. The study suggests that in the presence of high noise and IIH, the presented algorithm works well and establishes its superiority over other methods. Furthermore, to investigate whether the improvement is statistically significant or not, we conduct one tailed paired t-test between the developed algorithm and all other comparative methods. For this purpose a null hypothesis H_0 is set as: 'The mean value of the developed algorithm is same as that of the other method'. The alternative hypothesis H_1 is set as: 'The mean value of the presented algorithm is higher as that of the other method'. We present the summary of the significant analysis in TABLE 2.2. Results show that the developed algorithm is statistically significant over the MEI, REFCM and FCM methods at $p = 0.05$ for WM region. It is also statistically significant over MEFCM, MREFCM and FCM methods at $p = 0.01$ for GM and CSF regions.

Furthermore, we compare our algorithm with some of the recently proposed algorithms like, KIFECM (SNF, YNF) [54], TW-k-means [42] and IMV-FCM [44] methods. For a fair comparison, in line with the above methods, we also consider the average segmentation accuracy (ASA) and Dice similarity coefficient

TABLE 2.1: Segmentation accuracy on 3D simulated brain MR images. The best values are shown in bold.

(Noise, IIH)	Region	Developed algorithm	MEI	REFCM	MEFCM	MREFCM	FCM
5-20	WM	0.961	0.953	0. 906	**0.970**	0.963	0.848
	GM	**0.906**	0.906	0.845	0.851	0.837	0.834
	CSF	0.886	**0.915**	0.972	0.881	0.819	0.881
5-40	WM	0.930	0.934	0.877	**0.952**	0.920	0.840
	GM	0.881	**0.895**	0.880	0.838	0.840	0.825
	CSF	0.891	**0.909**	0.887	0.857	0.838	0.837
7-20	WM	**0.960**	0.918	0.959	0.943	0.960	0.829
	GM	**0.901**	0.860	0.766	0.791	0.836	0.818
	CSF	**0.887**	0.851	0.849	0.780	0.830	0.819
7-40	WM	**0.920**	0.896	0.843	0.920	0.914	0.795
	GM	**0.875**	0.845	0.840	0.776	0.839	0.782
	CSF	**0.888**	0.841	0.842	0.775	0.834	0.807
9-20	WM	**0.951**	0.864	0.891	0.902	0.949	0.781
	GM	**0.891**	0.807	0.772	0.722	0.846	0.755
	CSF	**0.880**	0.772	0.808	0.690	0.825	0.753
9-40	WM	**0.910**	0.846	0.767	0.891	0.888	0.765
	GM	**0.874**	0.789	0.796	0.711	0.843	0.742
	CSF	**0.880**	0.760	0.797	0.688	0.835	0.742

TABLE 2.2: Tabulation of statistical significance analysis for SA index.

Region	Paired t-test(1-tailed)	Developed algorithm	MEI	REFCM	MEFCM	MREFCM	FCM
WM	Mean of SA value	0.940	0.901	0.873	0.929	0.932	0.809
		-	0.040	0.021	0.284	0.341	0.000
GM	Mean of SA value	0.888	0.846	0.859	0.781	0.840	0.792
		-	0.061	0.151	0.000	0.000	0.000
CSF	Mean of SA value	0.885	0.841	0.859	0.859	0.830	0.806
		-	0.070	0.172	0.009	0.004	0.005

(DSC) indices for the slices 90 and 95 of T1-weighted BrainWeb images. TABLE 2.3 shows the comparative results, in terms of ASA and DSC, for the different methods with varying levels of noise and IIH. It is observed that, in almost all the cases the developed algorithm achieves better result than its competitive methods.

For TSA index, we present the summary of findings in TABLE 2.4. It shows that almost in all cases the presented algorithm performs better than the other methods. Like the previous index, we present the summery of the significant analysis in TABLE 2.5. It shows that except in two cases, the presented algorithm is statistically significance over its competitive algorithms at $p = 0.03$ for all the regions.

2.4.4 Quantitative Analysis on clinical MR image volumes

In this section, we present the experimental results of different methods in TABLE 2.6. The results indicate that the presented algorithm outperforms the other comparative methods except the MREFCM method.

2.4.5 Quantitative Analysis on a 3D synthetic image

We present the results of the developed method on a 3D synthetic image, where we added Rician noise, in TABLE 2.7. Here also, results reflect its efficiency as it satisfactorily segments the different regions.

2.5 Complexity analysis of the developed algorithm

As discussed earlier, let the size of the 3D brain MR image volume is $V = H \times W \times D$ (height $\times$ width $\times$ depth). The image

TABLE 2.3: Comparative results between the KIFECM, TW-k-means, IMV-FCM and the developed methods. The best values are shown in bold.

(Noise, IIH)	Region	Developed Algorithm	KIFECM SNF	KIFECM YNF	TW-k-means	IMV FCM
	ASA	-	-	-	-	-
0, 0	DSC-WM	**0.9859**	-	-	0.9428	0.952
	DSC-GM	**0.9509**	-	-	0.8761	0.8851
	DSC-CSF	**0.9403**	-	-	0.8283	0.8506
	ASA	-	-	-	-	-
3, 0	DSC-WM	**0.9724**	-	-	0.9377	0.9508
	DSC-GM	**0.9317**	-	-	0.8704	0.8762
	DSC-CSF	**0.9417**	-	-	0.8322	0.8441
	ASA	-	-	-	-	-
5, 0	DSC-WM	0.9332	-	-	0.9114	**0.9386**
	DSC-GM	**0.8685**	-	-	0.8466	0.8668
	DSC-CSF	**0.9190**	-	-	0.8023	0.8371
	ASA(Slice 90)	**0.9089**	0.8781	0.8781	-	-
7, 0	DSC-WM(Slice90)	**0.9421**	0.8909	0.8909	-	-
	DSC-WM(Slice95)	**0.9418**	-	-	0.9091	0.9295
	DSC-GM(Slice90)	0.8718	**0.8744**	0.8743	-	-
	DSC-GM(Slice95)	**0.8638**	-	-	0.8382	0.8545
	DSC-CSF(Slice90)	0.7958	0.8106	**0.8113**	-	-
	DSC-CSF(Slice95)	0.8007	-	-	0.7965	**0.8279**
	ASA (Slice 90)	**0.8890**	0.8428	0.8433	-	-
9, 0	DSC-WM(Slice90)	**0.9259**	0.8909	0.8909	-	-
	DSC-WM(Slice95)	**0.9423**	-	-	0.8862	0.9187
	DSC-GM(Slice90)	**0.8459**	0.8260	0.8257	-	-
	DSC-GM(Slice95)	**0.8623**	-	-	0.8189	0.8367
	DSC-CSF(Slice90)	0.7810	**0.7972**	0.7981	-	-
	DSC-CSF(Slice95)	0.7946	-	-	0.7779	**0.8132**
	ASA	**0.8925**	0.8843	0.8845	-	-
7, 20	DSC-WM	**0.9403**	0.9266	0.9266	-	-
	DSC-GM	0.8619	0.8777	**0.8780**	-	-
	DSC-CSF	0.7586	**0.8292**	0.8282	-	-
	ASA	**0.8787**	0.8434	0.8440	-	-
7, 40	DSC-WM	**0.9312**	0.8891	0.8891	-	-
	DSC-GM	**0.8498**	0.8235	0.8231	-	-
	DSC-CSF	0.7586	0.8044	**0.8052**	-	-
	ASA	**0.8874**	0.8702	0.8700	-	-
9, 20	DSC-WM	**0.9205**	0.9091	0.9091	-	-
	DSC-GM	0.8498	**0.8592**	0.8585	-	-
	DSC-CSF	0.7469	**0.8308**	0.8291	-	
	ASA	**0.8783**	0.8346	0.8350	-	-
9, 40	DSC-WM	**0.9174**	0.8814	0.8814	-	-
	DSC-GM	**0.8279**	0.8169	0.8165	-	-
	DSC-CSF	0.7354	**0.7958**	0.7955	-	-

TABLE 2.4: TSA on 3D images. The best values are shown in bold.

Volume	Tissue Region	Developed algorithm	MEI	REFCM	MEFCM	MREFCM	FCM
5-20	WM	**0.870**	0.829	0. 821	0.810	0.812	0.716
	GM	**0.801**	0.800	0.788	0.793	0.752	0.693
	CSF	0.592	0.610	**0.612**	0.601	0.546	0.439
5-40	WM	**0.850**	0.823	0.822	0.811	0.808	0.716
	GM	**0.781**	0.792	0.792	0.782	0.749	0.678
	CSF	0.589	**0.606**	0.573	0.587	0.553	0.419
7-20	WM	**0.866**	0.795	0.780	0.785	0.812	0.694
	GM	**0.800**	0.762	0.737	0.755	0.753	0.660
	CSF	**0.597**	0.578	0.575	0.540	0.551	0.417
7-40	WM	**0.849**	0.795	0.793	0.780	0.808	0.660
	GM	**0.780**	0.756	0.759	0.741	0.747	0.694
	CSF	**0.591**	0.568	0.541	0.535	0.554	0.390
9-20	WM	**0.861**	0.763	0.767	0.755	0.817	0.666
	GM	**0.796**	0.723	0.726	0.705	0.758	0.621
	CSF	**0.598**	0.522	0.516	0.473	0.556	0.377
9-40	WM	**0.845**	0.761	0.749	0.751	0.805	0.671
	GM	**0.776**	0.718	0.714	0.695	0.747	0.610
	CSF	**0.588**	0.510	0.486	0.468	0.552	0.361

TABLE 2.5: Tabulation of statistical significance analysis for TSA index.

Region	Paired t-test(1-tailed)	Developed Method	MEI	REFCM	MEFCM	MREFCM	FCM
WM	Mean of TSA	0.856	0.794	0.788	0.782	0.810	0.687
	value	-	0.000	0.000	0.000	0.000	0.000
GM	Mean of TSA	0.789	0.758	0.752	0.745	0.751	0.658
	value	-	0.031	0.013	0.013	0.000	0.000
CSF	Mean of TSA	0.592	0.565	0.550	0.534	0.552	0.400
	value	-	0.074	0.023	0.013	0.000	0.000

TABLE 2.6: Experimental results on clinical real patient 3D MR images.

Volume	Method	v_{pc}	v_{pe}
Clinical Patient 1	Developed algorithm	0.990	0.021
	MEI	0.960	0.040
	REFCM	0.891	0.343
	MEFCM	0.915	0.171
	MREFCM	0.992	0.012
	FCM	0.741	0.507
Clinical Patient 2	Developed algorithm	0.983	0.030
	MEI	0.890	0.153
	REFCM	0.837	0.331
	MEFCM	0.888	0.217
	MREFCM	0.994	0.009
	FCM	0.870	0.273
Clinical Patient 3	Developed algorithm	0.970	0.050
	MEI	0.965	0.080
	REFCM	0.931	0.126
	MEFCM	0.946	0.104
	MREFCM	0.991	0.014
	FCM	0.705	0.558
Clinical Patient 4	Developed algorithm	0.980	0.054
	MEI	0.976	0.039
	REFCM	0.875	0.264
	MEFCM	0.912	0.182
	MREFCM	0.981	0.017
	FCM	0.791	0.253

TABLE 2.7: Experimental results on a synthetic image volume.

Index	Segmented Region	Value
SA	Black	0.820
	Gray	0.985
	Light white	0.980
	White	0.960
Dice similarity coefficient		0.947
v_{pc}		0.980
v_{pe}		0.051

volume is to be segmented into C different regions or clusters. In this study, in order to classify an image voxel, we compute f (here f=4) features for each voxel. The value of C is 4 corresponding to CSF, GM WM and background regions. For each iteration, the algorithm first computes the complemented global membership matrix, then complemented local membership matrix and lastly the class-level uncertainty matrix. Finally, it computes the final membership matrix, based on which the voxels are classified. First, it computes the Euclidean distances between the cluster centers and image voxels. Therefore, the total time required to generate the global membership matrix M is approximately O(fVC). Whereas, in case of the local membership matrix U it computes the mean of the neighboring voxels of size N_T with respect to each voxel and it completes in O(N_T). So the computational cost for the local membership matrix U is O(fVC + VN_T). Similarly, the computational cost of the uncertainty parameter matrix P for the image volume is O(VC). Finally, the cluster centers are calculated in O(VC). Therefore, for each iteration, the total time required is O($fVC + fVC + VN_T + VC + VC$) $\cong$ O($2(f+1)VC + VN_T$). After N iterations (here it takes 15-20 iterations), it further computes the final membership matrix G in O(VC).

To evaluate the space complexity of the presented algorithm, we require spaces for its membership matrices, Euclidean distances, neighborhood matrices, input image space and the memory space for temporary values. The space for the 3D input image volume is O(V). For complemented global membership matrix M, it requires spaces for the distance matrix and complemented global membership matrix, which is calculated at the previous iteration. Hence, it requires a space of O(VC + $VC + VC$) = O($3VC$). At the same way, the complemented local

membership matrix U requires the space of O($VC + VC + VC$) = O($3VC$). For the uncertainty parameter matrix P, it requires space O($2VC$). The cluster center matrices require a space O($2C$). The final membership matrix G requires a space O(VC). Therefore, the total memory space required for the presented algorithm is O($V + 3VC + 3VC + 2VC + 2C + VC$) $\cong$ O($9VC + V + 2C$). We implement the algorithm in C programming language on a workstation computer configured with Intel Core i7 CPU, 32 GB DRAM and Fedora 26 Linux operating systems.

2.6 Conclusion

In this contribution, we developed an uncertainty parameter weighted entropy-based FCM algorithm to segment 3D brain MR image volumes in the presence of noise. We introduce complemented global and neighborhood controlled local fuzzy membership functions. These membership functions are the complement of the conventional fuzzy membership function. Due to the inherent nature of the brain MR images we introduce a class-level uncertainty parameter for each voxel. This uncertainty parameter is conjugated with the complemented fuzzy global as well as local membership functions. Finally, we introduce Shannon entropy to define the underlying total information uncertainty with the help of the uncertainty parameter. We investigate the algorithm using 6 simulated and 4 clinical real patient brain MR image data. We also conduct experiments on a synthetic image volume by adding Rician noise. In all experiments the developed algorithm establishes its superiority over state-of-the-arts methods, which are developed recently.

The future work of this algorithm may be to find a way to

utilize dynamic neighborhood window to address close association of the voxels lying within a local spatial image domain. In the next chapter, this issue is addressed by incorporating type-1 and interval type-2 fuzzy sets along with relative entropy.

Chapter 3

Multi-objective framework for brain MR image segmentation

3.1 Source of the Chapter

Chapter 3 is based on the research work [61].

3.2 Introduction

Due to the advancement of non-invasive imaging technology, magnetic resonance imaging (MRI) is a very useful and affordable mechanism for viewing brain details. However, its segmentation into different regions, like gray matter (GM), cerebro spinal fluid (CSF), white matter (WM), etc. is a critical and obvious course of action to identify any kind of anomaly or disorder in human brain. Noise and intensity in-homogeneity (IIH) have an impact on brain MR images because of the uneven generation of radio frequency, patient movement during scanning and other factors that make it blurry throughout the image domain. As a result, the process of segmentation become more challenging and more often it is prone to error especially if a significant amount of noise and IIH is present. The outcome segmentation helps the radiologists to identify the diseases and plan for treatment appropriately. As a result, there is a constant effort from

the research community to devise algorithms for achieving better segmentation results.

According to the literature survey, the fuzzy clustering algorithm, especially the c-means (FCM) algorithm [18] is mostly used and studied for segmentation of medical images. However, the FCM algorithm has limitations for noisy data as it is not considering spatial information during the clustering process. To overcome the shortcomings, some modified FCM-based algorithms are proposed at recent past to segment brain MR images. Sing et al. [30] developed a modified FCM (mFCM) algorithm that makes use of scale-controlled spatial information. Using an auxiliary variable for each pixel, Adhikari et al. [31] proposed a spatial and conditional FCM algorithm. Chighoub et al. [62] proposed a FCM algorithm by undertaking fully integrated spatial information. The algorithm selects optimal pixel by utilizing compactness and separation information within the neighboring pixels. In order to segment 3D brain MR images using 3D spatial neighborhood information, Kahali et al. [33] created a fuzzy multi objective framework in two stages. Mahata et al. [39] introduced a fuzzy clustering technique that relies on Gaussian functions and local contextual information. It defines IIH correction and Gaussian surface while taking into account contextual information specific to the local area. Devi et al. [47] proposed a hybrid deep learning based clustering algorithm. The algorithm utilizes Moth flame optimization (HAB-WMFO) technique to select optimal features.

In addition to the above variants, recently researchers also proposed some other alternatives of the FCM algorithm. Miao et al. [63] presented an enhanced FCM algorithm based on self-adaptive dictionary learning. It uses a dictionary to cut down on noise and removes the non-target regions of the image by

considering gray scale features of the images and extracts the intended regions. Singh et al. [42] developed modified FCM algorithm by utilizing multi-objective antlion optimization process to generate fuzzy hyper volume fitness functions and cluster compactness minimization function. Mahata et al. [55] developed fuzzy clustering algorithm that minimizes the global and local entropies, constraint by spatially controlled likelihood measure. Hua et al. [44] proposed an improved multiview FCM (IMV-FCM) algorithm, which incorporates view weight adaptive learning procedure to get the optimal weight of each clustering information. It uses view ensemble method to ensure the final clustering. Kahali et al. [53] proposed an improved FCM algorithm inculcating entropy. The algorithm utilizes Gaussian probability density function and contra harmonic mean filter for this purpose. Verma et al. [64] proposed an intuitionistic fuzzy co-clustering (IICC) algorithm, which incorporates intuitionistic fuzzy set theory. It uses particle swarm optimization (PSO) technique for parameter optimization. Recently, Ray et al. [28] proposed an entropy based FCM algorithm, which uses the local and global membership functions as their complemented forms. Mishro et al. [65] developed a T2FCM algorithm by utilizing adjustable weighted factor by using spatial information of volumetric MR images. Wang et al. [66] proposed an outlier robust picture of clustering algorithm with T2FS. It uses different fuzzification coefficients and generates positive, neutral and refusal membership functions.

In this work, we suggest a multi-objective paradigm incorporating relative entropy-based type-1 (T1) and interval T2FCM

(IT2FCM) algorithms for segmenting noisy 3D brain MR images. The first objective function proposes a relative entropy-based T1 FCM algorithm utilizing spatial information and locally biased class-level possibility parameter to yield global membership functions (GMFs) together with local membership functions (LMFs). To create the membership functions (MFs), it makes use of the intensity distribution within the cubic neighborhood of the central voxel. Whereas, the second objective function uses this GMFs and introduces IT2FMFs, weighted with the above possibility parameter. Specifically, it utilizes the LMFs to generate the secondary MFs for the IT2 fuzzy set (IT2FS). Thus, it uses the correlation between the neighboring voxels of the center voxel in order to classify the voxels. The framework calculates the final cluster centers as the arithmetic mean of those yielded by the two objective functions. By combining the GMFs and interval type-2 fuzzy membership functions (IT2F-MFs), it finally produces the final MFs with the aid of two weighting parameters.

The main contributions of this work is highlighted below:

1) A multi-objective framework is presented, which incorporates a relative entropy-based T1 and IT2FCM algorithms.

2) The first objective function employs GMFs and LMFs together with relative entropy based on these membership functions to address the issue related to the class specific non-uniform intensity distribution within the image domain.

3) The LMF is biased by the intensity distribution within its cubic neighborhood and also weighted by a class-level possibility parameter to influence the center voxel to belong to a class that dominates in the cubic neighborhood.

4) The second objective function uses the above GMF and

introduces IT2F-MF, which is weighted by the above possibility parameter. The LMFs are utilized to calculate the secondary MFs for the T2FS. This is done to further influence the presence of neighboring homogeneous voxels and the possibility parameter to determine the T2 fuzzy MF of the central voxel.

5) The final MF is produced by merging the GMF and the IT2F-MF along with two weighted parameters, which control their relative contributions.

To obtain both qualitative and quantitative validation we use the suggested approach on four volumes of simulated brain MR images with high noise and IIH, IBSR brain MR images of five volumes, clinical brain MR images of four volumes, and a single volume of synthetic images affected by Rician noise. The results of the experiments reflect its superiority and efficiency over some most advanced methods that have been suggested recently.

The remaining parts of this contribution are organized like this. Second section describes the basics of T2 and IT2FSs. Third section presents the suggested multi-objective framework utilizing T1 fuzzy sets (T1FSs) and T2FSs. Fourth section highlights the experimental results along with comparative analyses by utilizing the most recent algorithms. The complexity analysis of the presented algorithm is provided in the fifth section. Finally, the conclusion is presented in the sixth section.

3.3 T2 and IT2FSs

Lotfi A. Zadeh first introduced the T2FS in 1975 [67]. The T2FS is found to be more effective while dealing with more uncertainties. In a T2FS, the MF itself is a T1FS. In other words, in a T2FS, the membership function has multiple values rather than

a single membership value as in a T1FS. Here is how a T2FS $\bar{S}$ is defined:

$$\bar{S} = \{((x,q),\mu_{\bar{S}}(x,q))\,|\forall\, x \in R, q\ \in\ [0,1]\} \tag{3.1}$$

where R is the universe of discourse and $0 \leq \mu_{\bar{S}}(x,q) \leq 1$.

A specific instance of T2FS is an IT2FS., where the secondary membership values (MV) are equal to 1. It is expressed as follows.

$$\bar{S} = \{((x,q),\mu_{\bar{S}}(x,q)) = 1|\forall\, x \in R, q\ \in\ [0,1]\} \tag{3.2}$$

For each value of x the secondary MF $\mu_{\bar{S}}(x,q)$ represents a vertical slice of $\bar{S}$. Therefore, an IT2FS can be defined as follows and is confined by its upper and lower membership functions:

$$\bar{S} = 1/\left[\bar{\mu}_{\bar{S}}(x), \underline{\mu}_{\bar{S}}(x)\right] \tag{3.3}$$

where $\underline{\mu}_{\bar{A}}(r)$ and $\bar{\mu}_{\bar{A}}(r)$ presented as the lower and upper MF, correspondingly. For further information regarding IT2FS, readers may look into the work of Wu et al. [68].

3.4 Multi-objective framework using relative entropy with T1 and IT2FCM algorithms

IIH and noise have an impact on brain MR imaging because of limitations of MRI scanner. As a results, the images become blur and ambiguous which result irregular intensity distribution of the soft brain tissues throughout the image domain and make some regions as brighter and others as darker with respect to a particular tissue. This phenomenon makes the tissue classification and segmentation task more difficult and uncertain, particularly where there are tissue borders. In order to deal with this

matter, we suggest a multi-objective framework incorporating relative entropy with T1 and IT2FCM algorithms for segmenting noisy 3D brain MR images. The relative entropy defines the degree of uncertainty in the voxels' classification and it reaches its peak at tissue borders. In the first objective function, we propose a relative entropy-based T1FCM algorithm utilizing both spatial information and locally biased class-level possibility parameter to yield GMFs and LMFs. This objective function is also responsible to minimize the relative entropy. The possibility parameter has greater influence for generating the local membership function. Therefore, this objective function utilizes the intensity distribution in the cubic local neighborhood as well as in the whole 3D image domain in order to produce the two MFs. Whereas, in the second objective function, we use this GMFs and introduce IT2F-MFs multiplied by the above possibility parameter. Specifically, it uses the LMFs to generate the secondary MFs for the IT2FSs. The aim of introducing IT2FS is to utilize the neighboring spatial information for generating the proper fuzzy MFs and cluster centers. The IT2FS is then reduced to T1FS by using the simplified version of the method proposed by Nie et al. [69]. Thus, it utilizes the influence of the neighboring voxels in order to classify the center voxel under consideration. The framework calculates the final cluster centers as the arithmetic mean of those yielded by the two objective functions. Finally, it generates the final MF by combining the GMFs and IT2F-MFs using two controlling parameters, which control the trade-off between them. Further, in order to mitigate the impact of IIH and noise, within the spacial neighborhood, four features are used to represent each voxel. These are the voxels' intensity value and the average intensity values within the neighborhood along the 3 coordinates of the 3D image domain, keeping the voxel under

consideration in the center of the neighborhood.

We formulate the multi-objective framework by two fuzzy objective functions as defined below.

$$J_1 = \sum_{c=1}^{C}\sum_{b=1}^{B}\sum_{h=1}^{H}\sum_{l=1}^{L}\left(\alpha\mu_{c_{hlb}}^{m}d_{c_{hlb}}^{2} + (1-\alpha)u_{c_{hlb}}^{m}\bar{d}_{c_{hlb}}^{2}\zeta_{c_{hlb}})\right) - \sum_{b=1}^{B}\sum_{h=1}^{H}\sum_{l=1}^{L}\sum_{c=1}^{C}\left(\mu_{c_{hlb}}^{m}\ln\left(\frac{\mu_{c_{hlb}}^{m}}{u_{c_{hlb}}^{m}}\right)\right) \tag{3.4}$$

$$J_2 = \sum_{c=1}^{C}\sum_{b=1}^{B}\sum_{h=1}^{H}\sum_{l=1}^{L}\left(\alpha\mu_{c_{hlb}}^{m}d_{c_{hlb}}^{2} + (1-\alpha)\tau_{c_{hlb}}^{m}\bar{d}_{c_{hlb}}^{2}\zeta_{c_{hlb}}\right) \tag{3.5}$$

with the following three constraints as stated below.

$$\sum_{c=1}^{C}\mu_{c_{hlb}} = 1, \forall h, l, b \tag{3.6}$$

$$\sum_{c=1}^{C}u_{c_{hlb}} = 1, \forall h, l, b \tag{3.7}$$

$$\sum_{c=1}^{C}\tau_{c_{hlb}} = 1, \forall h, l, b \tag{3.8}$$

where the number of clusters or regions is C in the 3D image volume. The image volume is constituted by B number of images, each one having the width and height as L and H, respectively. The GMFs and LMFs for the voxel x_{hlb} with respect to cluster c are represented by $\mu_{c_{hlb}}$ and $u_{c_{hlb}}$, respectively. v_c is the c^{th} cluster center.The Euclidean distance between the voxel x_{hlb} and the center of cluster v_c is denoted by $d_{c_{hlb}}$. The mean distance among the neighboring voxels x_{hlb} and the v_c is indicated by $\bar{d}_{c_{hlb}}$. For the voxel x_{hlb} belonging to class c, the class-level possibility parameter is denoted by $\zeta_{c_{hlb}}$. Finally, $m > 1.0$

denotes the level of fuzziness. The definitions of the above parameters are given below.

$$d^2_{c_{hlb}} = ||x_{hlb} - v_c||^2 \tag{3.9}$$

$$\bar{d}^2_{c_{hlb}} = \frac{1}{B_T} \sum_{x_{hlb} \in B_{hlb}} ||x_{hlb} - v_c||^2 \tag{3.10}$$

$$\zeta_{c_{hlb}} = \frac{\sum_{x_{hlb} \in B_{hlb}} \mu_{c_{hlb}} x_{hlb}}{\sum_{x_{hlb} \in B_{hlb}} x_{hlb}} \tag{3.11}$$

where B_T is the entire voxel count in the neighborhood B_{hlb} concerning the central voxel x_{hlb}.

In (3.4), first term is responsible to lessen the product of fuzzy GMFs and distances of the voxels from the cluster centers. The second term is responsible to keep the product of fuzzy LMFs, the mean distances of the neighboring voxels from the cluster centers and the possibility factors minimum. These two terms are complementary regularized by a positive parameter $\alpha; 0 \leq \alpha \leq 1$. The third term estimates the complete information uncertainty by means of relative entropy for the 3D image domain. Similarly, in (3.5), two terms are responsible to find the proper cluster centers by using GMFs and IT2F-MFs.

To find the iterative equations regrading the parameters, the objective functions are required to minimize satisfying the associated constraints. This can be accomplished by rewriting the (3.4) and (3.5) utilizing Lagrange multipliers and then performing partial derivatives with respect to $\mu_{c_{hlb}}$, $u_{c_{hlb}}$ and v_c to generate the iterative equations of $\mu_{c_{hlb}}$, $u_{c_{hlb}}$ and v_c, respectively. The detailed derivatives are given in the **Appendix A**. The objective function in (3.5) is used to find the another set of cluster centers using the IT2F-MFs. We calculate the final cluster centers, which

utilize the T1 fuzzy sets (T1FSs) and IT2FSs, as the mean of the above two types of cluster centers ${}^1v_c$ and ${}^2v_c$. The equations are given as follows.

$$\mu_{c_{hlb}} = \frac{1}{\sum_{t=1}^{C}\left(\frac{\alpha d^2_{c_{hlb}} - \ln\left(\frac{\mu^m_{c_{hlb}}}{u^m_{c_{hlb}}}\right) - 1}{\alpha d^2_{t_{hlb}} - \ln\left(\frac{\mu^m_{t_{hlb}}}{u^m_{t_{hlb}}}\right) - 1}\right)^{\frac{1}{m-1}}} \forall c, h, l, b \tag{3.12}$$

$$u_{c_{hlb}} = \frac{1}{\sum_{t=1}^{C}\left(\frac{\left(1-\alpha\right)\vec{d}^2_{c_{hlb}}\zeta_{c_{hlb}} + \left(\frac{\mu^m_{c_{hlb}}}{u^m_{c_{hlb}}}\right)}{\left(1-\alpha\right)\vec{d}^2_{t_{hlb}}\zeta_{t_{hlb}} + \left(\frac{\mu^m_{t_{hlb}}}{u^m_{t_{hlb}}}\right)}\right)^{\frac{1}{m-1}}} \forall c, h, l, b \tag{3.13}$$

$${}^1v_c = v_c = \frac{\sum_{b=1}^{B}\sum_{h=1}^{H}\sum_{l=1}^{L}\left(\alpha\mu^m_{c_{hlb}}\, x_{hlb} + \left(1-\alpha\right)u^m_{c_{hlb}}\,\zeta_{c_{hlb}}\bar{x}_{hlb}\right)}{\sum_{b=1}^{B}\sum_{h=1}^{H}\sum_{l=1}^{L}\left(\alpha\mu^m_{c_{hlb}} + \left(1-\alpha\right)u^m_{c_{hlb}}\zeta_{c_{hlb}}\right)} \quad \forall c \tag{3.14}$$

$${}^2v_c = v_c = \frac{\sum_{b=1}^{B}\sum_{h=1}^{H}\sum_{l=1}^{L}\left(\alpha\mu^m_{c_{hlb}}\, x_{hlb} + \left(1-\alpha\right)\tau^m_{c_{hlb}}\,\zeta_{c_{hlb}}\bar{x}_{hlb}\right)}{\sum_{b=1}^{B}\sum_{h=1}^{H}\sum_{l=1}^{L}\left(\alpha\mu^m_{c_{hlb}} + \left(1-\alpha\right)\tau^m_{c_{hlb}}\zeta_{c_{hlb}}\right)}, \quad \forall c \tag{3.15}$$

$$v_c = \frac{1}{2}({}^1v_c + {}^2v_c), \forall c \tag{3.16}$$

In the next stage, we generate the IT2F-MF $\tau_{c_{hlb}}$ by using the LMFs $u_{c_{hlb}}$ as the secondary MFs. For the simplicity, let X denotes the set of all voxels in the 3D image volume and $J_{x_c} = \{{u_c}^1, {u_c}^2, ..., {u_c}^N\}$ denotes the set of N LMFs with respect to class

c within the local neighborhood of the center voxel x. We define the IT2FSs $\bar{A}_c$ as follows.

$$\bar{A}_c = \left\{ \left((x, u_c), \gamma_{\bar{A}_c}(x, u_c) = 1 \right) | \forall x \in X, \forall u_c \in J_{x_c} \subseteq [0, 1] \right\} \tag{3.17}$$

where $\gamma_{\bar{A}_c}(x, u_c)$ denotes the secondary membership function with respect to class c.

Additionally, (3.17) can also be expressed by footprint of uncertainty of $\bar{A}_c$ as $FOU(\bar{A}_c)$, which is confined by lower MF of $\bar{A}_c$ $(L(\bar{A}_c))$ or $\underline{\gamma}_{\bar{A}_c}(u_c)$ and upper MF of $\bar{A}_c$ $(U(\bar{A}_c))$ or $\bar{\gamma}_{\bar{A}_c}(u_c)$. The secondary MF is then expressed as follows.

$$\gamma_{\bar{A}_c}(x, u_c) \equiv \gamma_{\bar{A}_c}(u_c) = \int_{u_c \in J_{x_c}} \left[\underline{\gamma}_{\bar{A}_c}(u_c), \bar{\gamma}_{\bar{A}_c}(u_c) \right] \tag{3.18}$$

The upper and lower MFs are formulated as follows.

$$\bar{\gamma}_{\bar{A}_c}(u_c) = \begin{cases} \mathrm{Y}(m_1, \sigma; u_c), & if\ u_c < m_1 \\ 1 \qquad\qquad , & if\ m_1 \leq u_c \leq m_2 \\ \mathrm{Y}(m_2, \sigma; u_c), & if\ u_c > m_2 \end{cases} \tag{3.19}$$

$$\underline{\gamma}_{\bar{A}_c}(u_c) = \begin{cases} \mathrm{Y}(m_2, \sigma; u_c), & if\ u_c \leq \frac{m_1 + m_2}{2} \\ \mathrm{Y}(m_1, \sigma; u_c), & if\ u_c > \frac{m_1 + m_2}{2} \end{cases} \tag{3.20}$$

$$\mathrm{Y}(m_i, \sigma; u_c) = e^{\frac{(u_c - m_i)^2}{2 \times \sigma^2}}, i = 1, 2 \tag{3.21}$$

where a and σ specify the mean and standard deviation of $\{J_{x_c}\}$, correspondingly. Again, $m_1 = a - \sigma$ and $m_2 = a + \sigma$.

Finally, we perform the type reduction using the following equation to generate the crisp outputs from $\bar{A}_c$ by using simplified form of Nie-Tan method [69].

$$\tau_{c_{hlb}} = \tau_{c_x} = \frac{\sum_{t=1}^{N} u_c^t \times \left(\underline{\gamma}_{\bar{A}_c}(u_c^t) + \bar{\gamma}_{\bar{A}_c}(u_c^t) \right)}{\sum_{t=1}^{N} \left(\underline{\gamma}_{\bar{A}_c}(u_c^t) + \bar{\gamma}_{\bar{A}_c}(u_c^t) \right)}, \forall c, x, h, l, b \quad (3.22)$$

Finally, we calculate the final MFs $f_{c_{hlb}}$ by combining the GMFs and T2FMFs, weighted according to two positive regulating factors as follows.

$$f_{c_{hlb}} = \frac{(\mu_{c_{hlb}})^p (\tau_{c_{hlb}})^q}{\sum_{t=1}^{C} (\mu_{t_{hlb}})^p (\tau_{t_{hlb}})^q} \quad (3.23)$$

The formulation of IT2F-MFs is presented in FIGURE 3.1 in a graphical manner.

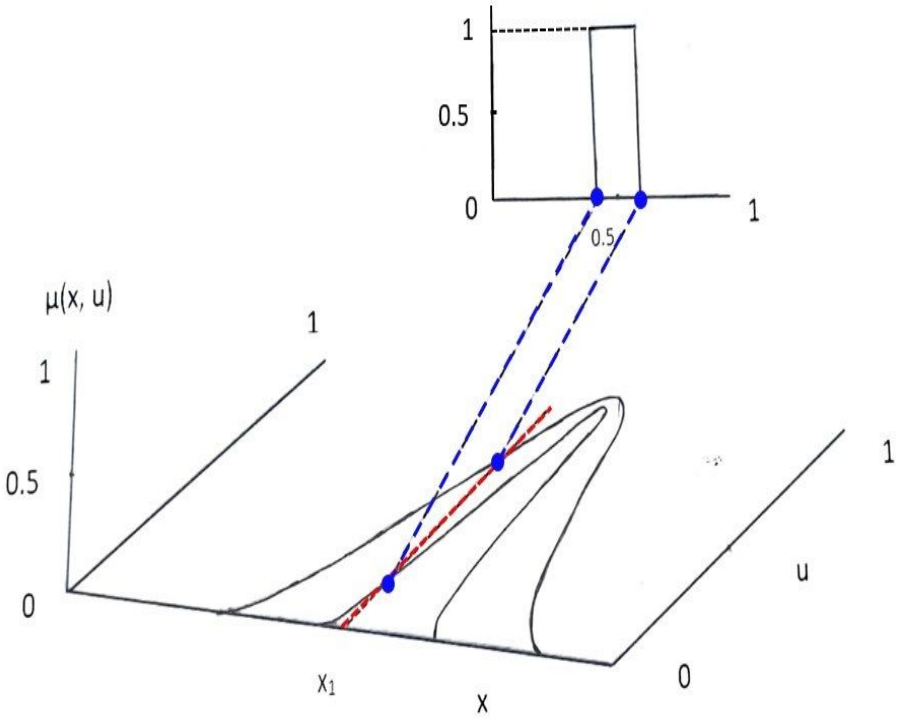

FIGURE 3.1: Graphical view of the suggested IT2F-MFs.

The suggested algorithm is summarized below for easier comprehension.

FIGURE 3.2 shows flow diagram of the developed method.

Algorithm 2: MOET1IT2FCM

Input: Three-dimensional magnetic resonance imaging of the brain of size $B \times H \times L$

Output: Segmented 3D CSF, GM, WM regions

Assign the values to p, q, m, iteration number $j = 0$ and error threshold ϵ;
Extract brain portion by using skull stripping algorithm;
Assign value to the cluster center $v_c^{(j)}, \forall c$ from the image histogram;
Initialize the GMFs $\mu_{c_{hlb}}$ and the LMFs $u_{c_{hlb}}$;
repeat
    Calculate the GMFs $\mu_{c_{hlb}}^{(j+1)}, \forall c, b, h, l$ by using (3.12);
    Calculate the class-level possibility parameter $\zeta_{c_{hlb}}, \forall c, b, h, l$ by using (3.11);
    Calculate the LMFs $u_{c_{hlb}}^{(j+1)}, \forall c, b, h, l$ by using (3.13);
    Generate the IT2F-MFs $\tau_{c_{hlb}}^{(j+1)}, \forall c, b, h, l$ by using (3.17)-(3.22);
    Calculate the cluster centers by using (3.14) and (3.15);
    Calculate the final cluster centres ${v_c}^{j+1}, \ \forall c$ by using (3.16);
    $j = j + 1$;
until $|| v_c^{(j)} - v_c^{(j-1)} || < \varepsilon, \forall c$
Determine the final fuzzy MF $f_{c_{hlb}}, \forall c, b, h, l$ by using (3.23);
Obtain the final cluster centers $V = \{v_1, v_2, v_3, ..., v_C\}$ and the membership matrix $F = \{f_{c_{hlb}}\}, \forall c, b, h, l$;
Allocate the voxel $x_{hlb}, \forall b, h, l$ to a class that produces the highest value of membership;

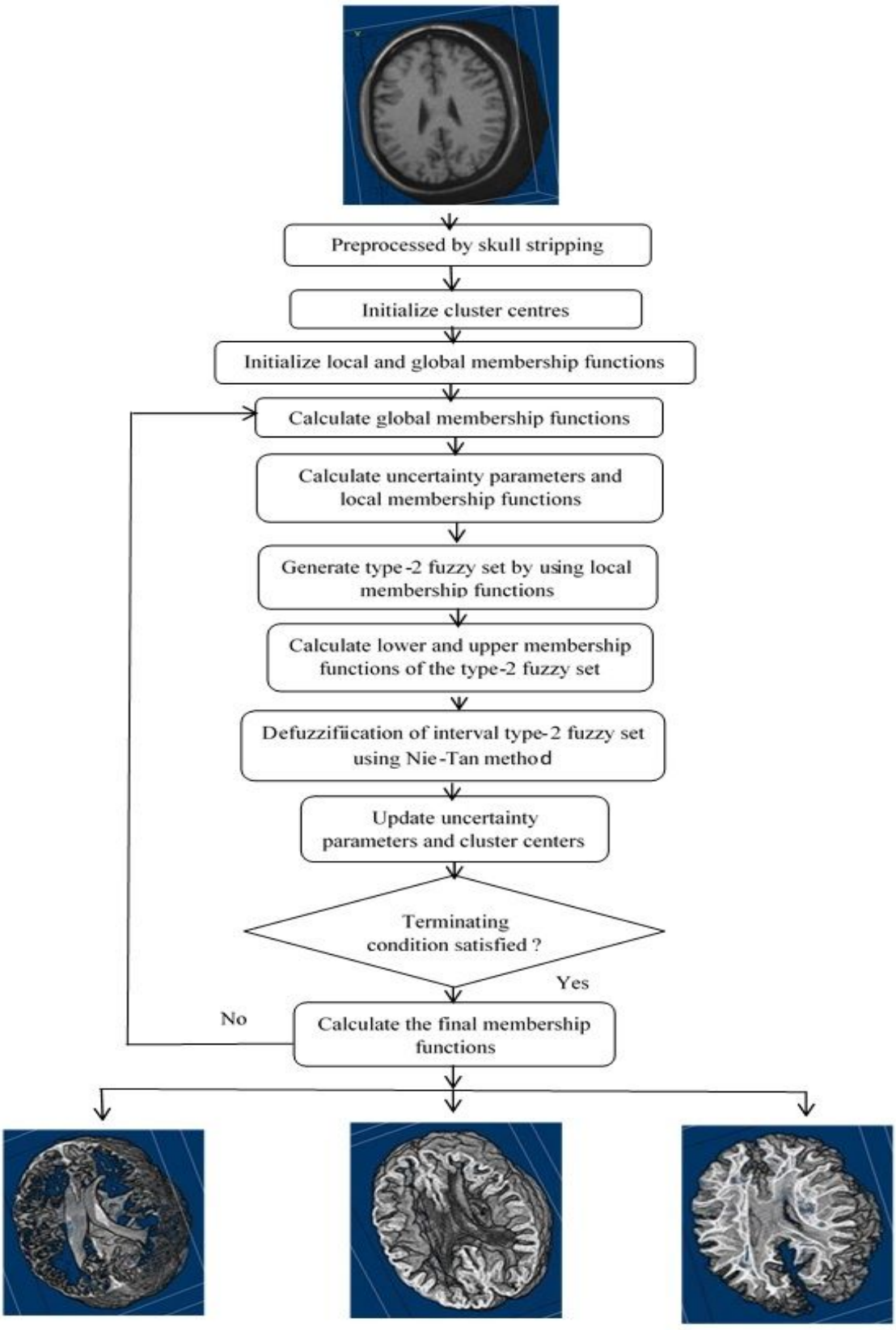

FIGURE 3.2: Work flow of the developed method.

3.5 Experiments

We analyze the effectiveness of the suggested algorithm by performing several experiments on different volumes of brain MR images. In doing so, we use 4 volumes of simulated BrainWeb images, 5 volumes of IBSR images, 4 volumes of clinical actual patients' MR images of brain and one volume of synthetic images, which is corrupted by high Rician noise. We use the BrainWeb [59] database with varying degrees of inhomogeneity (IIH) (20%-40%) and noise (1%-9%). To be specific, we utilize data volumes with high noise 7% and 9% and IIH with 20% and 40%. It may be stated that the image volume is $181 \times 217 \times 181$ $(height \times width \times depth)$ in size and thickness of voxel is $1 \times 1 \times 1$ mm^3. The IBSR image volume size is $256 \times 256 \times 128$ $(height \times width \times depth)$ with $1.5m^3$ of spacing. The resolutions of MR image volumes of clinical actual patient are $1105 \times 649 \times 20$, $552 \times 325 \times 58$, $256 \times 150 \times 20$ and $350 \times 206 \times 20$. Having four non-overlapping regions, the synthetic image volume is $200 \times 200 \times 80$. It may be noted that we segment a brain MR image into four regions as, the gray matter (GM), white matter (WM) and cerebro spinal fluid (CSF) and background.

3.5.1 Estimation of optimal parameters of the algorithm

We achieve optimal results of the presented algorithm utilizes different controlling factors, (a) fuzzifier weight m, (b) regularizing factor α, (c) two weighted parameters p and q and (d) neighborhood window size. First, we carry out experiments with various combination of p and q by using $m = 4.75, \alpha = 0.8$ and neighboring window size as $3 \times 3 \times 3$. FIGURE 3.3 shows the outcomes of the experiment expressed in terms of the dice similarity coefficient (DSC) over the MR image volume of the

brain with high noise (9%) and high IIH (40%). The results indicate that at $(p,q) = (4,3)$ the algorithm generates optimal results. Next, we study how well the algorithm performs using different data volumes by using different window sizes, keeping $m = 4.75$, $(p,q) = (4,3)$ and $\alpha = 0.8$. FIGURE 3.4 shows that with the neighboring window size as $3 \times 3 \times 3$, the DSC value attains maximum. Finally, by using the same data volume, we conduct the experiments with different values of m, keeping $(p,q) = (4,3)$, neighboring window size = $3 \times 3 \times 3$, and $\alpha = 0.8$. FIGURE 3.5 shows the results, which indicate that at $m = 4.75$ the algorithm yields better result. Similarly, for IBSR image volumes we conduct the same procedure to obtain the optimal values of these parameters as m = 2.00, (p,q) = (2,3) and neighboring window size = $3 \times 3 \times 3$.

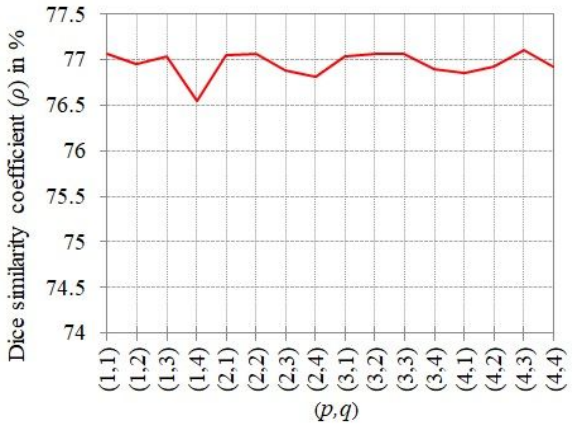

FIGURE 3.3: Dice similarity coefficients through varying combinations of (p,q).

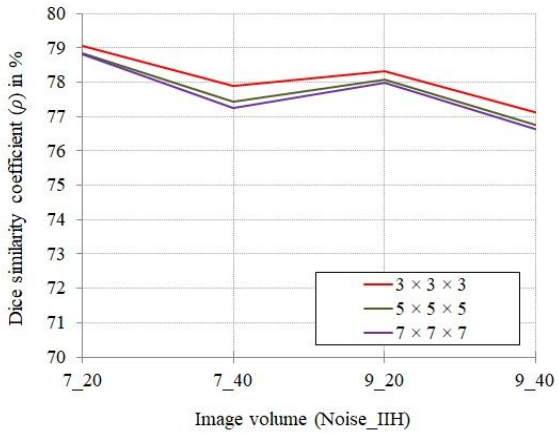

FIGURE 3.4: Dice similarity coefficients through varying window sizes.

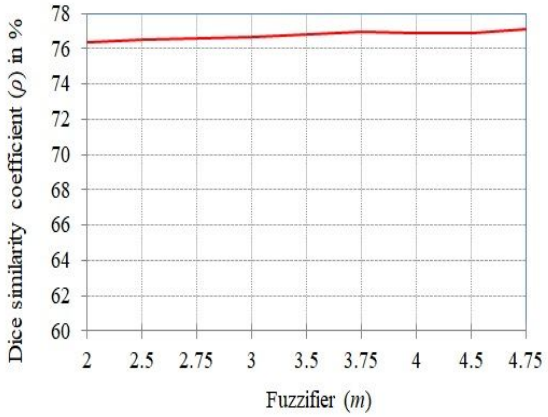

FIGURE 3.5: Dice similarity coefficients through different values of m.

3.5.2 Qualitative Analysis

The qualitative analysis represents the perceptible outcome of the suggested algorithm. At first, we investigate the suggested algorithm's performance on the volumes of simulated brain MR images, secondly, on the image volumes of the IBSR, next on the clinical data volumes and at the end on a noisy synthetic image volume.

BrainWeb image volumes

In this section, we display the outputs generated by the developed algorithm. Among the four volumes, we present the results of a volume with 9% noise and 40% IIH in or, FIGURE 3.6. To show the effectiveness, we also show the ground truths of these regions. Additionally, we also show the cross-sectional views of the segmented regions for better visualization. A thorough examination shows that the segmented outputs are very close to the ground truths; thereby demonstrating its efficacy. In addition, the ground truth's two-dimensional color mapped and the segmented image volumes are shown in or, FIGURE 3.7 for better understanding.

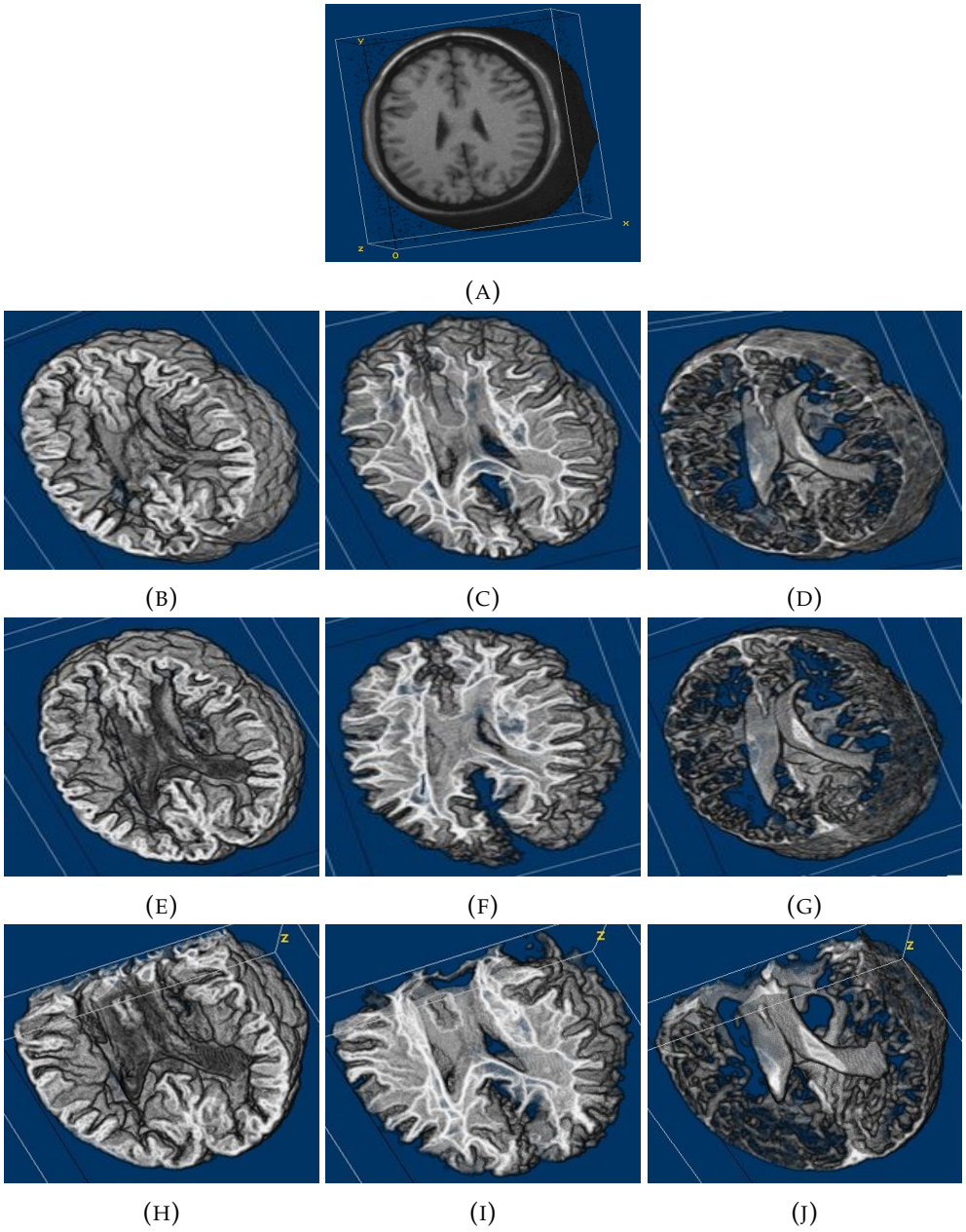

(A)

(B) (C) (D)

(E) (F) (G)

(H) (I) (J)

FIGURE 3.6: Outputs on BrainWeb data. (A): Input; (B)-(D): Ground truths of the GM, WM and CSF, correspondingly; (E)-(G): Outputs of the GM, WM and CSF, correspondingly and (H)-(J): Cross-sectional view of the GM, WM and CSF, correspondingly.

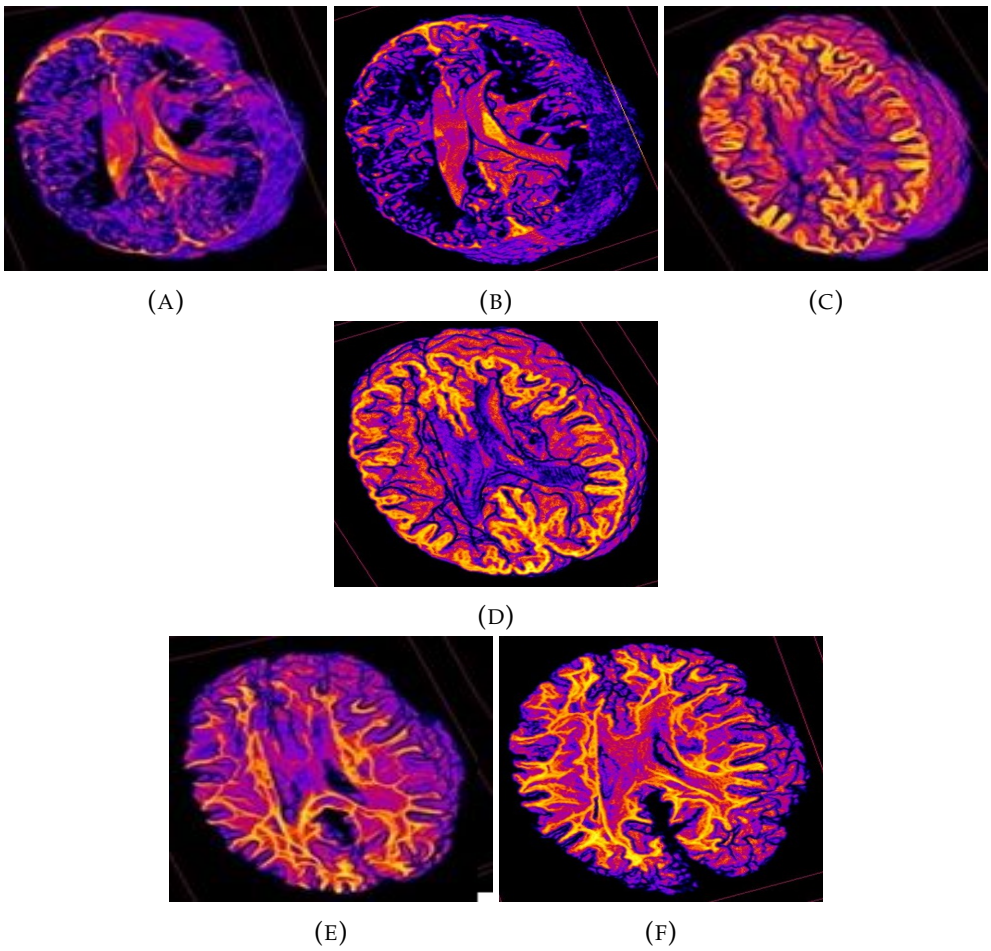

(A) (B) (C)

(D)

(E) (F)

FIGURE 3.7: 2D color mapped of the ground truth and the segmented image volumes. (A)-(B): Ground truth and segmentation of the CSF region, correspondingly; (C)-(D): Ground truth and segmentation of the GM region, correspondingly; (E)-(F): Ground truth and segmentation of the WM region, correspondingly.

IBSR image volumes

Like the previous section, we present the outputs of the algorithm along with the ground truths and cross-sectional views in FIGURE 3.8. Additionally, for a deeper comprehension, we present the two-dimensional color mapped of ground truth and the segmented image volumes in FIGURE 3.9. Again, the results are promising as compared to the ground truths.

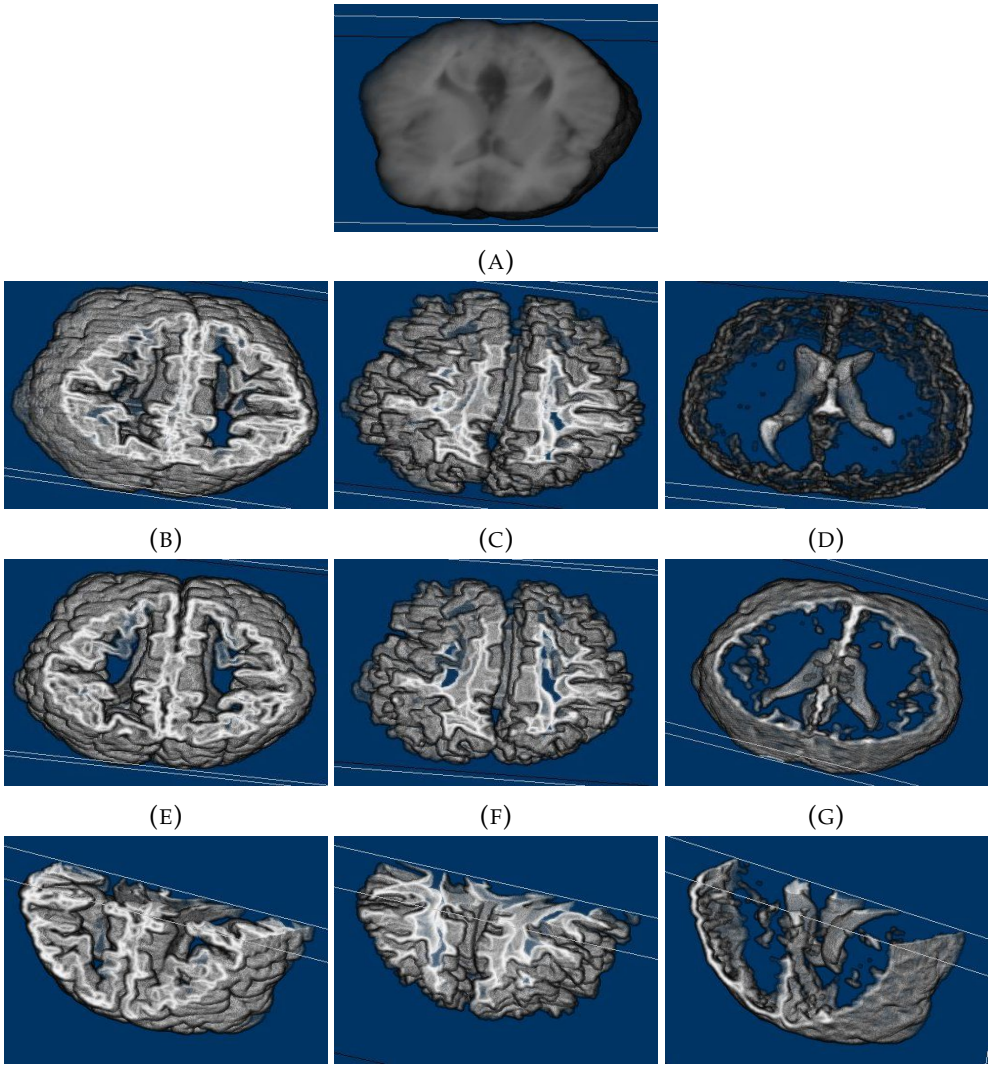

(A)

(B) (C) (D)

(E) (F) (G)

(H) (I) (J)

FIGURE 3.8: Outputs on IBSR data. (A): Input; (B)-(D): Ground truths of the GM, WM and CSF, regions, correspondingly; (E)-(G): Outputs of the GM, WM and CSF, correspondingly and (H)-(J): Cross-sectional view of the GM, WM and CSF regions, correspondingly.

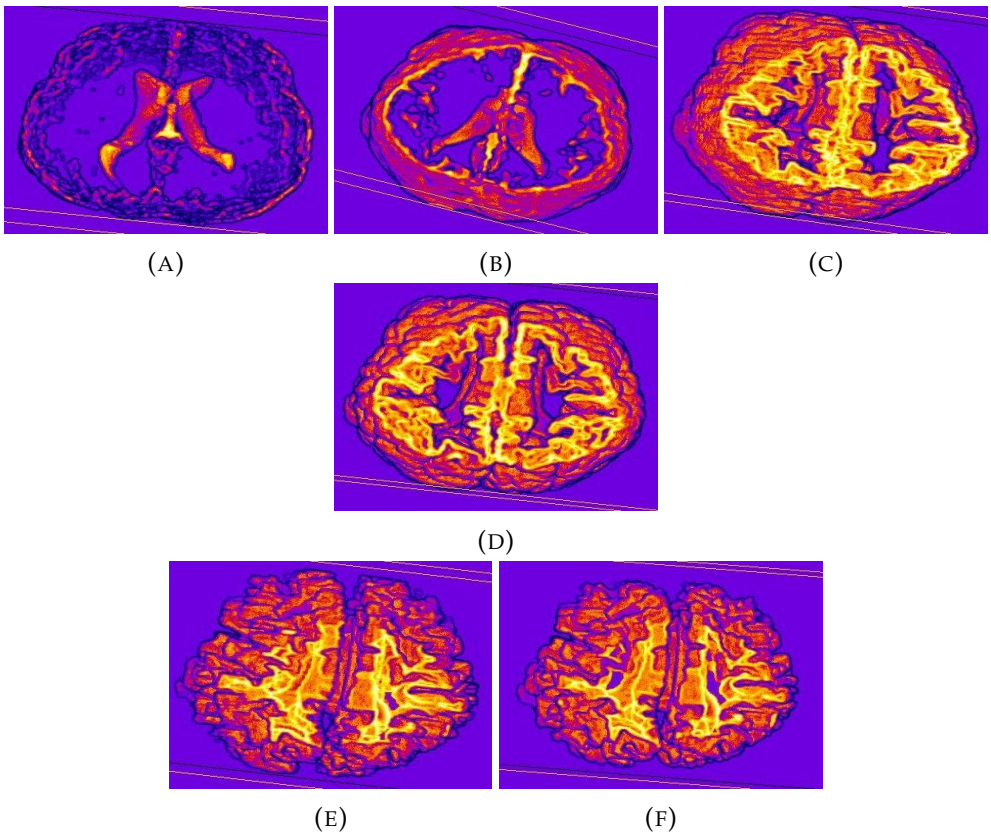

FIGURE 3.9: 2D color mapped of an IBSR image volume. (A)-(B): Ground truth and the segmented image of the CSF region, correspondingly; (C)-(D): Ground truth and the segmented image of the GM region, correspondingly; (E)-(F): Ground truth and the segmented image of the WM region, correspondingly.

Clinical Image Volumes

Among the four volumes of clinical data, the outputs of one such volume is presented in FIGURE 3.10. Further, better visualization, we also show the two-dimensional color mapped volumes and the cross-sectional views.

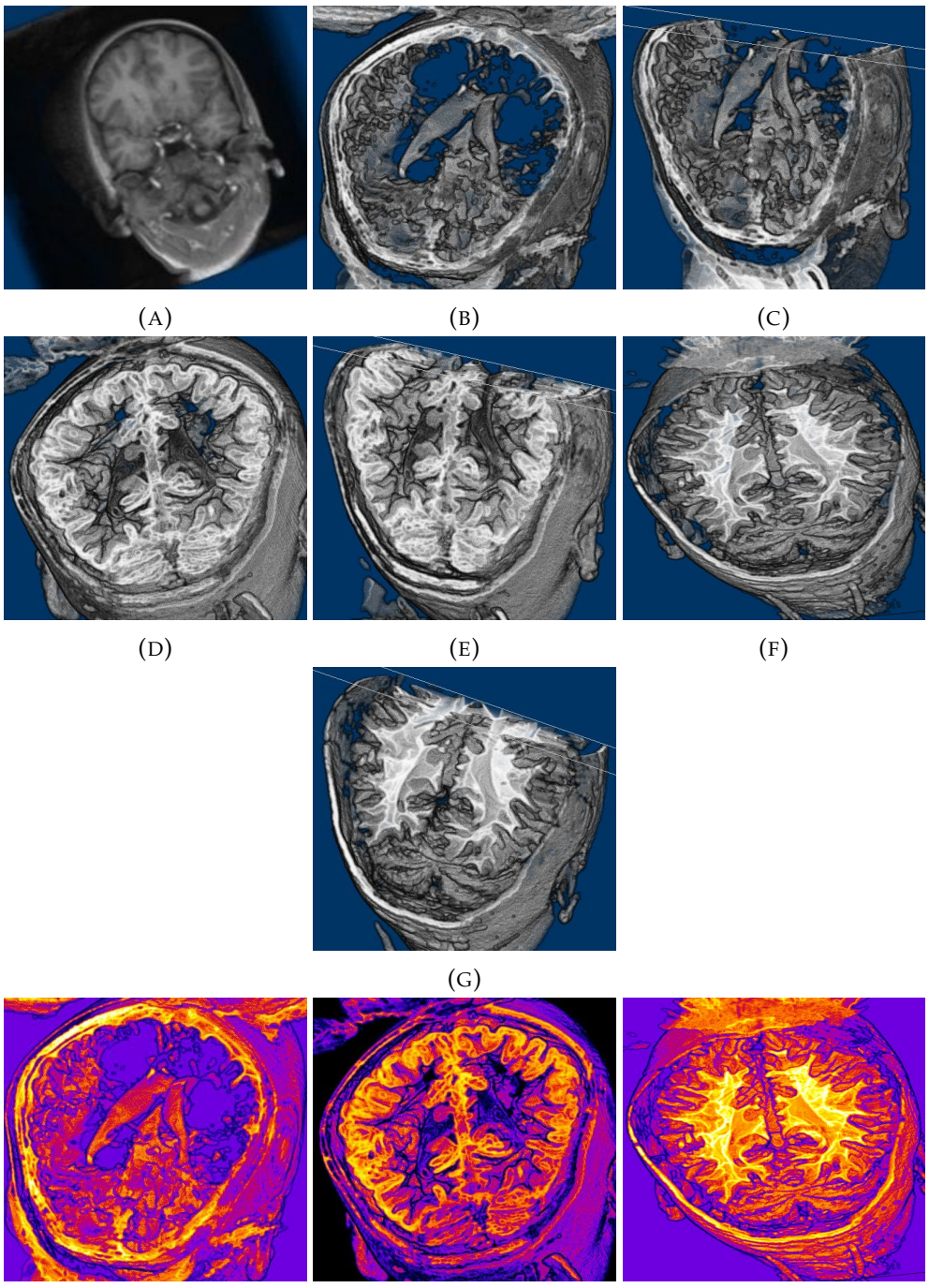

(A) (B) (C)

(D) (E) (F)

(G)

(H) (I) (J)

FIGURE 3.10: Segmented outcome of a clinical actual patient MR image volume of brain. (A): Input volume of images; (B), (D), and (F): Segmented outcome of CSF, GM and WM regions, correspondingly; (C), (E) and (G): Cross-sectional view of the CSF, GM and WM regions, correspondingly; (H)-(J): The segmented CSF, GM and WM regions by means of 2D color mapped, correspondingly.

Synthetic image volume

In this study, we show the segmentation results on a noisy volume of synthetic images. To make it noisy, we add the Rician noise manually. Generally, it is believed that the behavior of IIH in MR image is quite similar to that of Rician noise [60]. FIGURE 3.11 show the synthetic volume, its noisy version and the segmented volume. Here also, results prove its efficacy.

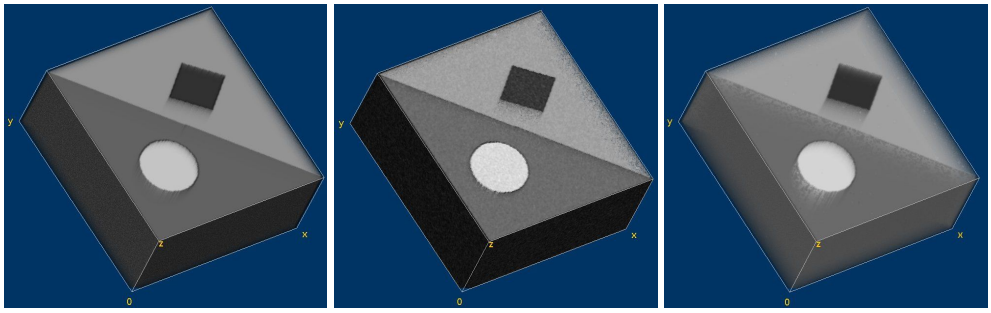

(A) (B) (C)

FIGURE 3.11: The outcome of segmented image volume of synthetic images including Rician noise. (A) Input volume of images; (B)-(C) Noisy and segmented image volumes, respectively.

3.5.3 Quantitative study

In this study, Several comparative performance analyses are presented between the developed algorithm and other similar algorithms by using different indices, namely (i) segmentation accuracy (SA), (ii) tissue segmentation accuracy (TSA), (iii) Dice similarity coefficient (ρ), (iv) partition coefficient (v_{pc}) and (v) partition entropy (v_{pe}) [31].

BrainWeb image volumes

This section presents the efficacy of the suggested algorithm along with other alike state-of-the-art algorithms like, MEI [49], REFCM [51], MEFCM [50], MREFCM [52] and the UPWEFCM [28]

algorithms. TABLE 3.1 presents the comparative results among the competitive methods using SA as a performance index. Results show that baring two cases, the suggested algorithm yields better results. In addition, we conduct t-test to examine whether this improvement is statistically significant or not by setting null hypothesis H_0 and the alternate hypothesis H_1 as defined by Ray et al. [28]. The outcome of this test is shown in TABLE 3.2, where it proves that in all most all the cases the improvement is significant at $p = 0.01$; thus proving its supremacy over the other methods.

TABLE 3.1: Segmentation results over brain MR simulated image volumes for SA index. Bold text designates the highest value.

(Noise,IIH)	Region	Developed algorithm	UPWEFCM	MEI	REFCM	MEFCM	MREFCM
7,20	WM	0.950	**0.960**	0.918	0.959	0.943	0.960
	GM	**0.918**	0.901	0.860	0.766	0.791	0.836
	CSF	**0.910**	0.887	0.851	0.849	0.780	0.830
7,40	WM	**0.920**	0.920	0.896	0.843	0.920	0.914
	GM	**0.900**	0.845	0.875	0.840	0.776	0.839
	CSF	**0.910**	0.888	0.841	0.842	0.775	0.834
9,20	WM	0.940	**0.951**	0.864	0.891	0.902	0.949
	GM	**0.901**	0.891	0.807	0.772	0.722	0.846
	CSF	**0.893**	0.880	0.772	0.808	0.690	0.825
9,40	WM	**0.910**	0.910	0.846	0.767	0.891	0.888
	GM	**0.888**	0.874	0.789	0.796	0.711	0.843
	CSF	**0.890**	0.880	0.760	0.797	0.688	0.835

TABLE 3.2: The calculative results of statistically significant analysis for the SA index

Region	Paired t-test(1-tailed)	Developed algorithm	UPWEFCM	MEI	REFCM	MEFCM	MREFCM
WM	Mean of SA	0.93	0.935	0.881	0.865	0.914	0.927
	value	-	0.0912	0.014	0.065	0.075	0.392
GM	Mean of SA	0.901	0.877	0.832	0.793	0.75	0.841
	value	-	0.052	0.014	0.006	0.001	0.002
CSF	Mean of SA	0.895	0.882	0.783	0.811	0.710	0.832
	value	-	0.008	0.002	0.001	0.001	0.001

Similarly, for TSA, we present the comparative performance and statistically significant analysis in TABLE 3.3 and TABLE 3.4, correspondingly. The findings demonstrate that the recommended method outperforms all other approaches. Further, excluding in three cases, at $p = 0.01$, this improve performance is statistically significant.

TABLE 3.3: Comparative performance among the different methods over the simulated brain MR image volumes using TSA. Bold text designates the highest value.

(Noise, IIH)	Region	Developed algorithm	UPWEFCM	MEI	REFCM	MEFCM	MREFCM
7-20	WM	**0.867**	0.866	0.795	0.780	0.785	0.812
	GM	**0.811**	0.800	0.762	0.737	0.755	0.753
	CSF	**0.610**	0.597	0.578	0.575	0.540	0.551
7-40	WM	**0.850**	0.849	0.795	0.793	0.780	0.808
	GM	**0.790**	0.780	0.756	0.759	0.741	0.747
	CSF	**0.600**	0.591	0.568	0.541	0.535	0.554
9-20	WM	**0.861**	0.861	0.763	0.767	0.755	0.817
	GM	**0.801**	0.796	0.723	0.726	0.705	0.758
	CSF	**0.600**	0.598	0.522	0.516	0.473	0.556
9-40	WM	**0.850**	0.845	0.761	0.749	0.751	0.805
	GM	**0.781**	0.776	0.718	0.714	0.695	0.747
	CSF	**0.590**	0.588	0.510	0.486	0.468	0.552

TABLE 3.4: The calculative results of statistically significant analysis for the TSA index.

Region	Paired t-test(1-tailed)	Developed algorithm	UPWEFCM	MEI	REFCM	MEFCM	MREFCM
WM	Mean of TSA	0.846	0.855	0.803	0.771	0.770	0.795
	value	-	0.242	0.122	0.003	0.002	0.001
GM	Mean of TSA	0.795	0.788	0.739	0.734	0.724	0.751
	value	-	0.008	0.004	0.004	0.004	0.001
CSF	Mean of TSA	0.600	0.593	0.544	0.529	0.504	0.553
	value	-	0.048	0.013	0.009	0.005	0.0001

Further, we conduct the comparative performance analysis regarding the partition coefficient v_{pc}, partition entropy v_{pe} and Dice similarity coefficient ρ and present the results in FIGURE 3.12 - FIGURE 3.14, correspondingly. The outcomes revile that

the suggested algorithm outperforms all other alternative techniques.

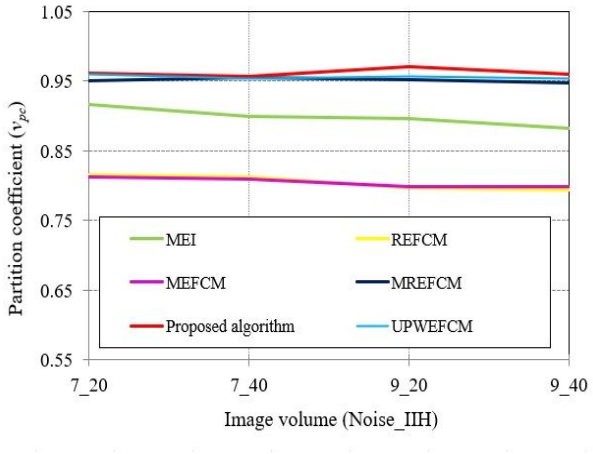

FIGURE 3.12: Comparative results of different algorithms by using V_{pc} on simulated image volumes.

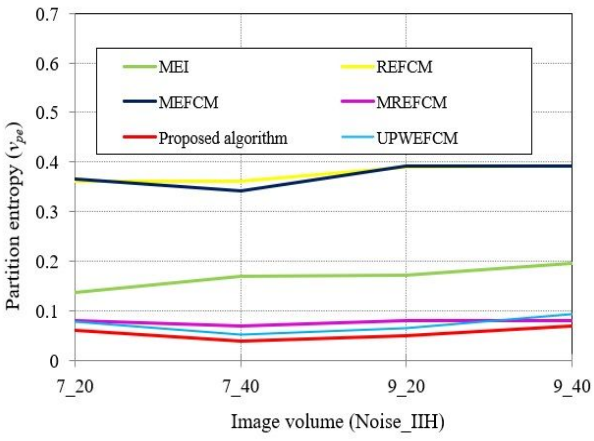

FIGURE 3.13: Comparative results of different algorithms by using V_{pe} on simulated image volumes.

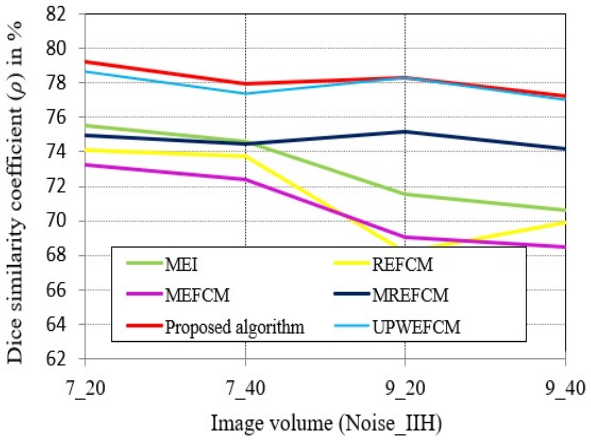

FIGURE 3.14: Comparative results of different algorithms by using ρ on simulated image volumes.

IBSR image volumes

In this study, we analyze the comparative performance between the suggested algorithm and the other methods on the IBSR image volumes. TABLE 3.5 shows the experimental results by using SA values. The results show that the suggested approach performs superior than the alternative approaches.

TABLE 3.5: SA values of different comparative algorithms on IBSR image volumes. Bold text designates the highest value.

(Noise,IIH)	Region	Developed algorithm	UPWEFCM	MEI	REFCM	MEFCM	MREFCM
vol 1	WM	**0.946**	0.901	0.925	0. 939	0.943	0.844
	GM	**0.701**	0.664	0.678	0.657	0.582	0.737
	CSF	**0.981**	0.900	0.904	0.907	0.938	0.797
vol 2	WM	**0.937**	0.900	0.914	0.935	0.889	0.882
	GM	**0.806**	0.744	0.683	0.746	0.684	0.791
	CSF	**0.986**	0.810	0.919	0.857	0.948	0.689
vol 5	WM	0.942	0.893	0.920	0.938	**0.952**	0.822
	GM	0.725	0.685	0.706	0.718	0.609	**0.780**
	CSF	**0.942**	0.804	0.840	0.824	0.881	0.652
vol 15	WM	0.912	0.855	0.925	0.911	**0.946**	0.854
	GM	**0.748**	0.682	0.740	0.699	0.650	0.853
	CSF	**0.891**	0.841	0.813	0.876	0.887	0.518
vol 17	WM	0.895	0.850	0.900	0.919	**0.934**	0.817
	GM	**0.860**	0.760	0.648	0.709	0.678	0.862
	CSF	**0.927**	0.913	0.770	0.894	0.831	0.843

The statistical significant analysis is shown in TABLE 3.6. It shows that this improvement is statistically significant over all various comparative techniques, excepting the MREFCM method, at $p = 0.03$ for the WM region. For the GM region, compared to all other approaches, it is statistically significant at $p = 0.03$. In case of the CSF region, at $p = 0.01$, its improvement is significant than the MREFCM method.

TABLE 3.6: Results of statistical significance analysis for SA index on IBSR volumes.

Region	Paired t-test(1-tailed)	Developed algorithm	UPWEFCM	MEI	REFCM	MEFCM	MREFCM
WM	Mean of SA	0.926	0.880	0.917	0.926	0.933	0.844
	value	-	0.001	0.140	0.283	0.351	0.001
GM	Mean of SA	0.768	0.707	0.691	0.706	0.640	0.846
	value	-	0.002	0.062	0.030	0.001	0.078
CSF	Mean of SA	0.945	0.853	0.856	0.871	0.890	0.700
	value	-	0.017	0.004	0.014	0.012	0.004

Similarly, TABLE 3.7 presents the outcomes of both the suggested approach and the alternative approaches in terms of TSA. Here also the results of the suggested method appear better than those of the other algorithms. The statistical significant analysis is shown in TABLE 3.8 and it shows that in all most all cases its improvement is significant at p=0.01.

TABLE 3.7: Comparative TSA values on IBSR image volumes. Bold text indicates the highest values.

(Noise, IIH)	Region	Developed algorithm	UPWEFCM	MEI	REFCM	MEFCM	MREFCM
vol 1	WM	**0.949**	0.853	0.905	0.898	0.889	0.869
	GM	**0.806**	0.753	0.779	0.779	0.721	0.799
	CSF	0.376	**0.387**	0.200	0.284	0.266	0.289
vol 2	WM	**0.951**	0.881	0.918	0.917	0.913	0.886
	GM	**0.863**	0.801	0.784	0.827	0.791	0.831
	CSF	**0.347**	0.326	0.273	0.201	0.0.200	0.201
vol 5	WM	**0.954**	0.891	0.912	0.912	0.909	0.859
	GM	**0.818**	0.736	0.796	0.811	0.739	0.808
	CSF	**0.351**	0.306	0.200	0.200	0.201	0.230
vol 15	WM	**0.950**	0.899	0.942	0.938	0.945	0.896
	GM	**0.818**	0.780	0.842	0.792	0.769	0.866
	CSF	**0.310**	0.304	0.212	0.200	0.200	0.205
vol 17	WM	**0.936**	0.883	0.914	0.915	0.912	0.862
	GM	**0.884**	0.847	0.759	0.842	0.789	0.866
	CSF	0.412	**0.492**	0.287	0.334	0.230	0.386

TABLE 3.8: Results of statistical significance analysis for TSA index on IBSR image volumes.

Region	Paired t-test(1-tailed)	Developed algorithm	UPWEFCM	MEI	REFCM	MEFCM	MREFCM
WM	Mean of TSA	0.948	0.881	0.918	0.916	0.913	0.874
	p value	-	0.000	0.005	0.005	0.010	0.000
GM	Mean of TSA	0.838	0.783	0.792	0.810	0.761	0.834
	p value	-	0.001	0.074	0.004	0.000	0.397
CSF	Mean of TSA	0.359	0.324	0.234	0.243	0.219	0.262
	p value	-	0.142	0.001	0.000	0.000	0.004

In FIGURE 3.15– FIGURE 3.17, we also visually represent the comparative outcomes of the various methods in terms of v_{pc},

v_{pe}, and ρ, respectively. The results clearly indicate the suggested method's superiority over competing techniques.

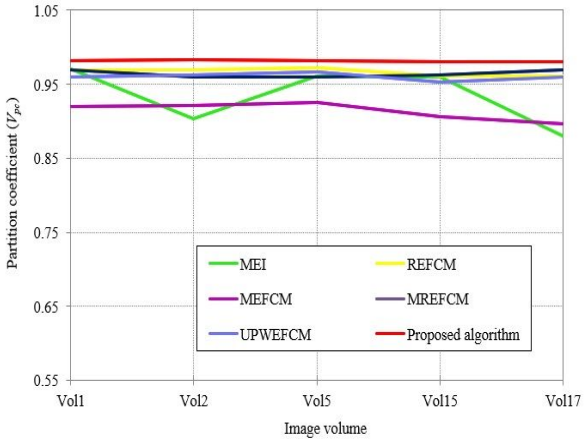

FIGURE 3.15: Comparative results of V_{pc} on IBSR image volumes.

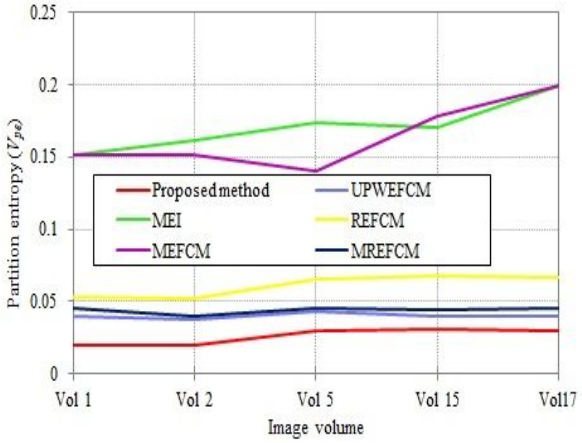

FIGURE 3.16: Comparative results of V_{pe} on IBSR image volumes.

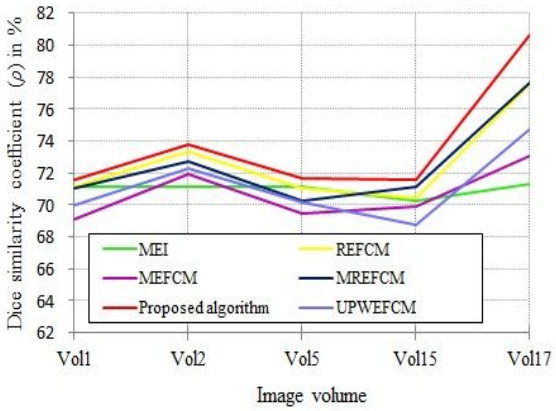

FIGURE 3.17: Comparative results of ρ on IBSR image volumes.

Clinical image volumes

We present the investigation outcomes of the suggested method along with other different methods over brain MR image volumes of actual patient in TABLE 3.9. Additionally, the experiment's results clearly demonstrate its superiority over all other comparative techniques.

TABLE 3.9: Comparative results on actual patient MR image volumes of brain. Bold text indicates the highest values.

Volume	Method	v_{pc}	v_{pe}
	Developed algorithm	0.992	0.01
	UPWEFCM	0.990	0.021
	MEI	0.960	0.040
Patient 1	REFCM	0.891	0.343
	MEFCM	0.915	0.171
	MREFCM	0.991	0.012
	Developed algorithm	0.986	0.011
	UPWEFCM	0.983	0.030
	MEI	0.890	0.153
Patient 2	REFCM	0.837	0.331
	MEFCM	0.888	0.217
	MREFCM	0.993	0.009
	Developed algorithm	0.985	0.023
	UPWEFCM	0.970	0.050
	MEI	0.965	0.080
Patient 3	REFCM	0.931	0.126
	MEFCM	0.946	0.104
	MREFCM	0.990	0.014
	Developed algorithm	0.987	0.023
	UPWEFCM	0.980	0.054
	MEI	0.960	0.040
Patient 4	REFCM	0.875	0.264
	MEFCM	0.912	0.182
	MREFCM	0.981	0.017

Noisy synthetic image volume

In this study, we provide the performance analysis of the suggested method on a Rician noise additive noisy synthetic image volume. TABLE 3.10 presents the results of the suggested method and other comparative methods. The findings again suggest its superiority over the alternative approaches.

TABLE 3.10: Results of an experiment using a synthetic image volume that is noisy.

Index	Segmented Region	Developed Method	UPWEFCM
SA	Black	**0.838**	0.820
	Gray	**0.986**	0.985
	Light white	**0.982**	0.980
	White	**0.962**	0.960
Dice similarity coefficient		**0.956**	0.947
v_{pc}		**0.997**	0.980
v_{pe}		**0.004**	0.051

Let size of the 3D brain MR image be S, where $S = H \times L \times B$ (height $\times$ width $\times$ depth) be the volume. The algorithm segments the volume of the images into R different regions according to the background regions, GM, WM, and CSF regions. At first, the presented algorithm calculates global fuzzy membership matrix (FMM) (G), class-level possibility matrix (U), local FMM (L) and lastly, interval type-2 FMM (I). The voxels are classified once the final FMM (F) is computed. First, the presented algorithm calculates the Euclidean distance between the cluster centers and the image voxels. Hence, $O(SR)$ is the total time needed to compute the global FMM matrix. The computational cost of class-level possibility matrix is $O(SR)$. For local FMM calculation, it determines the mean of distances between the neighboring voxels of size $O(N_W)$ and center voxel. So, total computational cost of local FMM is $O(SR + SN_W)$. The developed algorithm calculates interval type-2 FMM by taking $O(SR + SN_W)$ time. Finally, it calculates the cluster centers in $O(SR)$ time. Therefore, total computational cost in each iteration is $O(SR + SR + SR + SN_W + SR + SN_W + SR) \cong O(5SR + 2SN_W)$. Finally, it computes the final FMM in $O(SR)$ time.

For computation of the presented algorithm, the spaces required for 3D image volume, global FMM and local FMMs, mean distance matrix, Euclidean distance matrix, interval type-2 matrix, cluster center matrix and final FMM.

Space required for the volumetric image is $O(S)$. For the global FMM G, the required space is for distance matrix and the its space required for the previous iteration. So, the total space required for G is $O(SR + SR + SR) = O(3SR)$. Similarly, for local FMM, it is $O(SR + SR + SR) = O(3SR)$. The required space for class-level possibility matix U is $O(2SR)$ for IT2-FMM is $O(2SR)$ and for calculating cluster centre using local and global MFs required space is $O(2R)$, the cluster centre using global and IT2F-MFs required $O(2R)$ space and the final cluster center need $O(2R)$ space. So, the total space required for the cluster centre calculation is $O(2R) + O(2R) + O(2R) = O(6R)$ Final FMM requires $O(SR)$ space. So, the memory space consumed by the presented algorithm is $O(R) + O(3SR) + O(3SR) + O(2SR) + O(2SR) + O(6R) + O(SR)) \cong O(S + 11(SR) + 6R)$.

We conduct the experiments on a workstation computer that have a Intel Core i7 processor and RAM size as 32 GB. The coding is done using the C programming language in Fedora operating systems environment.

3.6 Conclusion

In this suggested work, we present a multi-objective framework utilizing relative entropy-based T1 and IT2FCM algorithms for segmentation of volumetric brain MR images. This framework utilizes three MFs namely, (i) global fuzzy MFs, (ii) class-level

possibility parameter weighted local fuzzy MFs and (iii) IT2F-MFs. It generates two set of cluster centers using the aforesaid fuzzy MFs. Finally, it generates the final cluster centers by taking arithmetic mean of these cluster centers. Further, it integrates the GMFs and IT2F-MFs utilizing two positive parameters to produce the final fuzzy MF depending on which the voxels are categorized within the recognized classes. This framework utilizes the underlying relationship among the voxels by means of various fuzzy MFs. We investigate the effectiveness of the presented algorithm by using (i) four volumes of simulated brain MR images with high IIH and noise, (ii) five volumes of the IBSR MR images of brain, (iii) four volumes of actual patients' MR images of brain and (iv) a Rician noise additive synthetic image volume. The experimental results establish its superiority over some other similar state-of-the-art methods, which are developed in recent times.

The limitation of this method arises when the intensity values of voxels of different regions appear similar within a close neighborhood. This results misclassification of voxels and yields poor segmentation. This can be addressed by using higher degree of fuzzy MFs in addition with selecting dynamic neighborhood region. To address this issue, the next chapter presents a FCM-based algorithm by incorporating fuzzy entropy.

Appendix A

Derivation of the iterative equations

The objective function (3.4) can be rewritten with the help of the Lagrange multipliers by incorporating the associated constraints, as given below.

$$J_1 = \sum_{c=1}^{C}\sum_{b=1}^{B}\sum_{h=1}^{H}\sum_{l=1}^{L}\left(\alpha\mu_{c_{hlb}}^{m}d_{c_{hlb}}^{2} + (1-\alpha)u_{c_{hlb}}^{m}\bar{d}_{c_{hlb}}^{2}\zeta_{c_{hlb}})\right) - \sum_{b=1}^{B}\sum_{h=1}^{H}\sum_{l=1}^{L}\sum_{c=1}^{C}\left(\mu_{c_{hlb}}^{m}\ln\left(\frac{\mu_{c_{hlb}}^{m}}{u_{c_{hlb}}^{m}}\right)\right) - \sum_{b=1}^{B}\sum_{h=1}^{H}\sum_{l=1}^{L}\left(\lambda_{hlb}\sum_{c=1}^{C}(\mu_{c_{hlb}}-1) + \gamma_{hlb}\sum_{c=1}^{C}(u_{c_{hlb}}-1)\right) \tag{A.1}$$

By carrying out partial derivatives of (A.1) with respect to $\mu_{c_{hlb}}$, $u_{c_{hlb}}$ and v_c and equating them to zero, we get the corresponding final iterative equations of these parameters. The detailed procedure is given below.

$$\frac{\delta J_1}{\delta \mu_{c_{hlb}}} = 0; \tag{A.2}$$

$$\frac{\delta J_1}{\delta u_{c_{hlb}}} = 0; \tag{A.3}$$

$$\frac{\delta J_1}{\delta v_c} = 0; \tag{A.4}$$

By using (A.2), the calculations of $\mu_{c_{hlb}}$ is given below.

$$\alpha\, m\, \mu_{c_{hlb}}^{m-1}\, d_{c_{hlb}}^2 + \ln\left(\frac{\mu_{c_{dhw}}^m}{u_{c_{hlb}}^m}\right) m\, \mu_{c_{hlb}}^{m-1} - \mu_{c_{hlb}}^m \frac{1}{\frac{\mu_{c_{hlb}}^m}{u_{c_{hlb}}^m}} \frac{u_{c_{hlb}}^m\, m\, \mu_{c_{hlb}}^{m-1}}{u_{c_{hlb}}^{m\ 2}} - \lambda_{hlb} = 0 \tag{A.5}$$

$$m\, \mu_{c_{hlb}}^{m-1}\left[\alpha\, d_{c_{hlb}}^2 - \ln\left(\frac{\mu_{c_{hlb}}^m}{u_{c_{hlb}}^m}\right) - 1\right] = \lambda_{hlb} \tag{A.6}$$

or,

$$\mu_{c_{hlb}}^{m-1} = \left(\frac{\lambda_{hlb}}{m\left[\alpha\, d_{c_{hlb}}^2 - \ln\left(\frac{\mu_{c_{hlb}}^m}{u_{c_{hlb}}^m}\right) - 1\right]}\right) \tag{A.7}$$

or,

$$\mu_{c_{hlb}} = \left(\frac{\lambda_{hlb}}{m\left[\alpha\, d_{c_{hlb}}^2 - \ln\left(\frac{\mu_{c_{hlb}}^m}{u_{c_{hlb}}^m}\right) - 1\right]}\right)^{\frac{1}{m-1}} \tag{A.8}$$

Since, $\sum_{i=1}^{C} \mu_{i_{hlb}} = 1$, by replacing the value of $\mu_{i_{hlb}}$ in (A.7), the following equation has been derived.

$$\sum_{i=1}^{C}\left(\frac{\lambda_{hlb}}{m\left[\alpha\, d_{l_{hlb}}^2 - \ln\left(\frac{\mu_{i_{hlb}}^m}{u_{i_{hlb}}^m}\right) - 1\right]}\right)^{\frac{1}{m-1}} = 1 \tag{A.9}$$

$$\lambda_{hlb}^{\frac{1}{m-1}} = \frac{1}{\sum_{i=1}^{C}\left(\frac{1}{m\left[\alpha\, d_{i_{hlb}}^2 - \ln\left(\frac{\mu_{i_{hlb}}^m}{u_{i_{hlb}}^m}\right) - 1\right]}\right)^{\frac{1}{m-1}}} \tag{A.10}$$

We obtain the iterative equation of $\mu_{c_{hlb}}$, from (A.7) and (A.10). The equation of $\mu_{c_{hlb}}$ is defined below:

$$\mu_{c_{hlb}} = \frac{1}{\sum_{i=1}^{C} \left(\frac{m \left[\alpha \, d^2_{c_{hlb}} - \ln \left(\frac{\mu^m_{c_{hlb}}}{u^m_{c_{hlb}}} \right) - 1 \right]}{m \left[\alpha \, d^2_{i_{hlb}} - \ln \left(\frac{\mu^m_{i_{hlb}}}{u^m_{i_{hlb}}} \right) - 1 \right]} \right)^{\frac{1}{m-1}}} \tag{A.11}$$

or

$$\mu_{c_{hlb}} = \frac{1}{\sum_{i=1}^{C} \left(\frac{\left[\alpha \, d^2_{c_{hlb}} - \ln \left(\frac{\mu^m_{c_{hlb}}}{u^m_{c_{hlb}}} \right) - 1 \right]}{\left[\alpha \, d^2_{i_{hlb}} - \ln \left(\frac{\mu^m_{i_{hlb}}}{u^m_{i_{hlb}}} \right) - 1 \right]} \right)^{\frac{1}{m-1}}} \tag{A.12}$$

At the same way, by utilizing (A.3), the illustrations of $u_{c_{hlb}}$ is shown below.

$$(1 - \alpha) \, m \, u^{m-1}_{c_{hlb}} \, \bar{d}^2_{hlb} \, \zeta_{c_{hlb}} - \mu^m_{c_{hlb}} \frac{1}{\frac{\mu^m_{c_{hlb}}}{u^m_{c_{hlb}}}} \frac{-\mu^m_{c_{hlb}} \, m \, u^{m-1}_{c_{hlb}}}{u^{2}_{c_{hlb}{}^m}} - \gamma_{hlb} = 0 \tag{A.13}$$

$$(1 - \alpha) \, m \, u^{m-1}_{c_{hlb}} \, \bar{d}^2_{hlb} \, \zeta_{c_{hlb}} + \frac{\mu^m_{c_{hlb}}}{u^m_{c_{hlb}}} \, m \, u^{m-1}_{c_{hlb}} = \gamma_{hlb} \tag{A.14}$$

$$m \, u^{m-1}_{c_{hlb}} \left[(1 - \alpha) \, \bar{d}^2_{hlb} \, \zeta_{c_{hlb}} + \frac{\mu^m_{c_{hlb}}}{u^m_{c_{hlb}}} \right] = \gamma_{hlb} \tag{A.15}$$

or,

$$u^{m-1}_{c_{hlb}} = \left(\frac{\gamma_{hlb}}{m \left[(1 - \alpha) \, \bar{d}^2_{hlb} \, \zeta_{c_{hlb}} + \frac{\mu^m_{c_{hlb}}}{u^m_{c_{hlb}}} \right]} \right) \tag{A.16}$$

or,

$$u_{c_{hlb}} = \left(\frac{\gamma_{hlb}}{m \left[(1 - \alpha)\, \bar{d}^2_{hlb}\, \zeta_{c_{hlb}} + \frac{\mu^m_{c_{hlb}}}{u^m_{c_{hlb}}} \right]} \right)^{\frac{1}{m-1}} \tag{A.17}$$

Since, $\sum_{i=1}^{C} u_{i_{hlb}} = 1$, by replacing the value of $u_{i_{hlb}}$ in (A.17), the following equation has been generated.

$$\sum_{i=1}^{C} \left(\frac{\gamma_{hlb}}{m \left[(1 - \alpha)\, \bar{d}^2_{hlb}\, \zeta_{i_{hlb}} + \frac{\mu^m_{i_{hlb}}}{u^m_{i_{hlb}}} \right]} \right)^{\frac{1}{m-1}} = 1 \tag{A.18}$$

$$\gamma_{hlb}^{\frac{1}{m-1}} = \frac{1}{\sum_{i=1}^{C} \left(\frac{1}{m \left[(1-\alpha)\, \bar{d}^2_{hlb}\, \zeta_{i_{hlb}} + \frac{\mu^m_{i_{hlb}}}{u^m_{i_{hlb}}} \right]} \right)^{\frac{1}{m-1}}} \tag{A.19}$$

We obtain the final outcome of the iterative equation of $u_{c_{hlb}}$, from (A.17) and (A.19). The iterative equation of $u_{c_{hlb}}$ is defined below:

$$u_{c_{hlb}} = \frac{1}{\sum_{i=1}^{C} \left(\frac{m \left[(1-\alpha)\, \bar{d}^2_{hlb}\, \zeta_{c_{hlb}} + \frac{\mu^m_{c_{hlb}}}{u^m_{c_{hlb}}} \right]}{m \left[(1-\alpha)\, \bar{d}^2_{hlb}\, \zeta_{i_{hlb}} + \frac{\mu^m_{i_{hlb}}}{u^m_{i_{hlb}}} \right]} \right)^{\frac{1}{m-1}}} \tag{A.20}$$

or

$$u_{c_{hlb}} = \frac{1}{\sum_{i=1}^{C} \left(\frac{\left[(1-\alpha)\, \bar{d}^2_{hlb}\, \zeta_{c_{hlb}} + \frac{\mu^m_{c_{hlb}}}{u^m_{c_{hlb}}} \right]}{\left[(1-\alpha)\, \bar{d}^2_{hlb}\, \zeta_{i_{hlb}} + \frac{\mu^m_{i_{hlb}}}{u^m_{i_{hlb}}} \right]} \right)^{\frac{1}{m-1}}} \tag{A.21}$$

By employing (A.4), we acquire the iterative equation of cluster centre which is demonstrated below.

$$\sum_{c=1}^{C}\sum_{b=1}^{B}\sum_{h=1}^{H}\sum_{l=1}^{L}\alpha\,\mu_{c_{hlb}}^{m}\,2\left(x_{hlb}-v_c\right)\left(-1\right)\;+\;\left(1\;-\;\alpha\right)u_{c_{hlb}}^{m}\;2\left(\bar{x}_{hlb}\;-\;v_c\right)\left(-1\right)\zeta_{c_{hlb}}\Bigg)=0 \tag{A.22}$$

or,

$$\sum_{c=1}^{C}\sum_{b=1}^{B}\sum_{h=1}^{H}\sum_{l=1}^{L}\Bigg(\left[\alpha\,\mu_{c_{hlb}}^{m}\,v_c\;-\;\alpha\,\mu_{c_{hlb}}^{m}\,x_{hlb}\right]\;+\;\Big[\left(1\;-\;\alpha\right)u_{c_{hlb}}^{m}\,v_c\;\zeta_{hlb}\;-\;\left(1\;-\;\alpha\right)u_{c_{hlb}}^{m}\bar{x}_{hlb}\,\zeta_{c_{hlb}}\Big]\Bigg)=0 \tag{A.23}$$

here, $\bar{x}_{hlb}=\frac{1}{N}\sum_{x_{hlb}\epsilon N_{hlb}}x_{hlb}$

$$\sum_{c=1}^{C}\sum_{b=1}^{B}\sum_{h=1}^{H}\sum_{l=1}^{L}v_c\left[\alpha\,\mu_{c_{hlb}}^{m}\;+\;\left(1\;-\;\alpha\right)u_{c_{hlb}}^{m}\,\zeta_{hlb}\right]\;=\;\sum_{c=1}^{C}\sum_{b=1}^{B}\sum_{h=1}^{H}\sum_{l=1}^{L}\Big[\alpha\,\mu_{c_{hlb}}^{m}\,x_{hlb}\;+\;\left(1\;-\;\alpha\right)u_{c_{hlb}}^{m}\bar{x}_{hlb}\,\zeta_{c_{hlb}}\Big] \tag{A.24}$$

or,

$${}^{1}v_c=v_c=\frac{\sum_{c=1}^{C}\sum_{b=1}^{B}\sum_{h=1}^{H}\sum_{l=1}^{L}\left[\alpha\,\mu_{c_{hlb}}^{m}\,x_{hlb}\;+\;\left(1\;-\;\alpha\right)u_{c_{hlb}}^{m}\bar{x}_{hlb}\,\zeta_{c_{hlb}}\right]}{\sum_{c=1}^{C}\sum_{b=1}^{B}\sum_{h=1}^{H}\sum_{l=1}^{L}\left[\alpha\,\mu_{c_{hlb}}^{m}\;+\;\left(1\;-\;\alpha\right)u_{c_{hlb}}^{m}\,\zeta_{c_{hlb}}\right]} \tag{A.25}$$

Similarly, by employing (A.4), for (3.5) we compute the centres in the following way.

$$\sum_{c=1}^{C}\sum_{b=1}^{B}\sum_{h=1}^{H}\sum_{l=1}^{L} \alpha\, \mu_{c_{hlb}}^{m}\, 2\left(x_{hlb}-v_c\right)\left(-1\right) + \left(1-\alpha\right)\tau_{c_{hlb}}^{m}\, 2\left(\bar{x}_{hlb}-v_c\right)\left(-1\right)\zeta_{c_{hlb}}\Bigg) = 0 \tag{A.26}$$

or,

$$\sum_{c=1}^{C}\sum_{b=1}^{B}\sum_{h=1}^{H}\sum_{l=1}^{L}\Bigg(\left[\alpha\, \mu_{c_{hlb}}^{m}\, v_c - \alpha\, \mu_{c_{hlb}}^{m}\, x_{hlb}\right] + \left[\left(1-\alpha\right)\tau_{c_{hlb}}^{m}\, v_c\, \zeta_{hlb} - \left(1-\alpha\right)\tau_{c_{hlb}}^{m}\bar{x}_{hlb}\,\zeta_{c_{hlb}}\right]\Bigg) = 0 \tag{A.27}$$

here, $\bar{x}_{hlb} = \frac{1}{N}\sum_{x_{hlb}\epsilon N_{hlb}} x_{hlb}$

$$\sum_{c=1}^{C}\sum_{b=1}^{B}\sum_{h=1}^{H}\sum_{l=1}^{L} v_c\left[\alpha\, \mu_{c_{hlb}}^{m} + \left(1-\alpha\right)\tau_{c_{hlb}}^{m}\,\zeta_{hlb}\right] = \sum_{c=1}^{C}\sum_{b=1}^{B}\sum_{h=1}^{H}\sum_{l=1}^{L}\left[\alpha\, \mu_{c_{hlb}}^{m}\, x_{hlb} + \left(1-\alpha\right)\tau_{c_{hlb}}^{m}\bar{x}_{hlb}\,\zeta_{c_{hlb}}\right] \tag{A.28}$$

or,

$${}^{2}v_c = v_c = \frac{\sum_{c=1}^{C}\sum_{b=1}^{B}\sum_{h=1}^{H}\sum_{l=1}^{L}\left[\alpha\, \mu_{c_{hlb}}^{m}\, x_{hlb} + \left(1-\alpha\right)\tau_{c_{hlb}}^{m}\bar{x}_{hlb}\,\zeta_{c_{hlb}}\right]}{\sum_{c=1}^{C}\sum_{b=1}^{B}\sum_{h=1}^{H}\sum_{l=1}^{L}\left[\alpha\, \mu_{c_{hlb}}^{m} + \left(1-\alpha\right)\tau_{c_{hlb}}^{m}\,\zeta_{c_{hlb}}\right]} \tag{A.29}$$

The iterative equations for the other set of cluster centers can be found from (3.5) by employing the above procedure.

Chapter 4

Fuzzy entropy-based FCM algorithm for brain MR image segmentation

4.1 Source of the Chapter

Chapter 4 is based on the work entitled, "3D MR image segmentation using a fuzzy entropy-based fuzzy clustering algorithm," in *Proc. 2nd International Conference on Advancement in Computation & Computer Technologies (InCACCT)*, Chandigarh University, Chandigarh, Punjub, India, May 2-3, 2024.

4.2 Introduction

In medical imaging field, brain magnetic resonance (MR) image segmentation task is a mandatory requirement for accurate diagnosis of any kind of ailment of human brain. The MR images become blurry as intensity in-homogeneity (IIH) and noise imposed within the image at the time of scanning due to many factors like, (i) movement of patients (ii) generation of improper magnetic field of the scanner and (iii) other inherent factors. The resultant image become more blurry at the soft tissue regions and makes the segmentation procedure more complex.

By means of the developed algorithm, primary regions of human brain namely, white matter (WM), gray matter (GM) and cerebrospinal fluid (CSF) are identified and segmented from a 3D brain MR image. Literature survey reveals the fact that regarding segmentation of the soft tissue regions of brain MR images, the fuzzy c-means (FCM) algorithm [1] is used abruptly. The performance of the FCM algorithm degrades for noisy input data as it does not consider the spatial information of the image. Identifying this shortfall of traditional FCM algorithm, some improved modified methods are proposed in near past. To name a few, Mahata et al. [39] developed a fuzzy clustering algorithm, which utilizes the local information and Gaussian functions in the fuzzy objective function to segment brain MR images. In addition to segmentation, it also extracts the bias field to make the image intensity inhomogeneity free. This work also reviewed some of the improved FCM-based methods, such as (i) an improved FCM algorithm by considering scale-controlled spatial information of images (ii) a conditional FCM method using auxiliary variables and spatial information and (iii)a FCM-based algorithm by using multi objective architecture in two phases. In the first stage, it uses probability distribution induced spatial information in the fuzzy clustering process. Secondly, the cluster centers, thus generated, are utilized in the second objective function to generate the final cluster centers and membership functions.

Researchers have also developed some different approaches of FCM algorithm based on entropy, some of them are discussed in this chapter. Boulanouar et al. [70] suggested a different approach regarding brain MR image segmentation by utilizing the hybrid algorithm combined with FCM algorithm and alternative approach of fuzzy bat algorithm. The algorithm generates

new fitness function by combining validity indices of fuzzy cluster and distance of intra cluster. Lohit et al. [71] developed a modified FCM algorithm by representing the data in a picture fuzzy manner and utilize the fuzzy set theory of picture. The algorithm uses total Bregman divergence in a modified way. Jia et al. [72] suggested a different approach of fuzzy clustering by utilizing Gaussian metric to generate sparse memberships of voxels for reduction of non-homogeneous interference. Prakash et al. [73] developed entropy-based FCM algorithm by incorporating genetic algorithm. The algorithm incorporates simulated binary crossover for hereditary calculation and constructs staggered thresholding, which divides restorative cerebrum. Khatri et al. [74] developed anther improved FCM algorithm by utilizing picture fuzzy sets and Gaussian kernel to calculate distances of the voxels from its canter voxel. The algorithm transforms data values in higher dimensional feature space for the image segmentation of brain. Kahali et al. [53] developed another approach based on entropy and incorporating Gaussian function along with contra harmonic means filter. This algorithm addresses the shortcomings of the traditional FCM algorithm by using an uncertainty parameter for each pixel. Instead of Euclidean distance as dissimilarity measure, it uses a Gaussian distribution function. Further, instead of using only the pixel value, it generates a feature vector by considering a small square window for each pixel to classify it. Mahata et al. [55] developed a modified FCM algorithm by incorporating global and local entropies. Very recently, Ray et al. [28] developed a fuzzy clustering algorithm, which integrates complemented local and global membership functions in the fuzzy objective function. In doing so, for each voxel, it defines class specific uncertainty parameters to integrate with the local membership functions. It

also uses the Shannon entropy utilizing the class specific uncertainty parameters for handling the inherent uncertainty. Sing et al. [30] proposed an improved FCM algorithm by considering spatial information of images and it is also scale-controlled. Using an auxiliary variable for each pixel, Adhikari et al. [31] developed a modified FCM algorithm that imposes spatial information and conditional factors for segmentation. Kahali et al. [33] developed a FCM based algorithm by using multi objective architecture in two phases for brain MR image segmentation.

Researchers developed some different approaches of FCM algorithm based on entropy, some of them are discussed at the following.

Dhanachandra et al.[15] developed a blending of FCM algorithm and an optimization technique called dynamic practical swarm for image segmentation. The algorithm uses parallel computing and global optimization searching procedure for this purpose.

Zhang et al. [75] incorporated a block-clustering approach with conventional FCM algorithm to handle large sample database. At first the algorithm imposes block processing for each image and at next by utilizing FCM algorithm it clusters the sub-images. Jiang et al. [76] developed a modified FCM algorithm which is distributive and multitask in nature. The algorithm uses co-learning architecture between different tasks by utilizing common information among them.

Senthilkumar et al. [77] presented fuzzy clustering method with neural network with back propagation for segmentation of brain MR images. The algorithm utilizes FCM algorithm with spatial information and curvlet transformation method for brain image segmentation.

Kumar et al. [78] developed an image fusion model which

have multi objective. In this method, the images are differentiate into two sub-bands, low-frequency and high-frequency by using discrete curvelet transform. For sub-images with low-frequency they have used averaging method and for the sub-images with high frequency the optimized Type-2 fuzzy entropy methods are used for segmentation of brain MR image segmentation.

Halder et al. [79] developed a modified clustering algorithms by using spatial information with kernel mapping. They considered the spatial information including some rank level. Jena et al. [80] incorporated an entropy based clustering algorithm for brain MR image segmentation which is multi level in nature. The algorithm minimizes the cross entropy and utilizes the African vulture optimization method for brain MR image segmentation. Habib et al. [81] developed another modified version of the FCM method for fuzzy clustering of brain tumor MR images. In this method they have used the FCM algorithm and records the negative function and iteration number and also used the threshold method for segmentation. Zhao et al. [82] suggested an improved FCM based on multitask strategy. The method allows for the utilization of both private information between tasks and inside tasks. The algorithm uses learning procedure with weighted factor and by achieving optimal weight the algorithm perform the fuzzy clustering. Pham et al. [38] developed a modified FCM algorithm which utilizes the particle swarm optimization technique which is based on multi-objective. The algorithm incorporates two fitness functions, which utilizes bias correction, spatial information along with adaptive energy weight merged with local and global active contour model for segmentation of MR brain images. Arulanandam et al. [83] developed a different approach of FCM

algorithm by using integrated energy minimization process for MR segmentation of brain. The algorithm utilizes spatial information of voxels and for each region there are an adaptive weighted parameter, which is used to recognize the segmented regions the brain MR images. Meftah et al. [84] incorporated a modified FCM algorithm by utilizing spatial information associated with each voxel and tree seed optimization procedure for segmentation. The algorithm avoid the problem of local minima for segmentation of brain MR image segmentation. Naghi et al. [85] developed an enhanced algorithm of FCM by combining the conventional FCM algorithm and possibilistic c-means algorithm. The algorithm uses low parameter for MR image of brain segmentation.

This suggested method incorporates fuzzy entropy with local membership functions (LMFs) for volumetric high noisy brain MR image segmentation. The objective function combines global membership functions (GMFs) and distance of the cluster centre and the intended voxel along with a controlling factor, as the first term. The LMFs, mean distance of neighboring voxels,a possibility parameter and the complemented controlling factor are combined in the second term.The third term realizes the fuzzy entropy to handle the uncertainty involved for soft tissue region clustering. In particular, fuzzy entropy uses the mean of the LMFs of the neighbouring voxels of the center voxel. Finally, the algorithm combines the LMFs and GMFs to obtain the final membership functions (FMFs). The key points of the suggested algorithm are described below: 1) A fuzzy entropy is defined by incorporating spatial information of the voxels at the local region by utilizes its LMFs. 2) The LMF is weighted by mean distance within the cubic region and a possibility parameter, which influences the center voxel to fall into its correct

class. 3) A parameter controls the influences of the GMFs and LMFs in the fuzzy objective function. 5) The final MF is computed by combining the LMFs and GMFs, in addition with two weighted parameters, which regulate their respective roles. The suggested algorithm validated in a quantitative and qualitative fashion. The investigation reveals the performance result of the algorithm by using 6 volumes of high noisy brain MR simulated images and 4 volumes of clinical brain MR images. The outcome of the investigations claim the superiority and efficiency of the developed algorithm over some related methods developed in recent past. The workflow of this suggested method is displayed at FIGURE 4.1.

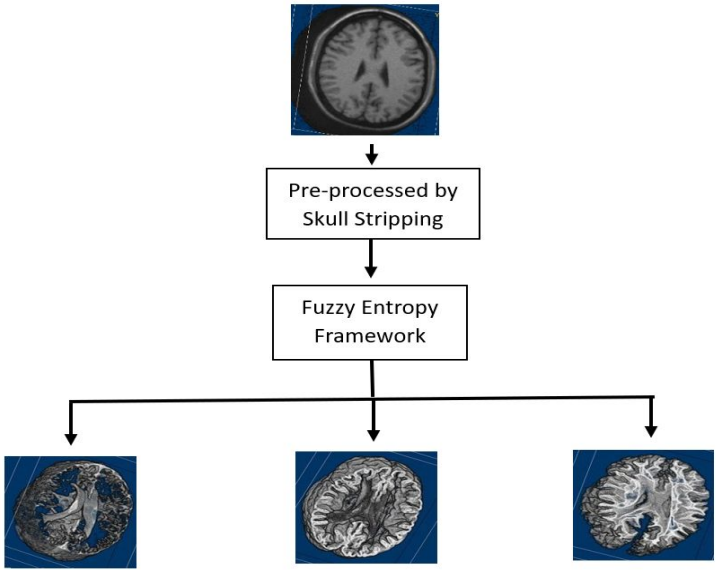

FIGURE 4.1: Segmented volumetric images of the developed algorithm for simulated image volumes.

4.3 Fuzzy entropy framework for volumetric MR image segmentation

In medical imaging field, brain MR image segmentation procedure is a critical task as the scanned images are influenced

by IIH and noise and make the images foggy, especially at the boundary region. Because of the noise and IIH, the intensity distribution becomes uneven all over the image domain.

To address this issue, a fuzzy framework has generated by integrating fuzzy entropy based FCM algorithm using the LMFs of the voxels for segmenting MR images of brain. The fuzzy entropy defines the degree of uncertainty in the classification of the voxels. This mechanism helps us to classify the voxels in the tissue boundary regions more precisely and accurately. Therefore, the objective function of the developed algorithm is so designed that it uses (i) fuzzy entropy, calculated within a local cubic image regions using only LMFs, (ii) LMF weighted by a possibility factor and local mean Euclidean distance and (iii) GMF weighted by Euclidean distance. The latter two are relatively controlled by a positive parameter. Since the uncertainty arises more in the tissue boundaries, the fuzzy entropy is defined by considering voxel intensity distribution within a local spatial region. Furthermore, to decrease the domination of IIH and noise, four features for each voxel has calculated by utilizing intensity distribution within a cubic local neighborhood.

The objective function is explained below.

$$J = \sum_{s=1}^{S}\sum_{i=1}^{I}\sum_{t=1}^{T}\sum_{o=1}^{O}\left(\alpha\mu_{s_{ito}}^{m}d_{s_{ito}}^{2} + (1-\alpha)u_{s_{ito}}^{m}\bar{d}_{s_{ito}}^{2}\zeta_{s_{ito}}\right) + \sum_{i=1}^{I}\sum_{t=1}^{T}\sum_{o=1}^{O}\epsilon_{x_{ito}} \tag{4.1}$$

subject to the following constraints-

$$\sum_{s=1}^{S}\mu_{s_{ito}} = 1, \forall i, t, o \tag{4.2}$$

$$\sum_{s=1}^{S}u_{s_{ito}} = 1, \forall i, t, o \tag{4.3}$$

where, the number of clusters or regions is S in the volume of 3D brain MR image, I represents the total images, O and T indicate the width and height of an image, correspondingly. The GMFs and LMFs for the voxel x_{ito} with respect to cluster s are represented by $\mu_{s_{ito}}$ and $u_{s_{ito}}$ respectively. v_s is the s^{th} cluster center. Euclidean distance is denoted by $d_{s_{ito}}$. The mean Euclidean distance $\bar{d}_{s_{ito}}$, indicates the mean distance of x_{ito} and the cluster center v_s. For the voxel x_{ito} belonging to class s, the class-level possibility parameter is denoted by $\zeta_{s_{ito}}$. Finally, $m > 1.0$ denotes the level of fuzziness. The definitions of the above parameters are given below.

$$d^2_{s_{ito}} = ||x_{ito} - v_s||^2 \tag{4.4}$$

$$\bar{d}^2_{s_{ito}} = \frac{1}{N_B} \sum_{x_{ito} \in N_B} ||x_{ito} - v_s||^2 \tag{4.5}$$

$$\zeta_{s_{ito}} = \frac{\sum_{x_{ito} \in N_B} \mu_{s_{ito}} x_{ito}}{\sum_{x_{ito} \in N_B} x_{ito}} \tag{4.6}$$

$$\epsilon_{x_{ito}} = -\sum_{s=1}^{S} \left(u_{s_{ito}} \, \tau_s \ln(\tau_s) \right) \tag{4.7}$$

$$\tau_s = \frac{\sum_{x_{ito} \epsilon N_B} \left(u_{s_{ito}} \right)}{|N_B|} \tag{4.8}$$

The (4.8) satisfies the following constraints:

$$\sum_{s=1}^{S} \tau_{s_{ito}} = 1, \forall o, t, i \tag{4.9}$$

where, N_B is the entire voxel count in the neighborhood region concerning the central voxel x_{ito}.

In (4.1), first term is responsible to lessen the product of fuzzy

GMFs and distances of the voxels from the cluster centers. The second term is responsible to keep the minimum product of fuzzy LMFs, the mean distances of the neighboring voxels from the cluster centers and the possibility factors. These two terms are complementary regularized by a positive parameter $\alpha; 0 \leq \alpha \leq 1$. The third term incorporate the fuzzy entropy with local membership function and also conjugate with global membership function.

To find the iterative equations regrading the parameters, the objective functions are required to minimize by satisfying the associated constraints. This can be accomplished by rewriting (4.1) utilizing Lagrange multipliers and then performing partial derivatives with respect to $\mu_{s_{ito}}$, $u_{s_{ito}}$ and v_c to generate the iterative equations of $\mu_{s_{ito}}$, $u_{s_{ito}}$ and v_s, respectively. Calculate the cluster centers by utilizing v_s. The equations are given as follows.

$$\mu_{s_{ito}} = \frac{1}{\sum_{p=1}^{S} \left(\frac{d^2_{s_{ito}}}{d^2_{p_{ito}}} \right)^{\frac{1}{m-1}}} \forall s, o, t, i \tag{4.10}$$

$$u_{s_{ito}} = \frac{1}{\sum_{p=1}^{S} \left(\frac{\left(1-\alpha\right) m \bar{d}^2_{s_{ito}} \zeta_{s_{ito}} - \left(\frac{\lambda_s \ln(\lambda_s)}{u^{(m-1)}_{s_{ito}}} \right)}{\left(1-\alpha\right) m \bar{d}^2_{p_{ito}} \zeta_{p_{ito}} - \left(\frac{\lambda_p \ln(\lambda_p)}{u^{(m-1)}_{p_{ito}}} \right)} \right)^{\frac{1}{m-1}}} \forall s, o, t, i \tag{4.11}$$

$$v_s = \frac{\sum_{s=1}^{S} \sum_{i=1}^{I} \sum_{t=1}^{T} \sum_{o=1}^{O} \left(\alpha \mu^m_{s_{ito}} x_{ito} + \left(1-\alpha\right) u^m_{s_{ito}} \zeta_{s_{ito}} \bar{x}_{ito} \right)}{\sum_{s=1}^{S} \sum_{i=1}^{I} \sum_{t=1}^{T} \sum_{o=1}^{O} \left(\alpha \mu^m_{s_{ito}} + \left(1-\alpha\right) u^m_{s_{ito}} \zeta_{s_{ito}} \right)} \forall s \tag{4.12}$$

The final MFs $f_{s_{ito}}$ has been calculated by combining the GMFs

and LMFs, weighted according to two positive regulating factors as follows.

$$f_{s_{ito}} = \frac{(\mu_{s_{ito}})^p (u_{s_{ito}})^q}{\sum_{l=1}^{S} (\mu_{l_{ito}})^p (u_{l_{ito}})^q} \tag{4.13}$$

The algorithm of the developed work is demonstrated below:

Algorithm 3: FEFCM

Input: Volumetric brain MR images of size $I \times T \times O$
Output: Segmented volume of GM, CSF and WM regions

Initialize the values to p, q, m, iteration number $n = 0$ and threshold of error ϵ;
Draw out brain area by utilizing skull stripping algorithm;
Initialize the cluster center $v_s^{(n)}, \forall s$;
Initialize the GMFs $\mu_{s_{ito}}$ and the LMFs $u_{s_{ito}}$;
repeat
    Evaluate the global fuzzy MFs $\mu_{s_{ito}}^{(n+1)}, \forall s, i, t, o$ by using (4.10);
    Evalute the class-level possibility parameter $\zeta_{s_{ito}}, \forall s, i, t, o$ by using (4.6);
    Evaluate the local fuzzy MF $u_{s_{ito}}^{(n+1)}, \forall s, i, t, o$ by using (4.11);
    Evalulate the cluster centres ${v_s}^{n+1}, \ \forall s$ by using (4.12);
    $n = n + 1$;
until $||v_s^{(n)} - v_s^{(n-1)}|| < \varepsilon, \forall s$
Find out the final fuzzy MF $f_{s_{ito}}, \forall s, i, t, o$ by using (4.13);
Derive the final cluster centers $V = \{v_1, v_2, v_3, ..., v_s\}$ and the membership matrix $M = \{f_{s_{ito}}\}, \forall s, i, t, o$;
Assign the voxel $x_{ito}, \forall i, t, o$ to a class that produces the highest value of membership;

4.4 Experimental results and discussion

The efficacy of the presented algorithm has conducted by performing various experiments on distinct volumetric brain MR images. For this purpose, 6 volumes of high noisy simulated images, 4 volumes of real patients' MR images of brain have used. The BrainWeb [59] database with different degrees of IIH (20%-40%) and noise (1%-9%) are used to conduct the experiments.

More specifically, the volumetric images with 5%-9% noise and 20%-40% IIH has utilized. It is defined that the size of the volumetric image is $181 \times 217 \times 181$ $(height \times width \times depth)$ and voxel thickness is $1 \times 1 \times 1$ mm^3. The real patients' volumetric MR image resolutions are $552 \times 325 \times 58$, $350 \times 206 \times 20$, $256 \times 150 \times 20$ and $1105 \times 649 \times 20$.

4.4.1 Qualitative Analysis

The execution of the suggested method has been inspected on the simulated volumetric brain MR images, next on the real patient volumetric brain MR images.

Qualitative demonstration on volumetric simulated brain MR images

In this present work, the results of the developed method has been investigated by presenting the outcomes of the brain tissue regions of gray matter (GM), cerebro spinal fluid (CSF) and white matter (WM). The experiments have been conducted by utilizing six image volumes which is high IIH and noise prone and differentiate the results with the ground truths for detail analysis. The outcome of the volumetric MR images of brain with 9% noise and 40% IIH presents at FIGURE 4.2. In the FIGURE 4.2(A) shows the original image volume. 4.2(B)-(D) present the segmented gray matter, white matter and cerebro spinal fluid respectively. The detail insight view of the volumetric image regions has been represented by generating two-third part of the segmented volumes. FIGURE 4.2(E)-(G) show the two-thirds part of the GM, WM and CSF regions respectively. Segmented outcomes of the volume image with 7% noise and 40% IIH are

presented in FIGURE 4.3. FIGURE 4.3(A)-(C) show the segmented GM, WM and CSF regions of brain MR image volume of 7% noise and 40% IIH, respectively. .

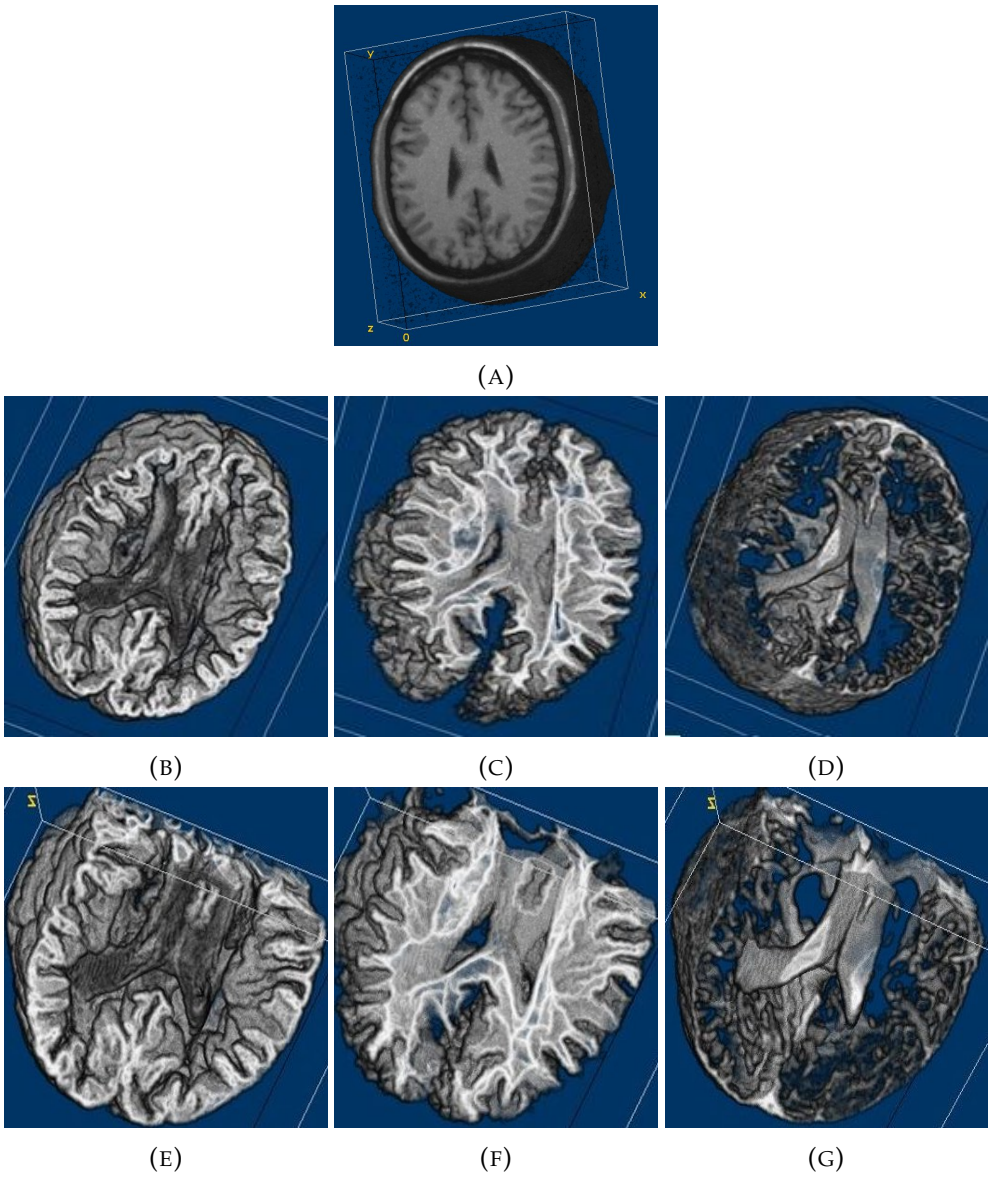

(A) (B) (C) (D) (E) (F) (G)

FIGURE 4.2: The segmented regions. (A) Segmented GM, (B) Segmented WM, (C) Segmented CSF, (D) Two-thirds of segmented GM, (E) Two-thirds of segmented WM and (F) Two-thirds of segmented CSF volumetric regions.

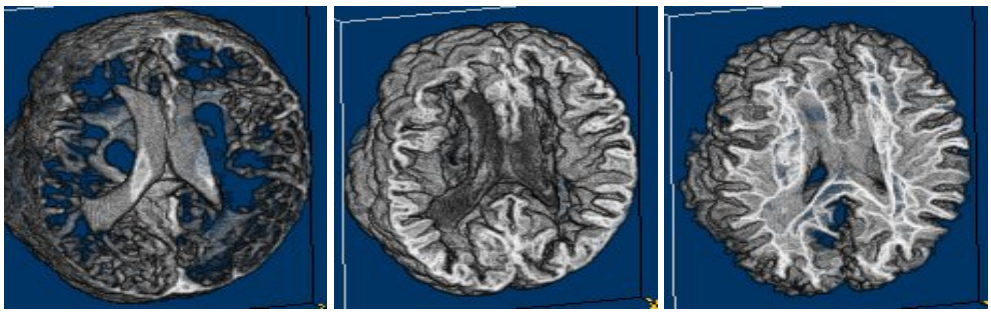

(A) (B) (C)

FIGURE 4.3: The segmented regions of 7% noise and 40%IIH prone brain image volume. (a) GM region, (b)WM region and (c) CSF region.

Qualitative Experiment of Volumetric Real Patient Images

In this investigation, the results of one volumetric real patients' brain MR images has been shown from the 4 volumes of subjects. The image volume accumulated from the EKO X-ray and Imaging Institute and AMRI Hospital, Kolkata, India. Image volume acquire at 1.5T MRI machines. The results shows at FIGURE 4.4. In the FIGURE 4.4(A) shows the original image volume. FIGURE 4.4(B)-(D) present the segmented CSF, GM and WM volumetric region of the original patient's MR image volume. For the insight view of the segmented regions two-third part of the images has been generated. FIGURE 4.4(E)-(G) presents two-thirds part of CSF, GM and WM regions respectively.

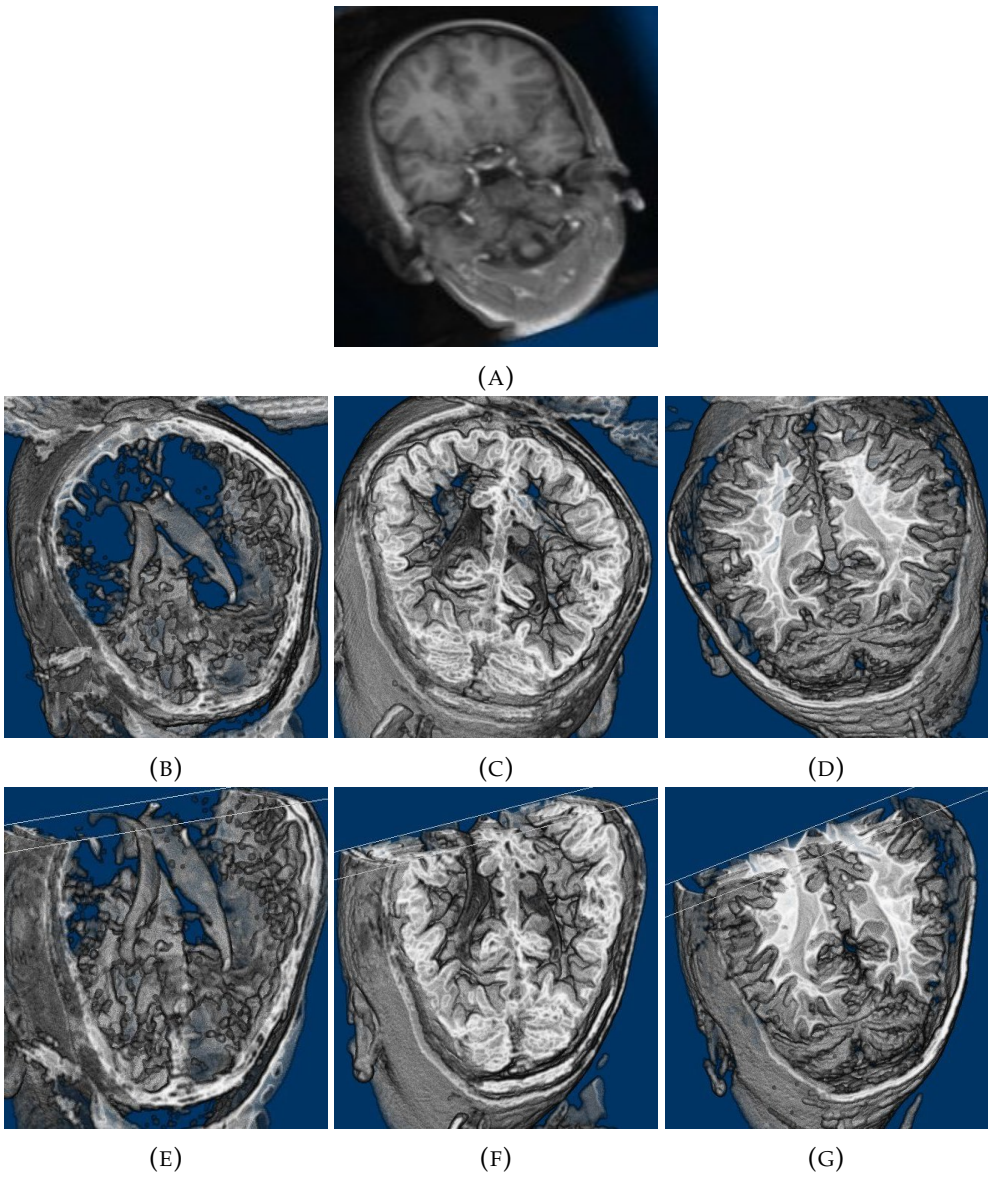

(A)

(B) (C) (D)

(E) (F) (G)

FIGURE 4.4: Segmented volumetric real patients' images. (A) Segmented volume of CSF, (B) Segmented volume of GM, (C) Segmented volume of WM, (D) - (F) Two-thirds of segmented CSF, GM and WM volumetric regions respectively.

4.4.2 Quantitative Analysis

In this analysis, different results of performance analyses between the suggested algorithm and other similar methods has been shown by utilizing different indices. The indices are (i) Dice similarity coefficient (ρ) [55], (ii) segmentation accuracy

(SA) [55], (iii) tissue segmentation accuracy (TSA) [33], (iv) partition entropy (v_{pe}) [55] and (v) partition coefficient (v_{pc}) [33] .

Quantitative study on simulated brain MR image volumes

In this analysis, the effectiveness of the developed algorithm along with other similar state-of-the-art algorithms like MRE-FCM [52], MEFCM [50], REFCM [51] and MEI [49] algorithms has shown. The comparative outcomes show in TABLE 4.1 by considering SA as a performance index. The TSA results show in TABLE 4.2. All the experimental results shows the superiority of the developed algorithm over the other comparative methods for the highest noisy image volume. The outcomes of the statistical significant analysis are shown at TABLE 4.3 for SA index and in TABLE 4.4 for TSA index. This method is statistically significant at $p = 0.05$ over MEI, REFCM and FCM for WM, statistically significant at $p = 0.01$ over all the comparative methods for GM and statistically significant at $p = 0.01$ over all the comparative methods for CSF of SA index. For TSA index this method is statistically significant at p= 0.01 for WM and GM over all other comparative methods and for CSF p= 0.03 for all other comparative methods.

TABLE 4.1: Results of T1-weighted simulated brain MR image volumes using SA Index. Best results are shown in bold.

(Noise,IIH)	Region	Developed algorithm	MEI	REFCM	MEFCM	MREFCM	FCM
5,20	WM	**0.954**	0.953	0.906	0.970	0.963	0.848
	GM	**0.934**	0.906	0.845	0.851	0.837	0.834
	CSF	0.926	0.915	**0.972**	0.881	0.819	0.881
5,40	WM	0.927	0.934	0.877	**0.952**	0.920	0.840
	GM	**0.910**	0.895	0.880	0.838	0.840	0.825
	CSF	**0.917**	0.909	0.887	0.887	0.838	0.837
7,20	WM	0.950	0.918	0.959	0.943	**0.960**	0.829
	GM	**0.919**	0.860	0.766	0.791	0.836	0.818
	CSF	**0.917**	0.851	0.849	0.780	0.830	0.819
7,40	WM	0.911	0.896	0.843	**0.920**	0.914	0.795
	GM	**0.897**	0.875	0.840	0.776	0.839	0.782
	CSF	**0.916**	0.841	0.842	0.775	0.834	0.807
9,20	WM	0.937	0.864	0.891	0.902	**0.949**	0.781
	GM	**0.902**	0.807	0.772	0.722	0.846	0.755
	CSF	**0.900**	0.772	0.808	0.690	0.825	0.753
9,40	WM	**0.901**	0.846	0.767	0.891	0.888	0.765
	GM	**0.880**	0.789	0.796	0.711	0.843	0.742
	CSF	**0.897**	0.760	0.797	0.688	0.835	0.742

TABLE 4.3: Results of statistical significance analysis for SA index on Brainweb image volumes.

Region	Paired t-test(1-tailed)	Developed algorithm	MEI	REFCM	MEFCM	MREFCM	FCM
WM	Mean of SA value	0.93 -	0.901 0.04	0.873 0.02	0.929 0.49	0.932 0.30	0.809 0.00
GM	Mean of SA value	0.907 -	0.855 0.007	0.816 0.002	0.781 0.000	0.840 0.000	0.791 0.00
CSF	Mean of SA value	0.912 -	0.841 0.011	0.859 0.001	0.764 0.005	0.838 0.001	0.806 0.000

TABLE 4.2: TSA results of T1-weighted simulated brain MR image volumes . The best results are in bold.

(Noise,IIH)	Region	Developed algorithm	MEI	REFCM	MEFCM	MREFCM	FCM
5,20	WM	**0.875**	0.829	0.821	0.810	0.812	0.716
	GM	**0.819**	0.800	0.788	0.793	0.752	0.693
	CSF	**0.606**	0.610	0.612	0.601	0.546	0.439
5,40	WM	**0.856**	0.823	0.822	0.811	0.808	0.716
	GM	**0.797**	0.792	0.792	0.782	0.749	0.678
	CSF	0.600	**0.606**	0.573	0.587	0.553	0.419
7,20	WM	**0.868**	0.795	0.780	0.785	0.812	0.694
	GM	**0.811**	0.762	0.737	0.755	0.753	0.660
	CSF	**0.606**	0.578	0.575	0.540	0.551	0.417
7,40	WM	**0.851**	0.795	0.793	0.780	0.808	0.660
	GM	**0.791**	0.756	0.759	0.741	0.747	0.694
	CSF	**0.597**	0.568	0.541	0.535	0.554	0.390
9,20	WM	**0.858**	0.763	0.767	0.755	0.817	0.666
	GM	**0.801**	0.723	0.726	0.705	0.758	0.621
	CSF	**0.598**	0.522	0.516	0.473	0.556	0.377
9,40	WM	**0.847**	0.761	0.749	0.751	0.805	0.671
	GM	**0.781**	0.718	0.714	0.695	0.747	0.610
	CSF	**0.585**	0.510	0.486	0.468	0.552	0.361

TABLE 4.4: Results of statistical significance analysis for TSA index on Brain Web image volumes.

Region	Paired t-test(1-tailed)	Developed algorithm	MEI	REFCM	MEFCM	MREFCM	FCM
WM	Mean of TSA	0.859	0.793	0.788	0.782	0.810	0.687
	p value	-	0.000	0.000	0.000	0.00	0.00
GM	Mean of TSA	0.8	0.758	0.752	0.745	0.751	0.659
	p value	-	0.006	0.005	0.004	0.00	0.000
CSF	Mean of TSA	0.598	0.565	0.550	0.535	0.552	0.400
	p value	-	0.0378	0.014	0.013	0.00	0.00

Moreover, the performance analysis of the developed algorithm has been displayed by utilizing the Dice similarity coefficient ρ index. FIGURE 4.5 shows the results of ρ. The results highlight the fact that the developed algorithm outperforms all other similar alternative techniques which are developed recent past. The graphical comparative results of the developed method has been presented in terms of v_{pc} and v_{pe}. FIGURE 4.6 shows the result of the v_{pc} index and FIGURE 4.7 shows the comparative results of v_{pe}. The graphical outcomes of the comparative methods show superiority of the developed method than other comparative methods except MREFCM.

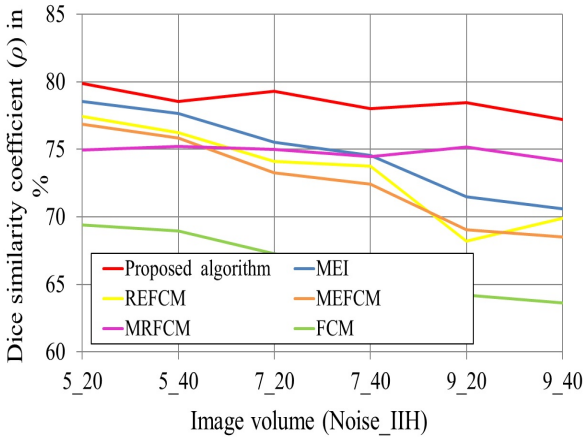

FIGURE 4.5: Results of ρ for simulated image volumes.

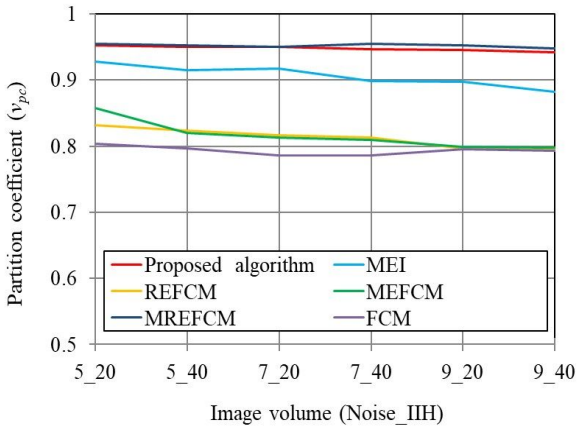

FIGURE 4.6: Results of v_{pc} for simulated image volumes.

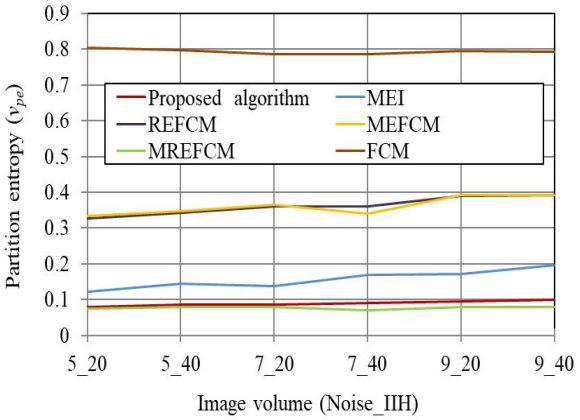

FIGURE 4.7: Results of v_{pe} for simulated image volumes.

Quantitative analysis on real patient volumetric brain MR images

TABLE 4.5 presents the experimental results of the suggested method with other comparative methods by using the volumetric real patient images. Additionally, the outcome of the experiments clearly demonstrate its superiority over all other comparative techniques. The results show the effectiveness of the algorithm over other similar methods.

TABLE 4.5: Results of MR real patient image volumes.

Volume	Method	v_{pc}	v_{pe}
Patient 1	Developed Method	0.990	0.020
	MEI	0.960	0.040
	REFCM	0.891	0.343
	MEFCM	0.915	0.171
	MREFCM	0.992	0.012
	FCM	0.741	0.507
Patient 2	Developed Method	0.989	0.019
	MEI	0.890	0.153
	REFCM	0.837	0.331
	MEFCM	0.888	0.217
	MREFCM	0.994	0.009
	FCM	0.870	0.273
Patient 3	Developed Method	0.989	0.018
	MEI	0.9650	0.080
	REFCM	0.931	0.126
	MEFCM	0.946	0.104
	MREFCM	0.991	0.014
	FCM	0.705	0.558
Patient 4	Developed Method	0.986	0.021
	MEI	0.976	0.039
	REFCM	0.875	0.264
	MEFCM	0.912	0.182
	MREFCM	0.981	0.017
	FCM	0.791	0.253

4.5 Conclusion

The suggested algorithm develops a fuzzy entropy-based FCM algorithm for volumetric brain MR image segmentation. This framework uses the GMFs, LMFs, class-level possibility parameter, local spatial information of the voxels and fuzzy entropy. The fuzzy entropy is defined by using the LMFs within a cubic neighborhood of a central voxel. By combining GMFs and LMFs with two weighted positive parameters, the algorithm generates the final fuzzy MF, which is responsible to categorize the voxels into one of the predefined classes. The efficacy of the suggested algorithm proof on six volumetric simulated MR images of brain affected by high noise as well as IIH and four volumetric real patients' brain MR images. The outcomes of the experiments show the supremacy of the presented method over other state-of-the-art algorithms. The presented algorithm may be extended to segment brain tumors from 3D MR image volumes. This work requires more detailed study regarding utilization of spatial information and inherent intensity distribution.

The fuzzy entropy framework provides better accuracy in the context of dice similarity coefficient than other two methods that are discussed in chapter 2 and chapter 3. Hence the three developed framework's performance increases gradually from one method to another as well.

Chapter 5

Concluding remarks and future directions work

5.1 Concluding remarks

The conclusion of the thesis is described in this chapter. This thesis includes three different entropy based enhanced fuzzy c-means algorithms for high noisy brain medical resonance image segmentation. The new framework will be more helpful to segments the volumetric brain MR images accurately and diagnosis the diseases of the patients correctly.

In my enhanced FCM-based framework, I have utilized the spatial correlation between voxels at the local cubic neighbouring window region. To handle the uncertainty in high noisy IIH prone MR volumetric image segmentation, the association between the neighbouring voxels play important role significantly. Three distinct frameworks has been developed and the scale of improvement gradually increases from first to second and second to third contribution.

The first chapter of the thesis is about the brief description of different image segmentation techniques and there pros and cons. Brief overview of the work.

The second chapter of the thesis highlighted my first contribution, which is entropy based complemented FCM framework

for brain MR image segmentation. In this framework the non-association of the image voxel corresponding to its respective cluster has been imposed by doing complement of the membership functions. The framework also emphasize the uncertainty parameter with local and global membership functions of the image domain. The total uncertainty is handled by means of Shannon entropy which has utilized the underlying uncertainty parameters as its definition.

The third chapter enlighten my second contribution that is the multi-objective paradigm based on relative entropy. The type-1 and interval type-2 fuzzy c-means algorithms are incorporated for volumetric noisy brain MR image segmentation. In this contribution interval type-2 fuzzy membership functions has been utilized at the local neighbouring cubic image domain by using local membership functions. The local-membership functions has been used as a secondary membership functions for interval type-2 fuzzy set. The interval type-2 fuzzy set has been generated from the type-2 fuzzy set by considering the footprint of uncertainty, which are bounded in between the lower and upper membership functions. Next the defuzzification process has been performed on the interval type-2 fuzzy set by using Nie-Tan defuzzification method. The final membership functions has been calculated by means of global membership functions and Interval type-2 fuzzy membership functions.

The fourth chapter of this thesis introduces my third contribution, which is the fuzzy entropy-based fuzzy c-means framework with global and local membership functions along with the possibility parameters and the fuzzy entropy at the local cubic neighbourhood region. In this contribution the local fuzzy membership functions has been utilized to generate fuzzy entropy at the local neighbourhood region. This fuzzy entropy

framework utilizes the global membership functions, local membership functions with possibility parameters and mean distance in cubic neghbouring region along with the fuzzy entropy.

The developed frameworks are validated by using ten volumes of T1-weighted BrainWeb simulated images, five volumes of Internet Brain Segmentation Repository (IBSR) images, four volumes of clinical patient images and a synthetic image volume corrupted with recian noise. The experimental outcomes shows the efficacy of the frameworks over other recent developed entropy-based FCM framework for brain MR image segmentation.

5.2 Future directions of work

In future these algorithm may utilize dynamic neighborhood window to utilize close association of the voxels which are lying within the local spatial image domain. To avoid miss classification higher degree of fuzzy membership functions may be incorporated with dynamic neighbourhood window. In medical imaging domain I utilize normal brain tissues. So in future I will work on the segmentation of abnormal and unhealthy brain tissues, which is very much required, as at the present days disorder and anomalies of human brain has increased rapidly. The future works on the basis of abnormal brain MR images are highlighted below:
i) Segmentation of brain tumor images by using new framework based on FCM.
ii) Segmentation of brain tumor image segmentation using deep learning techniques like CNN and other CNN based model.
iii) Identification of different type of tumor using deep learning.

Bibliography

[1] P. Suetens, *Fundamentals of medical imaging*. Cambridge university press, 2017.

[2] B. Abhisheka, S. K. Biswas, B. Purkayastha, D. Das, and A. Escargueil, "Recent trend in medical imaging modalities and their applications in disease diagnosis: A review," *Multimedia Tools and Applications*, pp. 1–36, 2023.

[3] A. Elangovan and T. Jeyaseelan, "Medical imaging modalities: a survey," in *2016 International Conference on emerging trends in engineering, technology and science (ICETETS)*. ieee, 2016, pp. 1–4.

[4] A. M. Khan and S. Ravi, "Image segmentation methods: A comparative study," *International Journal of Soft Computing and Engineering*, vol. 3, no. 4, pp. 84–92, 2013.

[5] K. Ramesh, G. K. Kumar, K. Swapna, D. Datta, and S. S. Rajest, "A review of medical image segmentation algorithms," *EAI Endorsed Transactions on Pervasive Health and Technology*, vol. 7, no. 27, pp. e6–e6, 2021.

[6] N. R. Pal and S. K. Pal, "A review on image segmentation techniques," *Pattern recognition*, vol. 26, no. 9, pp. 1277–1294, 1993.

[7] N. Shrivastava and J. Bharti, "Automatic seeded region growing image segmentation for medical image segmentation: a brief review," *International Journal of Image and Graphics*, vol. 20, no. 03, p. 2050018, 2020.

[8] R. Kohler, "A segmentation system based on thresholding," *Computer Graphics and Image Processing*, vol. 15, no. 4, pp. 319–338, 1981.

[9] R. Kashyap and P. Gautam, "Modified region based segmentation of medical images," in *2015 International Conference on Communication Networks (ICCN)*. IEEE, 2015, pp. 209–216.

[10] O. Monga, "An optimal region growing algorithm for image segmentation," *International Journal of Pattern Recognition and Artificial Intelligence*, vol. 1, no. 03n04, pp. 351–375, 1987.

[11] J. Preetha, S. Selvarajan, and P. Suresh, "Comparative analysis of various image edge detection techniques for two dimensional CT scan neck disc image," *Int. J. Comput. Sci. Commun*, vol. 3, pp. 57–61, 2012.

[12] D. Chaudhuri and A. Agrawal, "Split-and-merge procedure for image segmentation using bimodality detection approach," 2010.

[13] L. Caponetti, G. Castellano, and V. Corsini, "MR brain image segmentation: a framework to compare different clustering techniques," *Information*, vol. 8, no. 4, p. 138, 2017.

[14] M. A. Balafar, A. R. Ramli, M. I. Saripan, and S. Mashohor, "Review of brain MRI image segmentation methods," *Artificial Intelligence Review*, vol. 33, pp. 261–274, 2010.

[15] N. Dhanachandra and Y. J. Chanu, "An image segmentation approach based on fuzzy c-means and dynamic particle swarm optimization algorithm," *Multimedia tools and applications*, vol. 79, no. 25-26, pp. 18 839–18 858, 2020.

[16] S. N. Sulaiman and N. A. M. Isa, "Adaptive fuzzy k-means clustering algorithm for image segmentation," *IEEE Transactions on Consumer Electronics*, vol. 56, no. 4, pp. 2661–2668, 2010.

[17] A. Saxena, M. Prasad, A. Gupta, N. Bharill, O. P. Patel, A. Tiwari, M. J. Er, W. Ding, and C.-T. Lin, "A review of clustering techniques and developments," *Neurocomputing*, vol. 267, pp. 664–681, 2017.

[18] J. C. Bezdek, R. Ehrlich, and W. Full, "FCM: The fuzzy c-means clustering algorithm," *Computers & geosciences*, vol. 10, no. 2-3, pp. 191–203, 1984.

[19] Y. Alzahrani and B. Boufama, "Biomedical image segmentation: a survey," *SN Computer Science*, vol. 2, no. 4, p. 310, 2021.

[20] S. Shirly and K. Ramesh, "Review on 2D and 3D MRI image segmentation techniques," *Current Medical Imaging*, vol. 15, no. 2, pp. 150–160, 2019.

[21] A. Halder and N. A. Talukdar, "Robust brain magnetic resonance image segmentation using modified rough-fuzzyC-means with spatial constraints," *Applied Soft Computing*, vol. 85, p. 105758, 2019.

[22] M. H. Al Aqad and L. M. O. de Barros Cardoso, "Ant colony optimization (ACO) based fuzzy c-means (FCM) clustering approach for MRI images segmentation," *Wasit Journal of*

Computer and Mathematics Science, vol. 2, no. 4, pp. 115–125, 2023.

[23] M. Tavakoli-Zaniani, Z. Sedighi-Maman, and M. H. F. Zarandi, "Segmentation of white matter, grey matter and cerebrospinal fluid from brain MR images using a modified FCM based on double estimation," *Biomedical Signal Processing and Control*, vol. 68, p. 102615, 2021.

[24] B. Jai Shankar, K. Murugan, A. Obulesu, S. Finney Daniel Shadrach, and R. Anitha, "MRI image segmentation using bat optimization algorithm with fuzzy c means (BOA-FCM) clustering," *Journal of Medical Imaging and Health Informatics*, vol. 11, no. 3, pp. 661–666, 2021.

[25] A. Alrosan, W. Alomoush, N. Norwawi, M. Alswaitti, and S. N. Makhadmeh, "An improved artificial bee colony algorithm based on mean best-guided approach for continuous optimization problems and real brain MRI images segmentation," *Neural Computing and Applications*, vol. 33, pp. 1671–1697, 2021.

[26] Kamarujjaman and M. Maitra, "3D unsupervised modified spatial fuzzy c-means method for segmentation of 3D brain MR image," *Pattern Analysis and Applications*, vol. 22, no. 4, pp. 1561–1571, 2019.

[27] W. Alomoush, A. Alrosan, Y. M. Alomari, A. A. Alomoush, A. Almomani, and H. S. Alamri, "Fully automatic grayscale image segmentation based fuzzy c-means with firefly mate algorithm," *Journal of Ambient Intelligence and Humanized Computing*, vol. 13, no. 9, pp. 4519–4541, 2022.

[28] M. Ray, N. Mahata, and J. K. Sing, "Uncertainty parameter weighted entropy-based fuzzy c-means algorithm using

complemented membership functions for noisy volumetric brain MR image segmentation," *Biomedical Signal Processing and Control*, vol. 85, p. 104925, 2023.

[29] Z. Ji, Y. Xia, Q. Sun, Q. Chen, and D. Feng, "Adaptive scale fuzzy local Gaussian mixture model for brain MR image segmentation," *Neurocomputing*, vol. 134, pp. 60–69, 2014.

[30] J. K. Sing, S. K. Adhikari, and D. K. Basu, "A modified fuzzy c-means algorithm using scale control spatial information for MRI image segmentation in the presence of noise," *Journal of Chemometrics*, vol. 29, no. 9, pp. 492–505, 2015.

[31] S. K. Adhikari, J. K. Sing, D. K. Basu, and M. Nasipuri, "Conditional spatial fuzzy c-means clustering algorithm for segmentation of MRI images," *Applied soft computing*, vol. 34, pp. 758–769, 2015.

[32] H. Verma, R. Agrawal, and A. Sharan, "An improved intuitionistic fuzzy c-means clustering algorithm incorporating local information for brain image segmentation," *Applied Soft Computing*, vol. 46, pp. 543–557, 2016.

[33] S. Kahali, S. K. Adhikari, and J. K. Sing, "A two-stage fuzzy multi-objective framework for segmentation of 3D MRI brain image data," *Applied Soft Computing*, vol. 60, pp. 312–327, 2017.

[34] A. Namburu, S. K. Samay, and S. R. Edara, "Soft fuzzy rough set-based MR brain image segmentation," *Applied Soft Computing*, vol. 54, pp. 456–466, 2017.

[35] C. Singh and A. Bala, "An unsupervised orthogonal rotation invariant moment based fuzzy C-means approach for

the segmentation of brain magnetic resonance images," *Expert Systems with Applications*, vol. 164, p. 113989, 2021.

[36] T. Ren, H. Wang, H. Feng, C. Xu, G. Liu, and P. Ding, "Study on the improved fuzzy clustering algorithm and its application in brain image segmentation," *Applied Soft Computing*, vol. 81, p. 105503, 2019.

[37] C. Singh and A. Bala, "A local zernike moment-based unbiased nonlocal means fuzzy C-means algorithm for segmentation of brain magnetic resonance images," *Expert Systems with Applications*, vol. 118, pp. 625–639, 2019.

[38] T. X. Pham, P. Siarry, and H. Oulhadj, "A multi-objective optimization approach for brain MRI segmentation using fuzzy entropy clustering and region-based active contour methods," *Magnetic Resonance Imaging*, vol. 61, pp. 41–65, 2019.

[39] N. Mahata, S. Kahali, S. K. Adhikari, and J. K. Sing, "Local contextual information and Gaussian function induced fuzzy clustering algorithm for brain MR image segmentation and intensity inhomogeneity estimation," *Applied Soft Computing*, vol. 68, pp. 586–596, 2018.

[40] M. Alruwaili, M. H. Siddiqi, and M. A. Javed, "A robust clustering algorithm using spatial fuzzy C-means for brain MR images," *Egyptian Informatics Journal*, vol. 21, no. 1, pp. 51–66, 2020.

[41] R. Basnet, M. O. Ahmad, and M. Swamy, "A deep dense residual network with reduced parameters for volumetric brain tissue segmentation from MR images," *Biomedical Signal Processing and Control*, vol. 70, p. 103063, 2021.

[42] M. Singh, V. Venkatesh, A. Verma, and N. Sharma, "Segmentation of MRI data using multi-objective antlion based improved fuzzy c-means," *Biocybernetics and Biomedical Engineering*, vol. 40, no. 3, pp. 1250–1266, 2020.

[43] J. Xu, G. Feng, B. Fan, W. Yan, T. Zhao, X. Sun, and M. Zhu, "Landcover classification of satellite images based on an adaptive interval fuzzy c-means algorithm coupled with spatial information," *International Journal of Remote Sensing*, vol. 41, no. 6, pp. 2189–2208, 2020.

[44] L. Hua, Y. Gu, X. Gu, J. Xue, and T. Ni, "A novel brain MRI image segmentation method using an improved multi-view fuzzy c-means clustering algorithm," *Frontiers in Neuroscience*, vol. 15, p. 662674, 2021.

[45] J. Xu, T. Zhao, G. Feng, M. Ni, and S. Ou, "A fuzzy C-means clustering algorithm based on spatial context model for image segmentation," *International Journal of Fuzzy Systems*, vol. 23, pp. 816–832, 2021.

[46] G. Feng, M. Ni, S. Ou, W. Yan, and J. Xu, "A preferential interval-valued fuzzy c-means algorithm for remotely sensed imagery classification," *International Journal of Fuzzy Systems*, vol. 21, pp. 2212–2222, 2019.

[47] R. S. Devi, B. Perumal, and M. P. Rajasekaran, "A hybrid deep learning based brain tumor classification and segmentation by stationary wavelet packet transform and adaptive kernel fuzzy c means clustering," *Advances in Engineering Software*, vol. 170, p. 103146, 2022.

[48] T. Wei, X. Wang, X. Li, and S. Zhu, "Fuzzy subspace clustering noisy image segmentation algorithm with adaptive

local variance & non-local information and mean membership linking," *Engineering Applications of Artificial Intelligence*, vol. 110, p. 104672, 2022.

[49] R.-P. Li and M. Mukaidono, "A maximum-entropy approach to fuzzy clustering," in *Proceedings of 1995 IEEE International Conference on Fuzzy Systems.*, vol. 4. IEEE, 1995, pp. 2227–2232.

[50] M. Yasuda and T. Furuhashi, "Fuzzy entropy based fuzzy c-means clustering with deterministic and simulated annealing methods," *IEICE TRANSACTIONS on Information and Systems*, vol. 92, no. 6, pp. 1232–1239, 2009.

[51] M. Zarinbal, M. F. Zarandi, and I. Turksen, "Relative entropy collaborative fuzzy clustering method," *Pattern Recognition*, vol. 48, no. 3, pp. 933–940, 2015.

[52] R. R. Gharieb, G. Gendy, and A. Abdelfattah, "C-means clustering fuzzified by two membership relative entropy functions approach incorporating local data information for noisy image segmentation," *Signal, Image and Video Processing*, vol. 11, no. 3, pp. 541–548, 2017.

[53] S. Kahali, J. K. Sing, and P. K. Saha, "A new entropy-based approach for fuzzy c-means clustering and its application to brain MR image segmentation," *Soft Computing*, vol. 23, no. 20, pp. 10 407–10 414, 2019.

[54] D. Kumar, R. Agrawal, and H. Verma, "Kernel intuitionistic fuzzy entropy clustering for MRI image segmentation," *Soft Computing*, vol. 24, pp. 4003–4026, 2020.

[55] N. Mahata and J. K. Sing, "A novel fuzzy clustering algorithm by minimizing global and spatially constrained

likelihood-based local entropies for noisy 3D brain MR image segmentation," *Applied Soft Computing*, vol. 90, p. 106171, 2020.

[56] C. Wu and Z. Kang, "Robust entropy-based symmetric regularized picture fuzzy clustering for image segmentation," *Digital Signal Processing*, vol. 110, p. 102905, 2021.

[57] F. Salehi, M. R. Keyvanpour, and A. Sharifi, "SMKFC-ER: Semi-supervised multiple kernel fuzzy clustering based on entropy and relative entropy," *Information Sciences*, vol. 547, pp. 667–688, 2021.

[58] C. Ouchicha, O. Ammor, and M. Meknassi, "A new approach based on exponential entropy with modified kernel fuzzy c-means clustering for MRI brain segmentation," *Evolutionary Intelligence*, pp. 1–15, 2022.

[59] C. A. Cocosco, V. Kollokian, R. K.-S. Kwan, G. B. Pike, and A. C. Evans, "Brainweb: Online interface to a 3D MRI simulated brain database," in *NeuroImage*. Citeseer, 1997.

[60] H. Gudbjartsson and S. Patz, "The Rician distribution of noisy MRI data," *Magnetic resonance in medicine*, vol. 34, no. 6, pp. 910–914, 1995.

[61] M. Ray and J. K. Sing, "A novel relative entropy based FCM algorithm using interval type-2 fuzzy set at local membership functions for brain MR image segmentation," in *2024 IEEE 3rd International Conference on Control, Instrumentation, Energy and Communication (CIEC)*, 2024, pp. 91–96.

[62] F. Chighoub and R. Saouli, "Fully integrated spatial information to improve FCM algorithm for brain MRI image segmentation," *Automatic Control and Computer Sciences*, vol. 56, no. 1, pp. 67–82, 2022.

[63] J. Miao, X. Zhou, and T.-Z. Huang, "Local segmentation of images using an improved fuzzy c-means clustering algorithm based on self-adaptive dictionary learning," *Applied Soft Computing*, vol. 91, p. 106200, 2020.

[64] O. P. Verma and H. Hooda, "A novel intuitionistic fuzzy co-clustering algorithm for brain images," *Multimedia Tools and Applications*, vol. 79, no. 41-42, pp. 31 517–31 540, 2020.

[65] P. K. Mishro, S. Agrawal, R. Panda, and A. Abraham, "A novel type-2 fuzzy C-means clustering for brain MR image segmentation," *IEEE Transactions on Cybernetics*, vol. 51, no. 8, pp. 3901–3912, 2020.

[66] Y. Wang, L. Chen, J. Zhou, T. Li, and C. P. Chen, "Interval type-2 outlier-robust picture fuzzy clustering and its application in medical image segmentation," *Applied Soft Computing*, vol. 122, p. 108891, 2022.

[67] L. Zadeh, "The concept of a linguistic variable and its application to approximate reasoning—i," *Information Sciences*, vol. 8, no. 3, pp. 199–249, 1975. [Online]. Available: https://www.sciencedirect.com/science/article/pii/0020025575900365

[68] D. Wu and J. M. Mendel, "Recommendations on designing practical interval type-2 fuzzy systems," *Engineering Applications of Artificial Intelligence*, vol. 85, pp. 182–193, 2019. [Online]. Available: https://www.sciencedirect.com/science/article/pii/S0952197619301514

[69] M. Nie and W. W. Tan, "Towards an efficient type-reduction method for interval type-2 fuzzy logic systems," in *2008 IEEE International Conference on Fuzzy Systems (IEEE World Congress on Computational Intelligence)*, 2008, pp. 1425–1432.

[70] S. Boulanouar and C. Lamiche, "A new hybrid image segmentation method based on fuzzy c-mean and modified bat algorithm," *International Journal of Computing and Digital Systems*, vol. 9, no. 4, pp. 677–687, 2020.

[71] H. Lohit and D. Kumar, "Modified total bregman divergence driven picture fuzzy clustering with local information for brain MRI image segmentation," *Applied Soft Computing*, vol. 144, p. 110460, 2023.

[72] X. Jia, T. Lei, X. Du, S. Liu, H. Meng, and A. K. Nandi, "Robust self-sparse fuzzy clustering for image segmentation," *IEEE Access*, vol. 8, pp. 146 182–146 195, 2020.

[73] N. Prakash and G. Hemalakshmi, "Efficient brain image segmentation technique based on entropy with genetic algorithm," *Bioscience Biotechnology Research Communications (Special Issue)*, vol. 12, no. 6, pp. 134–141, 2019.

[74] I. Khatri, D. Kumar, and A. Gupta, "A noise robust kernel fuzzy clustering based on picture fuzzy sets and KL divergence measure for MRI image segmentation," *Applied Intelligence*, vol. 53, no. 13, pp. 16 487–16 518, 2023.

[75] H. Zhang and H. Zhang, "A novel segmentation method for brain MRI using a block-based integrated fuzzy c-means clustering algorithm," *Journal of Medical Imaging and Health Informatics*, vol. 10, no. 3, pp. 579–585, 2020.

[76] Y. Jiang, K. Zhao, K. Xia, J. Xue, L. Zhou, Y. Ding, and P. Qian, "A novel distributed multitask fuzzy clustering algorithm for automatic MR brain image segmentation," *Journal of medical systems*, vol. 43, pp. 1–9, 2019.

[77] C. Senthilkumar and R. Gnanamurthy, "A fuzzy clustering based MRI brain image segmentation using back propagation neural networks," *Cluster Computing*, vol. 22, no. Suppl 5, pp. 12 305–12 312, 2019.

[78] N. Nagaraja Kumar, T. Jayachandra Prasad, and K. Satya Prasad, "Multimodal medical image fusion with improved multi-objective meta-heuristic algorithm with fuzzy entropy," *Journal of Information & Knowledge Management*, vol. 22, no. 01, p. 2250063, 2023.

[79] A. Halder, R. Choudhuri, and A. Sarkar, "Enhanced kernelized conditional spatial fuzzy c means algorithm for noisy brain MRI tissue segmentation," in *Proceedings of the Thirteenth Indian Conference on Computer Vision, Graphics and Image Processing*, 2022, pp. 1–9.

[80] B. Jena, M. K. Naik, R. Panda, and A. Abraham, "A novel minimum generalized cross entropy-based multilevel segmentation technique for the brain MRI/dermoscopic images," *Computers in Biology and Medicine*, vol. 151, p. 106214, 2022.

[81] M. R. Habib, A. Y. Suhan, A. Vadher, M. A. R. Swapno, M. R. Arefin, S. Islam, K. A. Rahman, and M. S. Tanvir, "Clustering of MRI in brain images using fuzzy c means algorithm," in *Machine Learning and Autonomous Systems: Proceedings of ICMLAS 2021*. Springer, 2022, pp. 437–448.

[82] Y. Zhao, Z. Huang, H. Che, F. Xie, M. Liu, M. Wang, D. Sun *et al.*, "Segmentation of brain tissues from MRI images using multitask fuzzy clustering algorithm," *Journal of Healthcare Engineering*, vol. 2023, 2023.

[83] S. Arulanandam and S. Selvarasu, "Adaptive weighted fuzzy region based optimization for brain MR image segmentation," *Multimedia Tools and Applications*, vol. 79, pp. 3603–3621, 2020.

[84] B. Meftah and G. B. Ghaouti, "An optimized clustering approach using tree seed algorithm for the brain MRI images segmentation," *Inteligencia Artificial*, vol. 26, no. 72, pp. 44–59, 2023.

[85] M.-B. Naghi, L. Kovács, and L. Szilágyi, "A generalized fuzzy-possibilistic c-means clustering algorithm," *Acta Universitatis Sapientiae, Informatica*, vol. 15, no. 2, pp. 404–431, 2023.

Madhumita Ray
03/06/24